POLYMER MICROFIBER FOR SENSOR AND LASER APPLICATIONS

NINIK IRAWATI

INSTITUTE OF GRADUATE STUDIES
UNIVERSITY OF MALAYA
KUALA LUMPUR

2017

POLYMER MICROFIBER FOR SENSOR AND LASER APPLICATIONS

NINIK IRAWATI

THESIS SUBMITTED IN FULFILMENT OF THE REQUIREMENTS FOR THE DEGREE OF DOCTOR OF PHILOSOPHY

INSTITUTE OF GRADUATE STUDIES
UNIVERSITY OF MALAYA
KUALA LUMPUR

2017

UNIVERSITY OF MALAYA

ORIGINAL LITERARY WORK DECLARATION

Name of Candidate: NINIK IRAWATI

Matric No: HHE140004

Name of Degree: DOCTOR OF PHILOSOPHY

Title of Project Paper/Research Report/Dissertation/Thesis ("this Work"):

POLYMER MICROFIBER FOR SENSOR AND LASER APPLICATIONS

Field of Study: PHOTONICS ENGINEERING

I do solemnly and sincerely declare that:

(1) I am the sole author/writer of this Work;
(2) This Work is original;
(3) Any use of any work in which copyright exists was done by way of fair dealing and for permitted purposes and any excerpt or extract from, or reference to or reproduction of any copyright work has been disclosed expressly and sufficiently and the title of the Work and its authorship have been acknowledged in this Work;
(4) I do not have any actual knowledge nor do I ought reasonably to know that the making of this work constitutes an infringement of any copyright work;
(5) I hereby assign all and every rights in the copyright to this Work to the University of Malaya ("UM"), who henceforth shall be owner of the copyright in this Work and that any reproduction or use in any form or by any means whatsoever is prohibited without the written consent of UM having been first had and obtained;
(6) I am fully aware that if in the course of making this Work I have infringed any copyright whether intentionally or otherwise, I may be subject to legal action or any other action as may be determined by UM.

Candidate's Signature Date:

Subscribed and solemnly declared before,

Witness's Signature Date:

Name:

Designation:

ABSTRACT

Polymer microfiber devices have been attracting attention as a platform for manipulating light at the nanoscale. The high sensitivity of polymer microfibers to detect changes in the surrounding refractive index due to the large evanescent field propagating outside the microfiber can be utilized in various optical sensor and laser applications. In this thesis, the fabrication process of PMMA microfiber has been introduced using a direct drawing technique. The aim of this research is to establish a micro scale polymer optical fiber as a new sensor and laser technology which can create devices that are extremely small sized, ultra lightweight and have the potential to be manufactured at low cost. To enhance the performance of the sensing probe, PMMA microfibers were coated and doped with sensitive materials such as Zinc Oxide (ZnO) and Agarose gel for sensing different relative humidity (RH) levels. It is observed that the probe sensitivity improves due to the sensitive coating materials used. For instance, as the RH increases from 50% to 80%, the peak wavelength shifted against RH at a rate of 21.4 pm/% and 28 pm/%, and with a linearity of 98.36% and 98.83% for the un-doped PMMA and agarose doped PMMA microfiber, respectively. When the composite are exposed to an environment of humidity, rapid surface adsorption of water molecules occurs which changes its optical property. On the other hand, temperature sensor and laser applications have been proposed and demonstrated using CdSe QD doped PMMA microfiber. It is observed that the doping material managed to enhance the capabilities of generating, propagating, converting and modulating light at the microscale. For instance, a stable mode-locked Ytterbium-doped fiber laser operating at 1087.5 nm was successfully demonstrated with repetition rate of 12.6 MHz, maximum pulse energy of 1.1 nJ and output power of 14 mW.

ABSTRAK

Peranti gentian mikropolimer semakin menarik perhatian sebagai suatu platform untuk memanipulasi cahaya pada skala nano. Kepekaan gentian mikropolimer yang tinggi dalam mengesan perubahan indeks pembiasan persekitaran, yang disebabkan oleh penyebaran medan evanesan yang lebar boleh dimanfaatkan di dalam pelbagai aplikasi optik sensor dan laser. Di dalam tesis ini, penghasilan gentian mikropolimer melalui teknik '*direct drawing*' ". Matlamat penyelidikan ini adalah untuk menghasilkan gentian optik polimer pada skala nano sebagai sensor dan laser teknologi terbaru dimana ianya boleh menjadi suatu peranti yang sangat kecil saiznya, sangat ringan dan mempunyai potensi untuk dihasilkan pada kos yang rendah. Untuk meningkatkan keupayaan prob sensor, gentian mikro PMMA disadur dan didopkan dengan bahan-bahan berkepekaan tinggi seperti *Zinc Oxide (ZnO)* and gel *Agarose* untuk mengesan pelbagai aras kelembapan relatif (RH). Diperhatikan bahawa kepekaan prob meningkat disebabkan oleh penyaduran bahan berkepekaan tinggi. Misalnya, apabila RH meningkat dari 50% kepada 80%, puncak panjang gelombang berubah pada kadar 21.4 pm/% dengan kelinearan 98.36% untuk PMMA yang tidak didopkan manakala perubahan pada kadar 28 pm/%, dengan kelinearan 98.83% untuk *Agarose* didopkan dengan PMMA gentian mikro. Apabila komposit didedahkan dengan kelembapan persekitaran, penyerapan molekul air pada permukaan berlaku dengan cepat telah menyebabkan perubahan sifat optiknya. Selain daripada itu, sensor suhu dan aplikasi laser turut dicadang dan didemonstrasikan dengan menggunakan gentian mikropolimer yang didop dengan CdSe QD. Diperhatikan, bahan dop tersebut telah berjaya meningkatkan kebolehan dalam penghasilan, penyebaran, penukaran dan modulasi cahaya pada skala mikro. Misalnya, mode-locked Ytterbium didop dengan gentian laser yang stabil, beroperasi pada 1087.5 nm dengan kadar pengulangan 12.6 MHz, 1.1 nJ tenaga denyutan maksimum dan kuasa pengeluaran sebanyak 14 mW telah berjaya dihasilkan.

ACKNOWLEDGEMENTS

First and foremost I would like to thank the ALMIGHTY for the successful completion of this thesis. I wish to express my heartfelt indebtedness and deep sense of gratitude to my Supervisor, Prof. Dr. Sulaiman Wadi Harun and my co supervisor, Prof. Dr. Harith Ahmad. I want to express my profound thanks to them for giving me the independence in choosing my own subject of research, as well as for many fruitful discussions, which greatly contributed to my scientific work.

Thanks also to my external co supervisor Dr. Husna Abdul rahman, for sharing her expertise in the area of sensors. Words are inadequate to place my gratitude to her for valuable suggestions and constructive criticism to fulfil this work.

My appreciation also goes to the members of the Photonic Research Center. You have made the lab most enjoyable to work in despite the many challenges we have to put up with.

I wishes to express deepest thanks to my beloved the late of my father, my mother and my brother, for their understanding, endless love, and prayers.

Finally special thanks to Indonesia government for providing fund to support my study under Indonesia Endowment Fund for Education Grant.

TABLE OF CONTENTS

LIST OF FIGURES

LIST OF TABLES

LIST OF SYMBOLS AND ABBREVIATIONS

β	:	Propagating constant
k	:	Wavelength of the light in vacuum
n	:	Index of refraction
A	:	mode area
ν	:	The light speed
$\Delta\lambda$	:	Space between two adjacent resonance wavelengths
µW	:	Micro watt
AFM	:	Atomic Force Microscope
ASE	:	Amplified Spontaneous Emission
BP	:	Black phosphorus
CdO	:	Cadmium oxide
CdSe	:	Cadmium selenide
DNA	:	Deoxyribonucleic Acid
DPN	:	Dip-pen nanolithography
ER	:	Extinction Ratio
FESEM	:	Field Emission Scanning Electron Microscope
FWHM	:	Full wave at half maximum
FSR	:	Free Spectral Range
GOF	:	Glass Optical Fiber
GNRs	:	Single gold nanorods
HMTA	:	Hexamethylenetetramine
HRP	:	Horseradish peroxidase
ISAM	:	Ionic self-assembled monolayer
KMnO4	:	Potassium permanganate

Mn	:	Manganese
MS222	:	Tricaine methanesulfonate
NaCl	:	Sodium Chloride
Nm	:	Nanometer
NOLM	:	Nonlinear optical loop mirror
NPR	:	Nonlinear polarization rotation effect
OSA	:	Optical Spectrum Analyzer
PAM	:	Polyacrylamide
PMKR	:	Polymer microfiber knot resonator
PMLR	:	Polymer microfiber loop resonator
PMNF	:	Polymer micro-nanofiber
PMMA	:	Polymethyl Methacrylate
PVA	:	Poly Vinyl Alcohol
PEO	:	Poly Ethylene Oxide
QDs	:	Quantum dots
POF	:	Plastic Optical Fiber
RH	:	Relative Humidity
RI	:	Refractive Index
SA	:	Saturable absorber
Se	:	Selenium
SESAM	:	Semiconductor saturable absorber
SMF	:	Single Mode Fiber
SWCNTs	:	Single-walled carbon nanotubes
TCO	:	Transparent conduction oxide electrode
TMDs	:	Transition metal dichalcogenides
TMO	:	Transition metal oxide

UA	:	Uric Acid
ZnO	:	Zinc Oxide
$Zn(CH_3COO)_2 \cdot 2H_2O$	:	Zinc acetate dehydrate
Zn(NO3)2.6H2O	:	Zinc nitrate hexahydrate

CHAPTER 1

INTRODUCTION

1.1 General

The basic concept of any optical sensing system is divided into three main stages ; emitting the light from an optical source, guiding the light through the sensor structure while exposing it to measurand changes, detecting and processing the received light. Optical sensors modulate the light passing through the fiber in response to the changes in measurand. In the sensing region, measurand interacts with fiber or its coating resulting in a light modulation in a form of wavelength shifts, power intensity variations, or light phase changes. The optical sensor system have been attracting consideration due to their preferential advantages over their electrical counterparts, such as small size, low cost, high sensitivity, passive and reliability since single mode fiber avoids the problem of intermodal dispersion losses (Gambling, 2000; Golnabi, 2004). The applications of fiber optic in sensing can be used for the measurement of physical (e.g. strain, displacement, temperature, pressure, velocity, acceleration) and chemical (e.g. PH) quantities, as well as for the detection of specific chemical or bio-chemical molecules (e.g. air and water pollutants, glucose contents in blood, DNA sequencing) and refractive index change (Golnabi, 2000; Kwon et al, 2004; Xu et al, 2013; Zhao, Zhang, & Liao, 2003)

On the other hand, Q-switched fiber lasers have been widely used in material processing, optical communications, medicine, and optical sensing (Dausinger, Lichtner, & Lubatschowski, 2004; Ursula Keller, 2003; Schütze, Pösl, & Lahr, 1998). These lasers can be realized by using an artificial saturable absorber (SA) or placing a real saturable absorber (SA) in the resonant cavity. In general, lasers that use nonlinear

polarization rotation (NPR) as artificial SA are unstable (Wang et al., 2011). Apart from NPR, a material-based SA can also be used to generate stable Q-switching pulses. One type of material-based SA, the semiconductor saturable absorber mirror, however, always has a narrow transmission bandwidth and requires complex fabrication and packaging (Liu et al., 2016; Wu et al., 2015; Yan et al, 2015). Another material-based SA, based on single-walled carbon nanotubes (SWCNTs) though easier to fabricate and cost effective, has working wavelengths that are connected with the diameter of the nanotubes (Yamashita et al., 2004). A third material-based SA, graphene, has a higher optical damage threshold, lower loss and better wavelength-independence than SWCNTs. However, monolayer graphene always has a small absorption at 1550 nm (Bao et al., 2009; Luo et al., 2014; Sobon et al., 2015). Recently, several new and intensively investigated nanomaterials, including transition metal dichalcogenides (TMDs) and black phosphorus (BP) have been used as SAs. However, TMDs have sizeable bandgaps corresponding to only the visible and near-infrared spectrum ranges (Y et al, 2015), while BP is very sensitive to the environment because of the high reactivity of BP with air, and this might limit their applications in real devices (Yuan, Rudenko, & Katsnelson, 2015).

Quantum dots (QDs) semiconductor nanocrystals have been discovered as a new class of 0D nanomaterials that have drawn numerous attention in potential important application including laser power limiter, light-emitting diodes, optical switch, sensor, biological labeling, and solar cells. One of the QD material is cadmium selenide (CdSe) which has unique properties such as stronger extinction coefficient, narrower band gap, higher quantum confinement effect, higher optical gain, broader absorption profile, better photochemical stability and larger Stokes shift compared to bulk semiconductor. The QD CdSe exhibit resonant nonlinearity in slow time scales that induce huge optical nonlinearity, which an important feature for generating pulsed laser.

This thesis is concerned with the development of a simple and low cost polymer microfiber device for both sensor and laser applications. The polymer microfiber is fabricated using a direct drawing technique. This polymer microfiber is sensitive to change in the refractive index of its surrounding and thus it can be coated with various sensitive materials for sensing applications. In this thesis, a polymer microfiber doped with quantum dot CdSe materials is also developed for both sensor and laser applications.

1.2 Microfiber

Fiber-optic technology has historically achieved many developments especially in telecommunications and continues to be driven to a large extent due to reduction of the price of the optical components, coupled with integrated spatial miniaturized devices (G Brambilla, 2010; Gilberto Brambilla et al., 2009; Tong et al., 2003; Tong, Zi, Guo, & Lou, 2012). Recently, a new type of waveguide so called microfiber has been developed by combining fiber optic and nanotechnology. The microfiber has opened up new possibilities of new devices for a new range of applications. With its tiny size (diameter of hundreds of nanometers to several micrometers) (Tong et al., 2003), accompanied by high-fractional evanescent fields and high flexibilities, making it as a microscale waveguide that has higher sensitivity, faster responses and lower power consumption (Brambilla, 2010; Guo, Ying, & Tong, 2013; Tong et al., 2003; Tong & Sumetsky, 2011; Wu & Tong, 2013) over conventional optical fiber. In addition, light propagate in the microfiber shows low optical loss and high mechanical strength, owed to diameter uniformity and smoothness of atomic-level sidewall of fiber (Tong et al., 2003; X. Wu & Tong, 2013). The great evanescent fields and the sturdy confinement as well as the superb waist uniformity and the surface smoothness (Tong et al., 2003) make the microfibers prospective candidates for low loss optical sensing of refractive index (RI), temperature, humidity, displacement, acceleration, and other

parameters. Silica is one of the most popular optical materials to fabricate a microfiber. However, several different materials, including polymers are also used (Wang et al, 2013).

Polymer microfiber offers many unique characteristics such as strong evanescent field in which fraction of the transmitted power propagates outside the polymer microfiber and that leads to its potential usage in sensing applications. Polymer microfiber is flexible and has high configurability which can be easily bent and fabricated at different compact optical structures with small bending radius. Polymer microfiber as a new sensor technology which can create devices that are extremely small size, can be manufactured at low cost and hospitality to many functional dopants. All these attractive features of the microfiber have strongly motivated many researchers to do research in this topic. Here, doped and undoped optical polymer microfiber are developed for sensing and laser applications.

1.3 Research Justification

Various technologies are used in the photonics research field are based on silica microfibers leaving behind polymer microfibers (X. Wu & Tong, 2013). However due to the advantages such as the polymer matrix is hospitable to a variety of functional dopants and have perm-selective nature with respect to gas molecule, high surface volume ratios and excellent mechanical flexibility, polymer microfiber become important. Recently, the interest on the polymer microfiber is also increasing for sensor applications. The reduction in the diameter of fiber allows the evanescent field of the propagating mode of the fiber to extend into the external environment. The deposition of a sensitive material onto the polymer microfiber such as coating and doping allows for the transmission spectrum control via the interaction of the light propagating in a fiber with the overlay material. The coating and doping material expand their

capabilities of generating, propagating, converting and modulating light at the microscale. In this thesis, PMMA microfiber is fabricated using a simple and low cost direct drawing technique. The microfiber is then used for various sensor applications.

On the other hand, nanomaterials have recently emerged as promising solution for generating fiber laser pulse. In the last few years, numerous research activities have been carried out on passively Q-switched and mode-locked fiber lasers using various kind of nanomaterials as saturable absorber (SA). These materials are graphene, topology insulator (TI), transition metal di-chalcogenide (TMD) and transition metal oxide (TMO). In this thesis, two types of new nanomaterials have been investigated as a new SA device for both Q-switching and mode-locking applications. Despite the success of these materials, researchers are still exploring for new materials to compensate for any shortcomings and improves the performance of the pulse generations. In recent years, many studies focused on QDs because of its high luminescence quantum yield, narrow band gap and a variety of optoelectronic (J. Zhu, Palchik, Chen, & Gedanken, 2000). So far there is no scientific report of using QD for pulse generations. It is believed that QD materials provide a special attribute, which is the tunable bandgap that can be achieved by varying its particle size (L.-s. Li, Hu, Yang, & Alivisatos, 2001). This tunable bandgap is one of the very important feature required to become good SA which not achievable by bulk semiconductor that having fixed bandgap. One of the well-known QD material is the cadmium selenide (CdSe) that have been widely used in commercial optical components due to its high photoluminescence and high resistance to photobleaching (Empedocles, Norris, & Bawendi, 1996). CdSe material in the form of QD have higher optical gain, stronger extinction coefficient, better photochemical stability and larger Stoke shift due to high surface area to volume ratio and small size distribution (Xiaoyong Wang, Qu, Zhang, Peng, & Xiao, 2003). In the aspect of SA, QD CdSe exhibit resonant nonlinearity in slow time scales that induce

huge optical nonlinearity, an important feature for generating pulsed laser. In this thesis, we demonstrate Q-switched and mode-locked pulse generation in fiber laser cavity using QDs CdSe doped PMMA microfiber as a SA device.

1.4 Objectives of the Study

The aim of the study is to develop PMMA microfiber devices for sensor and laser applications. To achieve this, the following objectives have been outlined to guide the research route;

1. To fabricate polymer microfibers using a direct drawing technique and demonstrate a refractive index sensor to detect different concentration of chemicals.
2. To coat the polymer microfiber with sensitive material such as zinc oxide (ZnO) nanorods and agarose gel for relative humidity sensor.
3. To fabricate QD CdSe doped PMMA microfiber using direct drawing technique for temperature sensing, Q-switched and mode-locked laser applications.

1.5 Organization of the Thesis

This thesis is organized into 6 chapters to comprehensively demonstrate the development of undoped and doped PMMA microfibers for both sensor and laser applications. Chapter 1 is the brief introduction about the background and motivation of this study. This chapter briefly describes a recent development on optical fiber sensor, fiber lasers and microfiber. The aim and research objectives of this study are also highlighted in this chapter. In Chapter 2, a literature study on polymer microfiber, its fabrication techniques and applications.

Chapter 3 reports on the fabrication and characterization of polymer microfiber

using direct drawing technique. The fabricate polymer microfiber is then used as a sensor probe to measure the refractive index of various chemicals.

Chapter 4 demonstrates a polymer microfiber for relative humidity measurement. In this work, the polymer microfiber is coated with sensitive coating materials such as ZnO nanorods and agarose gel to enhance the sensitivity of the sensor. The sensitive materials change refractive indices in presence of water molecules. It is observed that the difference in refractive index between the cores and cladding influences the amount of light confinement inside the core. The polymer microfiber itself can play an active role by acting as a sensor when the cladding is replaced with chemical sensitive material.

Chapter 5 demonstrates functionalized polymer microfiber doped with Quantum doped as a temperature sensor and laser applications. In this work, the polymer microfiber after doping with quantum doped its used for Q-switch and mode lock application.

The finding of this work is concluded and summarized in Chapter 6. This chapter also discusses about possible areas for future research.

CHAPTER 2

BACKGROUND THEORY

2.1 Introduction

A brief review on the recent development in polymer microfiber and its properties are discussed in detail which divided into several sections. Various techniques for developing microfibers are discussed in this chapter including direct drawing, electrospinning and chemical synthesis for fabrication of the microfiber. In addition to this, the application of the polymer microfiber are also discussed in this chapter. Finally an overview of functional dopants is given in detail for explanation of the physical characteristic of the polymer microfiber.

2.2 Overview of Polymer Microfiber

Polymer optical fibers (POF) have gained tremendous interest in recent years (Jin & Granville, 2016; Koike & Asai, 2009; Koike & Koike, 2011; Peters, 2010). According to Agrawal that Brillouin scattering (Agrawal, 2007) was observed in the POF for the first time in 2007 and since then its properties have been investigated for distributed strain and temperature sensing applications (Hayashi, Mizuno, & Nakamura, 2012; Mizuno, Hayashi, & Nakamura, 2013; Mizuno & Nakamura, 2010). The POF have similar advantages as conventional silica optical fiber (SOF) for sensing applications. The POF also attracted considerable attention in physical, chemical, and biological sensors due to their unique geometry with low dimension and large surface-to-volume ratio. In addition to physical geometry, the POF offers its versatility for electrical and optical detection. Compared with the silica and glass counterparts, polymer materials possess many attractive properties including easy handling, great

flexibility, infrared transparency in long-wavelength, low-cost integration, good processability, excellent biocompatibility and tunable properties. The POF have great potential for short-distance networking (in-building), optical sensing and power delivery (Wang, et al., 2013). For sensor devices, the POF have additional advantages which include high elastic strain limits, high fracture toughness, high-flexibility bending, high-sensitivity strain and potential negative thermos-optic coefficients (Peters, 2010). Polymer material also have an excellent compatibility with organic material and have a great potential for use in biomedical applications. Previously, a multimode POF based sensor has been successfully applied to take advantages of these properties. Silica fiber sensors produce lower measurement accuracy and resolution due to the characteristic of multimode fibers since these sensors are generally larger than comparable single mode. However, recent successes in the fabrication of single mode POF and new integration methods for multimode POF sensors have enable the sensor manufacturer to produce a large deformation and high precision sensor.

A miniaturizing technology has led and contribute in reducing electronic circuit and components to their ultimately fundamental forms. This miniature technology have spurred great efforts in reducing the photonic structures and components to scales comparable to or less than the wavelength of light. Polymer waveguides in the form of free-standing optical fiber is potential building blocks for photonic circuitry and integration. The polymer waveguides can be shrunk to polymer nanofibers with diameters of tens or hundreds of nanometers attracting increasing attention as versatile platforms for manipulating light at the nanoscale. Compared with inorganic material microfiber such as glasses or semiconductors, polymer microfiber or nanofiber exhibit fascinating properties: First, the polymer matrix is hospitable to variety of functional dopants, ranging from quantum dots, noble metal nanoparticle, dye molecules and rare earth ions which can be readily employed to tailor the optical, electrical and magnetic

properties of the host micro/nanofibers with great versatility. Secondly, polymer micro/nanofibers have perm selective nature with respect to gas molecule, high surface to volume ratios and high flexibility of surface functionalities, offering more possibilities for polymer nanofibers in applications such as optical sensing. In addition, polymer micro/nanofibers exhibit excellent mechanical flexibility and biocompatibility as well as simple and low-cost fabrication. To date, polymer micro/nanofibers have been successfully applied in micro-nanometer scale waveguides (Gu et al, 2008; Guo et al., 2013; Harfenist et al., 2004; Yang et al., 2008), lasers (Camposeo et al., 2009; Das et al, 2011; Li et al, 2011), photodetectors (O'Brien et al, 2006), incoherent light emitting device (Camposeo, Persano, & Pisignano, 2013; Di Benedetto et al., 2011; Wang et al, 2013), optical sensors (Gu et al, 2013; Gu et al., 2008; Meng et al., 2011; Wang et al., 2012; Zhu, Wang, & Li, 2009).

2.3 Fabrication Techniques of Polymer Microfiber

A number of techniques, including electrospinning (Agarwal, Greiner, & Wendorff, 2013; Aussawasathien, Dong, & Dai, 2005; Bhardwaj & Kundu, 2010; Camposeo et al., 2013; Chang et al., 2010; Chang, Li, Xu, Wang, & Xue, 2016; Roskov et al., 2011; Wu et al., 2013) (Aussawasathien et al., 2005; Camposeo et al., 2013; Chang et al., 2010; Roskov et al., 2011), nanolithography (Noy et al., 2002; Wang et al., 2011), direct drawing (Berry et al., 2011; Duong Ta et al, 2013; Gu et al., 2013; Gu et al., 2008; Meng et al., 2011; Ong et al, 2015; Wang et al., 2013; Wang et al., 2012; Yang et al., 2008), and chemical synthesis (Cui et al., 2006; Huang & Kaner, 2004) have currently been developed for the fabrication of polymer micro/nanofiber.

2.3.1 Electrospinning

Electrospinning is a broadly used technology for electrostatic fiber formation which utilizes electrical force to produces polymer fibers with diameters ranging from 2

nm to several micrometers using polymer solutions of both natural and synthetic (Bhardwaj & Kundu, 2010; Garg & Bowlin, 2011). This process is a very powerful method for creating diverse kinds of microstructures and offers unique capabilities for producing novel natural nanofibers and fabrics with controllable pore structure (Cramariuc et al., 2013). Till date, electrospinning has been used for the fabrication of nanofibrous scaffolds from numerous biodegradable polymers, such as poly (ε-caprolactone) (PCL), poly (lactic acid) (PLA), poly (glycolic acid) (PGA), polyurethane (PU), copolymer poly (lactide-co-glycolide) (PLGA), and the copolymer poly (L-lactide-co-ε-caprolactone) for bone tissue engineering, cardiac grafts, wound dressings and for engineering of blood vessel substitutes (Holzwarth & Ma., 2011; Meinel et al, 2012; Unnithan et al., 2012). The electrospinning technique using electrostatic forces to produces fine fibers from polymer solutions or melts and the fibers thus produced have a thinner diameter and larger surface area than those obtained from conventional spinning processes. To generate the electrospinning, a DC voltage in the range of several tens of kV is necessary. There are two standard electrospinning setups i.e. vertical and horizontal. This method is conducted at room temperature with atmosphere conditions. Figure 2.1 shows the typical set-up of electrospinning apparatus. Electrospinning system consist of three major components: a high voltage power supply, a spinneret and a grounded collecting plate. The electrospinning utilizes a high voltage source to inject charge of a certain polarity into a polymer solution or melt, which is then accelerate towards a collector of opposite polarity. Most of the polymers are dissolved in some solvents before electrospinning, and when it completely dissolves which forms polymer solution. The polymer fluid is then introduced into the capillary tube for electrospinning. In the electrospinning process, a polymer solution held by its surface tension at the end of a capillary tube is subjected to an electric field. An electric charge is induced on the liquid surface due to this electric field. When the electric field

being applied reaches a critical value, the repulsive electrical forces overcome the surface tension forces. Eventually, a charged jet of the solution is ejected from the tip of the Taylor cone. An unstable and a rapid whipping of the jet occurs in the space between the capillary tip and collector which leads to evaporation of the solvent which leaving a polymer behind.

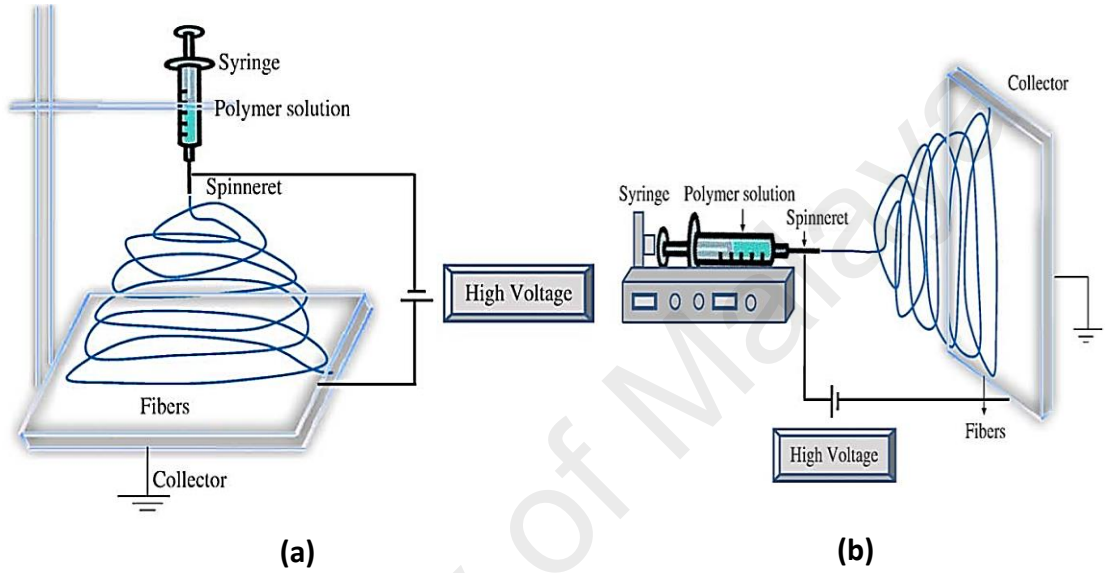

Figure 2.1: Schematic set-up of electrospinning apparatus (a) vertical set-up (b) horizontal set-up (Bhardwaj & Kundu, 2010).

Analysis of nanofibers structure still on-going for polymer solutions. The parameters such as concentration, molecular weight, surface tension, viscosity, conductivity and governing parameters, such as applied voltage, and the distance between electrodes are being analysed (Adomavičiūtė & Milašius, 2007).

2.3.2 Nanolithography

Nanolithography method often rely on patterning of resistive film, then followed by a chemical etch of the substrate. Noy et al., (2011) has explained this technique using dip-pen nanolithography (DPN) in details where DPN uses an atomic force microscope (AFM) tip as a “nip”, a solid state substrate as “paper”, and molecules with a chemical

affinity for the solid state substrate as “ink”. Capillary transport of molecules from the AFM tip to the solid substrate is used in nanolithography to directly write patterns consisting of a relatively small collection of molecules in sub-micrometer dimensions. The advantage of DPN it can turn on and off the ink flow at will, whereas prior DPN techniques apply ink to the surface as long as the tip stays in contact with it. The rate of the ink diffusion is tunable by controlling the tip temperature. Single lines were written less than 100 nm wide (Sheehan et al., 2004). In the DPN process, a drop of the solution in methanol was absorbed onto a thin paper membrane. Then, gently lowered the AFM tip into contact with the paper for 30-60 s using a custom-built translation stage under the optical microscope. Lithography was performed immediately after the “inking”. Figure 2.2, shows the schematic diagram illustrating the dip-pen nanolithography. The instrument combines atomic force microscopy and scanning confocal microscopy functionalities. A bioscope AFM head is mounted on a Nikon Eclipse 300 inverted microscope equipped with a custom-built translation stage that incorporates a closed-loop piezo scanner. The scanning stage is used in both the lithography procedure and confocal imaging. The fluorescence excited by 514-nm line Ar-Ion laser is collected with 100 x 1.4 NA lens, passed through a 50-μm pinhole to reject stray light and then detected by an avalanche photodiode. Excitation light was rejected by a long-pass filter.

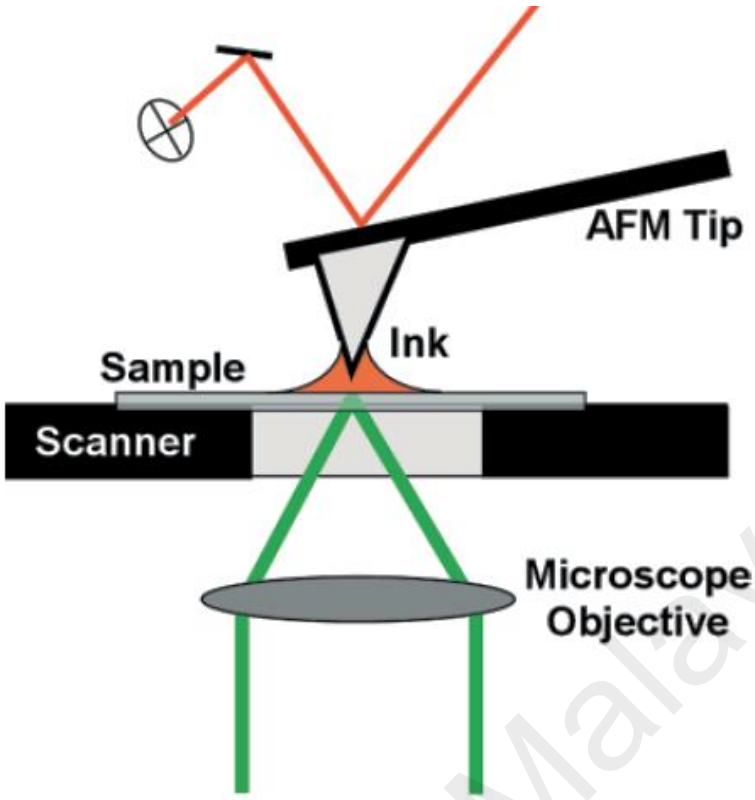

Figure 2.2: Schematic diagram used for dip-pen nanolithography (Noy et al., 2002).

2.3.3 Direct Drawing

Direct drawing is an optimal method for fabricating polymer micro-nanofibers with excellent surface qualities that area highly desired for low-loss optical waveguiding. A sharp tip tapered fiber probe is used to directly draw polymer microfiber out from molten polymer material (Xing, Zhu, Wang, & Li, 2008). The diameter of the drawn polymer microfiber can be roughly controlled by the drawing speed and the solution concentration. The step by step drawn polymer microfiber from the molten polymer material is shown in Figure 2.3. In the direct drawing process, a silica tip is dipped into the molten polymer material and then retracted from the molten polymer with a speed of 0.1-1 m/s. A polymer microfiber extending between the molten polymer and the tip. The extended polymer is quickly quenched in air and finally polymer microfiber is formed.

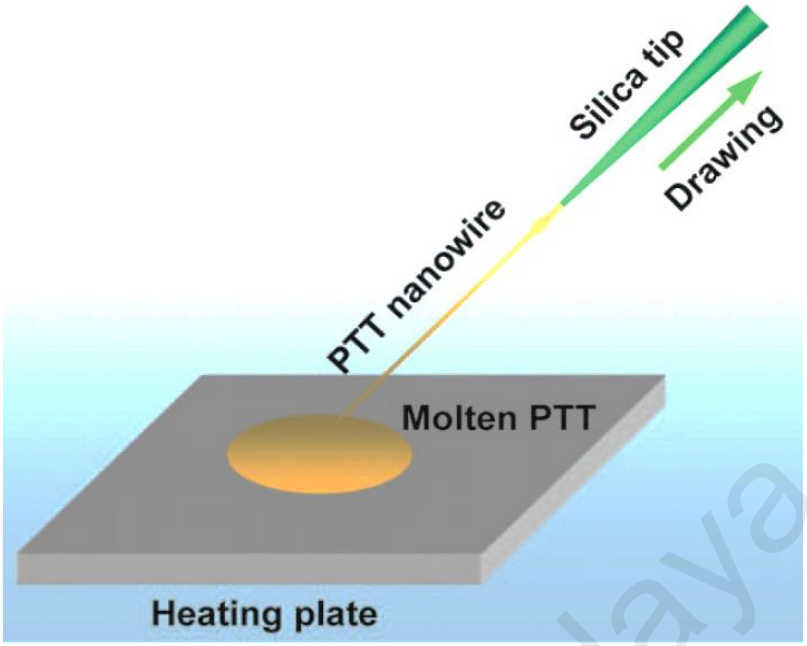

Figure 2.3: Schematic diagram direct drawing technique for the fabrication of polymer microfiber.(Xing et al., 2008)

2.3.4 Chemical Synthesis

Cui et al., (2006) has explained the chemical synthesis technique in details where fabrication of polymer composite nanofiber through the combined use of γ-irradiation and gas/solid reaction. Figure 2.4 shows the schematic diagram synthetic pathway for the preparation of PbS nanoparticles/polymer composite nanofibers. First step requires organic metal-salt (lead dimethacrylate $Pb(MA)_2$ powder to be dissolved in ethanol solution by heating and ultrasonication, then $Pb(MA)_2$ molecules could self-assemble into nanofibers in this system. Second step is the monomeric $Pb(MA)_2$ nanofibers were polymerized and formed poly(lead dimethacrylate) ($P\text{-}Pb(MA)_2$) nanofibers by ^{60}Co γ-ray irradiation. Final step is PbS nanoparticles were generated in situ by exposing the P-Pb $(MA)_2$ nanofibers to H_2S gas at room temperature. In this approach, γ-irradiation offers an ideal means to fabricate polymer nanofibers without obvious changing of the morphology and introducing any other reagent (Cui et al., 2006).

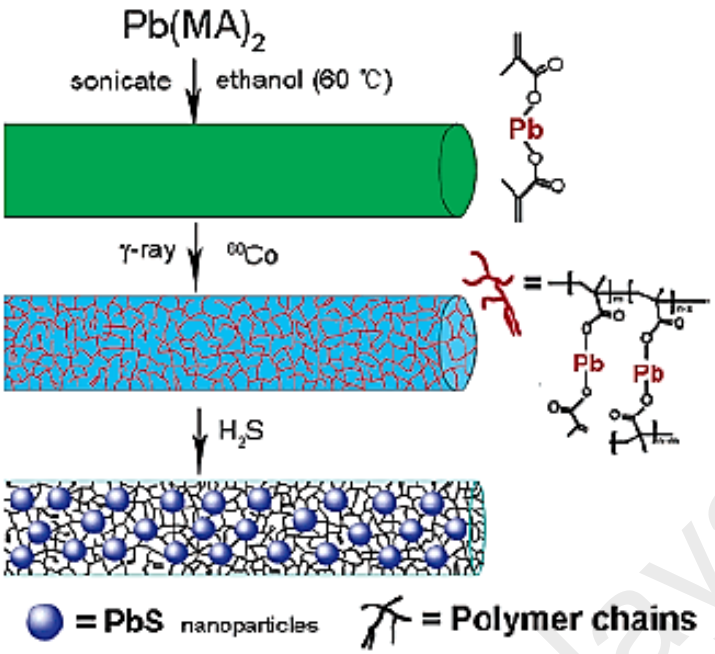

Figure 2.4: Schematic diagram synthetic pathway for the preparation of PbS nanoparticles/polymer composite nanofibers (Cui et al., 2006).

2.4 Optical Properties

This section introduces the optical techniques and mechanical properties of polymer micro-nanofiber sensor (PMNFs) including mode propagation, evanescent field, optical confinement, propagation loss and bend loss.

2.4.1 Mode Propagation

Figure 2.5 (a) shows the refractive indices of the PMNF and the surrounding medium are n_1 and n_2. The diameter of the PMNF is 2a. The index profile of the waveguiding PMNFs is expressed as

$$n(r) = \begin{cases} n_1, & 0 < r < a \\ n_2, & a \leq r < \infty \end{cases} \quad (2.1)$$

The waveguiding properties of a PMNF for non-absorptive polymers can be obtained by analytically solving the following Helmholtz equations:

$$(\nabla^2 + n^2k^2 - \beta^2)\,\vec{e} = 0,$$

$$(\nabla^2 + n^2k^2 - \beta^2)\,\vec{h} = 0 \qquad (2.2)$$

where is $k = 2\pi/\lambda$, λ is the wavelength of the light in vacuum, and β is the propagating constant.

Benefited from the circular cross section, Equation (2.2) can be analytically solved in cylindrical coordinate (Tong, Lou, & Mazur, 2004), with eigenvalue equations:

HE*vm* and EH*vm* modes

$$\left\{\frac{J_v'(U)}{UJ_v(U)} + \frac{K_v'(W)}{KW_v(W)}\right\}\left\{\frac{J_v'(U)}{UJ_v(U)} + \frac{n_2^2K_v'(W)}{n_1^2KW_v(W)}\right\} = \left(\frac{v\beta}{kn_1}\right)^2\left(\frac{V}{UW}\right)^4 \qquad (2.3)$$

For TE_{om} modes

$$\frac{J_1(U)}{UJ_0(U)} + \frac{K_1(W)}{WK_0(W)} = 0 \qquad (2.4)$$

For TM_{om} modes

$$\frac{n_1^2J_1(U)}{UJ_0(U)} + \frac{n_2^2K_1(W)}{WK_0(W)} = 0 \qquad (2.5)$$

where the β solutions are denoted with two indices *v* and *m*. *v* originates from the detailed calculations of the fields and describes the azimuthal dependence. *m* denotes the m^{th} root of the eigenvalue equation. J_v is the Bessel function of the first kind, K_v is the modified Bessel function of the second kind and $U = a(k_0^2n_1^2 - \beta^2)^{1/2}$, $W = a(\beta^2 - k_0^2n_2^2)^{1/2}$, $V = k_0a(n_1^2 - n_2^2)^1$.

By numerical solving Equations (2.3) – (2.5), the waveguiding modes (β) supported by the PMNFs can be obtained. Generally when its diameter goes close to or

smaller than the wavelength of the guided light, an PMNF with low index clad (e.g., water, air or vacuum) offers unusual properties such as tight optical confinement (Figure 2.5 (b)), high fractional evanescent field (Figure 2.5 (c)), and large tailorable waveguide dispersion, which intrigue new opportunities for manipulating light on the micro/nanoscale. Table 2.1 shown the summarized optical properties and potentials of PMNFs can be categorized into three types.

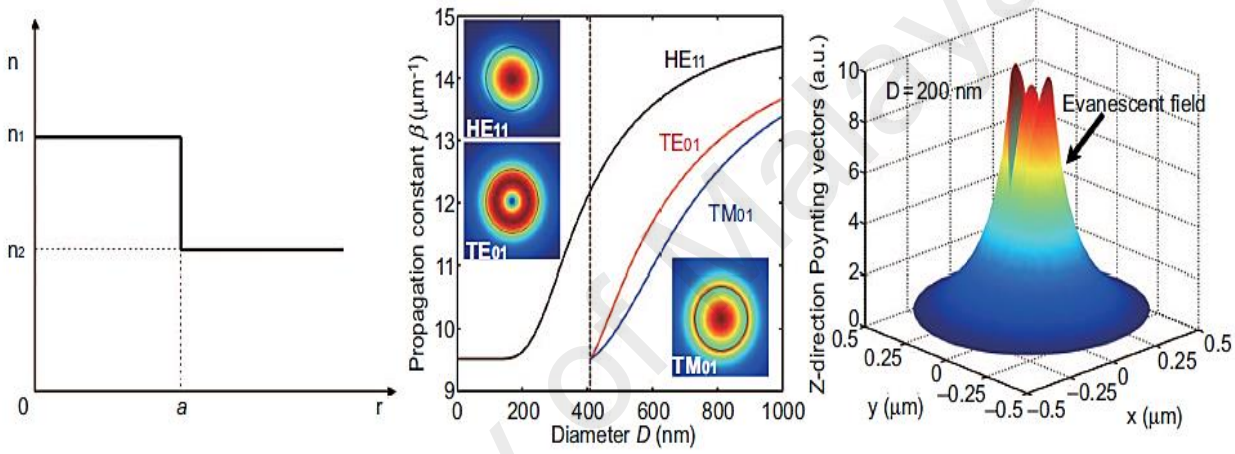

(a) **(b)** **(c)**

Figure 2.5: Mathematical modeling of a PMNF. (a) Index profile of a PMNF, (b) Numerical solutions of the propagation constant (β) of an air-clad polystyrene nanofiber at 660 nm, (c) Calculated pointing vectors of a 200 nm diameter polystyrene nanofiber (wang et al., 2013).

Table 2.1. Properties and potentials of optical PMNFs.

Fiber Parameter	Waveguiding Properties		Potentials for Applications
Wavelength/subwavelength diameter with high index contrast	Tight optical confinement	• Small allowable bending radius	• Short interconnection • Miniaturized circuits/devices
		• Small mode area	• Low-power-consumption devices • Low threshold nonlinear effects
	Strong evanescent fields	• Modified vacuum states of radiation strong near-field interaction	• Modified spontaneous rate of an atom • High sensitivity optical sensing • Efficient/convenient evanescent coupling
		• Steep field gradient	• Atom trapping and waveguiding • Large gradient force for optical trapping
	Small mass/weight	• Modifiable group velocity	• Large/manageable waveguiding dispersion
		• Photon-momentum-induced effect	• Optomechanical components/device • Efficient photon-photon coupling

2.4.2 Evanescent Field

Large evanescent field is particular important for sensor (Vienne et al., 2008; Xu et al., 2008) and resonator (e.g., rings/ loops/ knots/ coils), where a significant fraction of the propagating power needs to interact with surrounding medium (Sumetsky, 2008; Warken et al., 2007; Zhang et al, 2011) and especially for laser (Jiang et al., 2007; Li et al., 2006). A waveguiding PMNF can also provide evanescent field with steep gradient. The evanescent field with steep gradient may generate large gradient force for optical trapping and potential wells deep enough for cold atom

trapping and guiding (Dawkins et al., 2011; Le Kien et al., 2005; Nayak & Hakuta, 2008). When V « 2, a large portion of the optical power resides in the evanescent field outside the PMNF. The extension of the evanescent field and the fraction of power (η_{EF}) propagating in it depend on the λ/r ratio. It can be obtained from the component of the pointing vector along the direction of the beam propagation S_z $\int_{in} S_z \mathrm{d}A$ and $\int_{out} S_z \mathrm{d}A$ area over the MNF cross-sectional area (A) inside and outside the PMNF respectively.

The fractional power of the evanescent fields (propagating outside the fiber) is strongly dependent on the wavelength of the guided light or diameter of the fiber. The fractional power of the evanescent fields has indicated the possibility of significantly modifying group velocity of the guided modes, and resulting in large or manageable waveguide dispersion under single-mode operation (Lou, Tong, & Ye, 2006).

$$\eta_{EF} = \frac{\int_{out} S_z \mathrm{d}A}{\int_{in} S_z \mathrm{d}A + \int_{out} S_z \mathrm{d}A} = \frac{\int_r^{\infty} S_z \mathrm{d}A}{\int_0^r S_z \mathrm{d}A + \int_r^{\infty} S_z \mathrm{d}A} \tag{2.6}$$

Optical waveguiding in a single PMNF is implemented by an evanescent coupling method (see Figure 2.6). An evanescent coupling method has been proven to be very efficient with a high compactness (Gu, Yu, Wang, Yang, & Tong, 2010; K. Huang, Yang, & Tong, 2007). Figure 2.6 shows a fiber taper, which is drawn from a standard glass optical fiber is placed in close contact with one end of PMNF. The obvious color change in the orange light input versus green light output indicates wavelength dependent transmission. Light can be launched into the PMNF with high efficiency up to 90% due to the strong evanescent coupling between the PMNF with fiber taper (K. Huang et al., 2007). A large evanescent field is particularly important in resonators

because a significant fraction of the propagating power is needed to interact with surrounding medium.

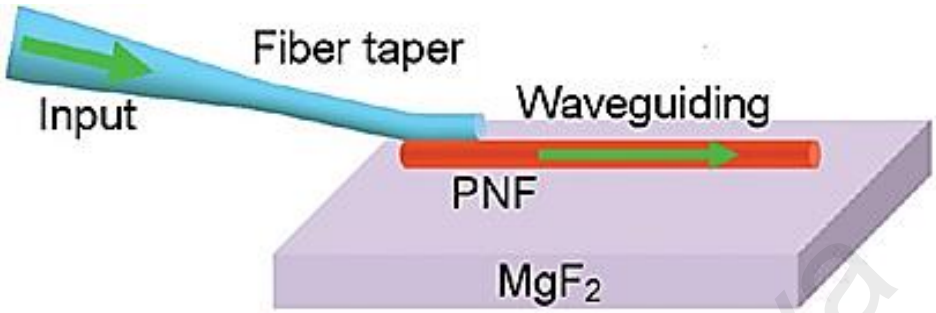

Figure 2.6: Schematic diagram of evanescent launching of PMNF using a fiber taper. (Gu et al., 2010).

2.4.3 Optical Confinement

Tight optical confinement allows optical waveguiding with small bending radius (low- loss waveguiding through sharp bends) and small mode area (Tong et al., 2005; Yu et al., 2009). These parameters in turn present advantages for developing optical circuits or devices with short optical paths, small footprints and low power consumption. Meanwhile, small mode area and field enhancement originated from the tight confinement suggests a promising approach to low-threshold or low power optical nonlinear effects (Foster et al., 2008). Also, within the close vicinity of the fiber surface, vacuum states for radiation is modified, which may significantly change the spontaneous rate of an atom nearby (Sagué et al., 2007).

2.4.4 Propagation Loss

Optical loss is of the most relevant parameters for photonics applications. For polymer PMNF, the greatest contributions to the optical loss come from material and geometric factors, including spectral absorption, diameter non-uniformity, surface non-uniformities, surface contamination, and impurities associated with the PMNF and its

surrounding medium (Kovalenko, Kurashov, & Kisil, 2008; Zhai & Tong, 2007). If the optical loss is increased, the PMNF diameter is decreasing correspondingly. This can be explained by the stronger interaction between the field intensity of the guided light and the surface of thinner PMNF. The waveguiding loss of PMNF usually is less than 0.1 dB mm^{-1} , which is acceptable in most micro-nanophotonic applications that require an effective length of less than 1mm (Gu et al., 2008; Meng et al., 2011; Wang et al., 2012).

2.4.5 Bend Loss

PMNFs have properties which allow them to be bent and manipulated. Sharp bent structures are often required to construct highly compact photonic device using PMNF (Tong et al., 2005; Yang et al., 2008). Benefiting from the tight optical confinement of the waveguiding modes in PMNF with low index surrounding, the additional bending loss remains low with a bending radius as low as several micrometers. Yu et al., (2009) reported a bending radius as small as 3μm, the bending loss of a 350 nm diameter polystyrene nanofiber at 633 nm is approximately 0.5 dB/90 ^{o}C (Yu et al., 2009), which is acceptable for photonic circuitry in most cases. The PMNF are good candidates for bent waveguides because the polymer material is a ductile material that presents high flexibility for bending. For PMNF that are connected to a single mode silica fibers and free standing in the air, they are easy to be manipulated into spatial geometries such as knot, loop, and Mach-Zehnder interferometer (MZI).

2.5 Sensing Parameters

Parameters for performing sensing on physical, chemical and biological variations can be included are sensitivity, resolution, stability, repeatability, reproducibility, operating range, and response time.

2.5.1 Sensitivity

A sensor that can detect the smallest value of the measurand is called sensitivity. The sensitivity is defined as the resolution of the sensor is divided by the responsivity of the sensor.

2.5.2 Resolution of Detection System

Resolution of the sensor is described as the smallest variable change in the detection system. The specification of the detection system has determined that the resolution is related to the precision in which the measurement is made.

2.5.3 Stability

Susceptibility of the sensor head to external effects such as temperature, vibration or electromagnetic interference (EMI) is called stability. The stability of the sensor must has an exact and accurate measurements over a long period of time.

2.5.4 Repeatability

The performance of the sample taken under same experiment conditions over different times is called repeatability. The stability and the life-time of the sensor head is depend on a good repeatability.

2.5.5 Reproducibility

The measured performance of the same sensor taken under the same experimental conditions at different times is called reproducibility. The mass production of sensor heads with the same specifications is an example a good reproducibility.

2.5.6 Operating Range

A range of value of the parameter under testing or investigation or examination by the sensor is defined as operating range.

2.5.7 Compactness

The most important consideration for a sensor is compactness. The compactness of the sensor enable easier deployment and minimizes intrusion in the measurement environment which allow remote interrogation, the size and weight of the detection system

2.6 Sensors Overview

The research on optical PMNFs have been attracting more attentions due to the great potential and curiosity of guiding light on a lower dimension. This section summarized PMNF based sensors reported to date for the measurement of the humidity, temperature, refractive index and bio-chemical. To integrate as drawn PMNF into miniaturized devices or circuits, micromanipulation techniques are desired for tailoring and assembling these tiny building blocks into functional structures or geometries (Tong et al., 2005; Yang et al., 2008). Using controlled tapered fiber probes with tip size a few of micro-nanometers, PMNF can be cut, picked up, transferred, bent and shaped under an optical microscope. PMNF can be firmly held in position by Van der Waals force and electrostatic interactions between the PMNF and the substrate (Wang, et al., 2013).

Typical structures of optical PMNF sensors illustrated in figure 2.7. Figure 2.7(a) shows the simplest straight PMNF and employ intensity dependent scheme. The straight PMNF is common configuration that exploits the strong evanescent field of the guided modes to interact with its surrounding medium.

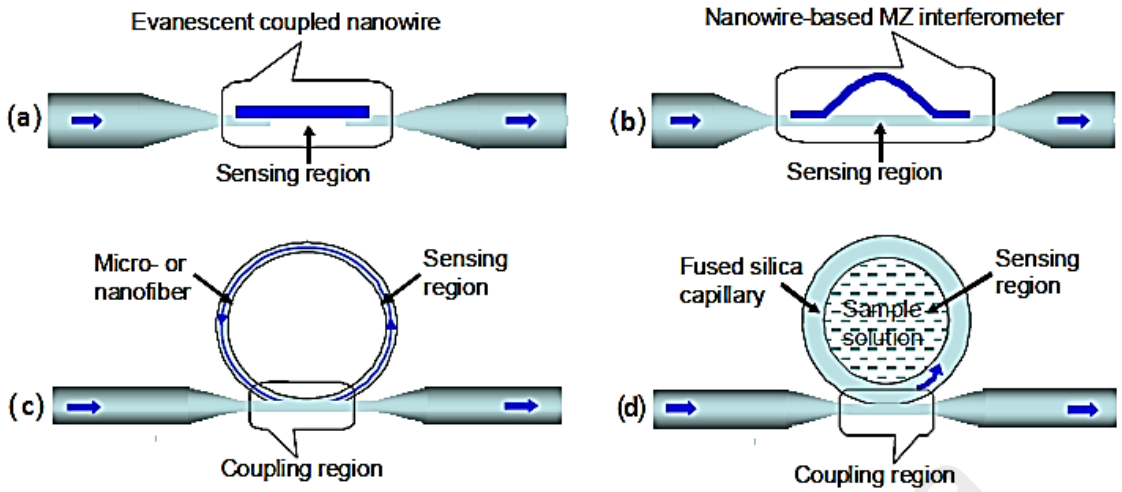

Figure 2.7: Illustration of typical structures of PMNF sensors: (a) Straight PMNF sensor, (b) PMNF MZI sensor, (c) PMNF loop/knot/coil resonator sensor, (d) PMNF liquid-core optical ring-resonator sensor (Zhang et al., 2011).

Figure 2.7 (b) shows a sensing structure relying on PMNF MZI where that features high responsivity to the phase difference between the sensing and the reference arms. The abrupt PMNF section can be exploited for modal interferometry in the configuration of either MZI. Figure 2.7 (c) shows optical sensors based on PMNF loop/knot/coil resonators that are assembled by micromanipulation. Figure 2.7 (d) shows a liquid-core optical ring resonator sensor using PMNF for input and output connection. Since high fractional guiding mode of PMNF propagates outside the fiber, transmission intensity of PMNF depends on the properties of ambient medium, which has been applied for chemical/biological sensing, humidity, and refractive index (RI). Sometimes, the surface of PMNF can be coated with reagents wider sensing applications.

2.6.1 Relative Humidity (RH) Sensor

Relative humidity sensors typically operate on RI changes in its external coating in response to variations in ambient humidity. The stability of the composite fiber structure varies depending on the coating material or doping material. Externally induced effect such as thermal expansion can cause shear stress to build-up along the

fiber coating interface, which will ultimately result in delamination above a certain threshold. A highly versatile nanosensors using polymer nanofibers has been reported (Gu et al., 2008). A polyacrylamide (PAM) nanowire drawn from a PAM aqueous solution was employed for RH sensing based on RH dependent evanescent power leakage. Wang et al. demonstrated PAM microwires to construct a microring as shown in figure 2.8. Self-coupling was achieved evanescently at the overlap region. The tapers were also firmly bonded on the substrate by low-RI UV fluoropolymer. By measuring the resonance dip shift, the sensor showed fast response time of 120 ms and a high sensitivity of 490 pm/%RH (Wang et al., 2011). The remarkably fast response of the sensor can be attributed to small diameter and large surface to volume ratio of the nanowire that enable rapid diffusion or evaporation of water molecules, as well as fast signal retrieval using optical approach. Batumalay et al. demonstrated agarose gel as alternative humidity sensitive material. A mixture of agarose powder dissolved in water was heated and then deposited on a PMMA with diameter 0.45 mm and tapering length of 10 mm. As the RH varies from 50 % to 80 % the sensitivity of the sensor is 0.0228 mV/%, 0.0103 mV/% and 0.0079 mV/% with agarose gel 0.5%, 1% and 1.5% weight content, respectively (Batumalay et al., 2014). Agarose gel is hydrophilic material which has a high porosity that allows the gel to absorb moisture and perform as a humidity sensor. The agarose gel used is based on swelling nature of hydrophilic materials which causes refractive index changes in accordance with humidity and modulates the light propagating through the fiber. As the concentration of agarose increases, the porosity of the agarose gel decreases correspondingly. (Stellan & Yao, 1981). Batumalay et al. proposed a PMMA fiber with diameter 0.45 mm and length of 10 mm coated with zinc oxide (ZnO) nanostructure using sol-gel immersion for RH measurement. The sensor provides better sensitivity at 0.0258 mV/% with limit of detection (LOD) 0.143%. The ZnO composites are exposed to an environment of

humidity causes rapid surface absorption of water molecules. The optical properties of ZnO composite surfaces are modulated by the surface absorption of water molecules. The increase of water molecules being absorbed by ZnO composite results in an increase of relative humidity (Batumalay et al., 2014; Batumalay et al., 2015; Harith et al., 2015; Liu et al., 2012).

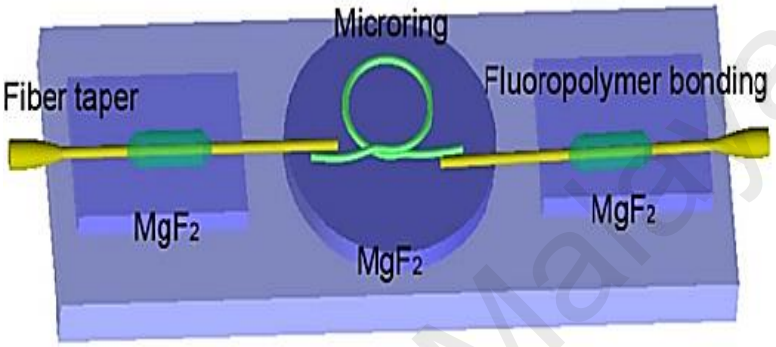

Figure 2.8: Schematic illustration of a PAM microring for RH sensing (Wang et al., 2011)

2.6.2 Refractive Index (RI) Sensor

Refractive index (RI) sensor is one of the basic physical properties in optical sensing. RI sensor most commonly used to measure the concentration of the solute in an aqueous solution and it is very important for chemical and biological sensing. According to the sensor structure, RI sensor can be classifies into the straight PMNF RI sensor (De-Jun, Mao-Sen, Liu, Xi-Lu, & Dong-Fang, 2014), looped/knot PMNF RI sensor (Huaqing Yu et al., 2014), whispering gallery mode (WGM) (Duong Ta et al., 2013) Mach–Zehnder interferometer (MZI) based PMNF RI sensor (Wo et al., 2012), twist PMNF RI sensor (Zhu et al., 2009), coupled polymer microfiber (Ta, Chen, & Sun, 2014). Zhu et al., (2009) demonstrated tunable refractive index sensor with ultracompact structure in a 2 x 2 poly(trimethylene terephthalate) (PTT) nanofiber coupling splitter assembled by twisting two fiber PTT. The highest measured

sensitivity of the sensor is 26.96 mW/RIU (refractive index unit) and the maximum limit detection on refractive index change is 1.85×10^{-7}.

2.6.3 Temperature Sensor

Temperature monitoring is vital for many applications in harsh environments, such as the oil and gas industries, power generation, or engine turbines. Because of their immunity to electromagnetic interference and possibility to work in contact with explosives, the use of optical fibers for temperature monitoring has been widely investigated (Grobnic et al., 2004; Kou et al., 2010). Wu et al. (2011) reported two fiber optic sensors based on silica/polymer microfiber knot resonators (SMKR/PMKR) (Wu et al., 2011). These sensors were composed of three layers: MgF_2 slab to keep it steady and immunity to environment fluctuations. Temperature sensitivity of SMKR was about 52 pm/°C within 30°C around 700°C, while the sensitivity of PMKR is about 266 pm/°C within 20°C around 80°C. Temporal response of SMKR and PMKR sensors were less than 1 ms and 5 ms, respectively. Zeng et al. (2009) demonstrated a compact temperature sensor based on MNF knot resonator that was placed on a plate glass substrate and coated with low index polymer to keep the system robust (Zeng et al., 2009). Sensitivities of this kind of temperature sensor of 0.27 nm/°C in heating process (when temperature ranged from 28°C to 140°C) and -0.28/°C in cooling process (when temperature ranged from 135°C to 25°C) were obtained. Temperature resolution of 0.5°C was demonstrated and higher resolution was predicted with a high-resolution spectrometer.

2.7 Polymer Microfiber Functionalized Structures

To enhance the responsivity to certain measurands, the surface of the PMNF can be functionalized to respond to specific chemical or biological species (Dıez, Andres, & Cruz, 2001). Doping in chemical indicators is another approach to activate the polymer

micro/nanofiber for optical sensing. In this section, polymer microfiber functionalized structures are explained in detail in following subsection.

2.7.1 Quantum Dots

Quantum dots (QD) in the form of semiconductor nanocrystals has shown fascinating optical and electric properties including the quantum confinement effect, broad absorption profiles, high optical gain and photochemical stability. The QD has found wide applications in areas such as photon sources, optical amplifications, sensing and fluorescent labeling (Medintz et al., 2005). To date, a variety of QD have been successfully incorporated into PMNF (Di Benedetto et al., 2011; Meng et al., 2011; Tatavarty et al., 2011). It is found that the QD is well dispersed into the PMNF without obvious aggregation. This effect thus avoiding the Förster resonance energy transfer between neighboring QD and preserving the fluorescence properties of the single QD. The well-dispersed QD dopants do not scatter waveguided light in the micro-nanofiber due to the small size of QD. This making the QD functionalized PMNF excellent active micro-nanowaveguides. Photobleaching is one of the most important issues for practical applications in functionalized PMNFs with active dopants. Compare to dye-doped PMNF (Q. Song, Liu, & Xu, 2009), QD doped shows a much higher resistance to photobleaching, which are offer great advantage for long term and high stability applications (Bruchez et al., 1998; Chan & Nie, 1998). The QD are highly sensitive to various chemical species and become promising sensor for variety analytes by optical means. It is because of their high surface to volume ratios and surface chemistry dependent photoluminescent properties. QD nanofiber optical sensor for RH detection with a low optical power (100 pW level) and fast response has been reported by Meng et al (Meng et al., 2011). This polymer matrix without aggregation has attributed to the fast evaporation rate of solvents during the PMNF drawing process. Figure 2.9 shows scanning electron microscopy (SEM) image of a 480-nm diameter QD PMNF with

uniform diameter and smooth sidewall, which favourable for low-loss optical waveguiding.

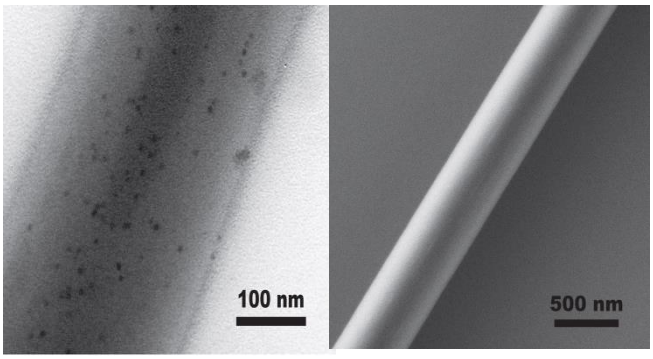

Figure 2.9: Electron microscope characterization of QD PMNF ; TEM image of a 280 nm diameter QD PMNF and SEM image of a 480nm diameter QD PMNF(Meng et al., 2011).

CHAPTER 3

FABRICATION AND CHARACTERISATION OF POLYMER MICROFIBER

3.1 Introduction

Optical microfibers have gained tremendous interest in recent years as promising components for subwavelength waveguiding and nanophotonics devices(Jiang et al., 2007; K. S. Lim et al., 2011; Sulaiman, Harun, Ahmad, Norizan, & Ahmad, 2012). This is due to a number of interesting optical properties of these devices, which can be used to develop low-cost, miniaturized and all-fiber based optical devices for various applications. For instance, they have been attracting considerable attention in physical, chemical, and biological sensors due to their unique geometry with low dimension and large surface-to-volume ratio and their versatility for electrical and optical detection. Furthermore, the higher portion of the evanescent field is travelling inside the cladding in the microfiber and thus the travelling wave characteristics becoming more sensitive to the physical ambience of its surrounding (Corres, Arregui, & Matias, 2006; Lim et al., 2011; Zibaii et al., 2010). In the previous works, silica microfiber has been used for various applications (John et al., 2015). Compared with the silica and glass counterparts, polymer optical microfibers may also play a key role in several rapidly developing areas of broadband communications because of their lightweight, chemical specificities, low cost, mechanical flexibility, tunable properties, easier processibility, and integration (Guo, Shi, & Li, 2008). Polymer microfibers, inherited from the perm-selective nature and biocompatibility of polymer materials, also offer a number of highly attractive advantages for sensing applications. For example, gas molecules to be detected can be

either selectively bound to their surface or diffused into the polymer matrix, which may be difficult for other materials such as semiconductor nanowires or glass microfibers.

To date, polymer-based microfibers or nanowires have been achieved by various techniques such as chemical synthesis (Cui et al., 2006), nano-lithography (Noy et al., 2002), electro-spinning (Li & Xia, 2004) and mechanical drawing (Nain et al., 2006). Chemical synthesis and nano-lithography are quite complicated and requires expensive facilities. Electro-spinning is only for microfiber mat fabrication but not for a single microfiber structure. The simplest and cheapest technique is based on mechanical drawing where the microfiber is normally drawn from solvated liquid polymer. In this technique, the main concerns are on the nature of solvent and concentration of polymers. Typical polymer's solvent are volatile organic compound which poses serious health risk to frontline worker.

In this chapter, we demonstrate a various optical sensors using a Polymethyl methacrylate (PMMA) polymer based microfiber as a probe. An eco-friendly and simple drawing method is used to fabricate the polymer microfibers. PMMA polymer is used in this work as it has many interesting properties such as high transmittivity for visible light and refractive index of 1.49, which provides a good optical confinement. In a rubber like state, PMMA poses a weak restoring force and will deform significantly under stress (Nain et al., 2006) and thus microfiber can be easily fabricated by the proposed direct drawing technique. The propagation loss of the microfiber is also investigated for different waist diameters. The fabricated PMMA microfiber is then used for the detection of various concentrations of potassium permanganate ($KMnO_4$) solution and detection of honey adulteration. An uric acid sensor is also demonstrated using a PMMA microfiber coated with an Al doped ZnO nanostructure as a probe. The PMMA microfiber is coated with Al-doped ZnO nanostructure using a sol-gel process.

3.2 Fabrication of PMMA microfiber

Using direct drawing technique, polymer microfiber with diameters down to 1.5 microns and lengths up to 3 mm were fabricated by one-step process as described in Figure 3.1. PMMA is selected as the polymer wave-guiding material in the experiment because of its high mechanical strength, good dimensional stability, good weather resistance, and natural transparent above deep ultraviolet. We use a heating plate to melt PMMA and keep the temperature constant during the fiber drawing process. For the polymer to maintain a desirable viscosity level, the temperature of the heating plate should be controlled within the temperature range between the glass transition temperature and the melting temperature of polymer and should be kept constant. As the glass transition temperature (T_g) of PMMA ranges from 85 to 165 °C, the heating plate temperature was kept at round 115°C during the fiber drawing. First, a tapered silica fiber with a diameter of about 125 μm is being used and its tip is immersed into the molten PMMA. Then the fiber tip is retracted from the molten polymer with a speed of 0.1−1 m/s, leaving a PMMA microfiber extending between the molten PMMA and the tip. The extended PMMA microfiber is quickly quenched in air and finally, a bare PMMA microfiber is formed. The microfiber diameter can be controlled by the pulling speed and viscosity of the polymer (which depends on the hot plate temperature). Microfibers produced by this technique are uniform in diameter over a long length with good flexibility.

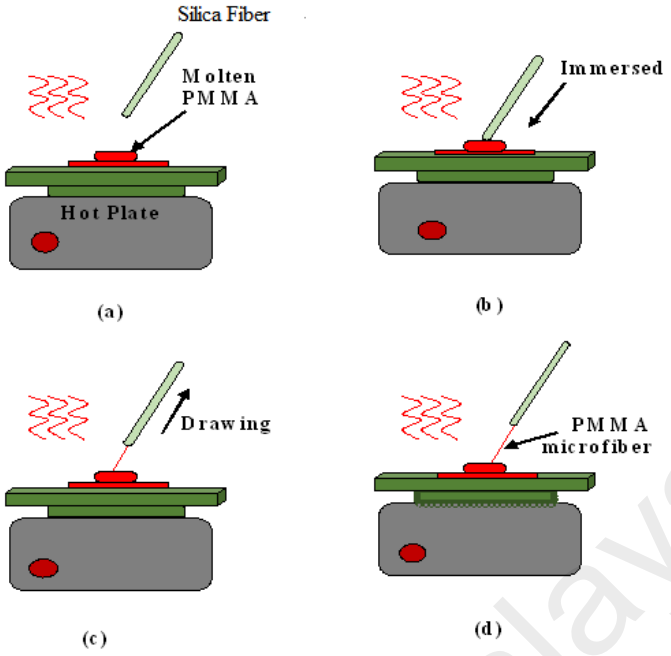

Figure 3.1: Schematic illustration of the polymer microfiber fabrication by direct drawing method from molten PMMA. (a) A cylindrical silica fiber is approaching the molten PMMA (b) The fiber tip is immersed into the molten PMMA (c) The fiber conglutinated PMMA is being drawn out. (d) A PMMA microfiber is formed.

We found that PMMA microfibers were easier to be fabricated when the viscosity of the PMMA is optimum. The attainable diameter of the microfiber reduces as the viscosity of the PMMA increases. Figure 3.2 shows the microscope image of the fabricated PMMA microfiber. As shown Figure 3.2(a), the microfiber can be easily formed between the molten PMMA and the fiber tip using the proposed direct drawing technique. During the drawing process, a He-Ne 632 nm laser is launched into the microfiber for easier monitoring. As the microfiber surface is relatively smooth, the leakage of light (Figure 3.2(b)) is probably due to dust, bending and transition region rather than surface roughness. The fabricated microfibers can be easily bent and curled, offering a wide range of optical sensors applications. It exhibits high uniformity, smooth surface and can be drawn up to the length of 500 mm long.

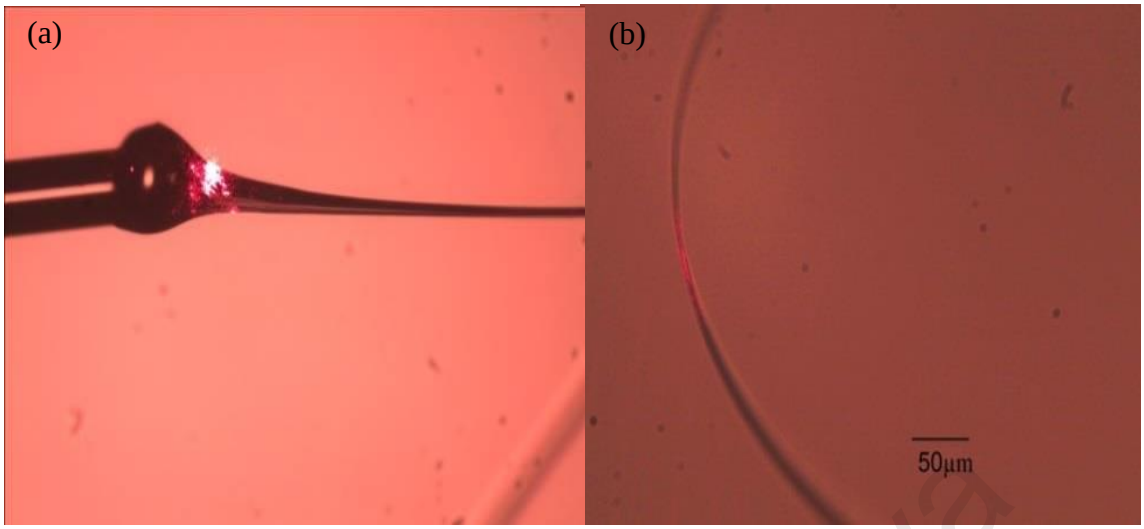

Figure 3.2: Microscope image of the fabricated PMMA microfiber. (a) PMMA microfiber is formed between the molten PMMA and the fiber tip (b) the middle part of the PMMA microfiber as a 632 nm laser is launched into the microfiber.

3.3 Loss Characteristic of the PMMA Microfiber

Figure 3.3 shows the fabricated microfibers with different waist diameter, which were obtained by varying the temperature of the heating plate and the speed of drawing. The excellent diameter uniformity and sidewall smoothness make the microfiber suitable for low-loss optical waveguiding and sensing. PMMA microfibers with diameters ranged from 6 to 12 μm and lengths up to few centimeters have been drawn by this method. The transmission loss of the fabricated microfiber is investigated for three different diameters; 6, 8 and 12 μm. Optical waveguiding in a single PMMA microfiber is implemented by an evanescent coupling method as shown in Figure 3.4. As shown Figure 3.4, a silica microfiber with a diameter of about 4 μm, which was fabricated by using the flame brushing technique is fixed at a fiber holder at two ends of the PMMA microfiber. The PMMA microfiber is then placed in parallel and close contact with these silica microfibers. Due to the strong evanescent coupling between the PMMA microfiber and the silica microfiber, light can be efficiently launched into and picked up from the PMMA microfiber within a few micrometers' overlap. The

transmitted light power against the PMMA microfiber length is investigated for all PMMA samples. The result is shown in Figure 3.5.

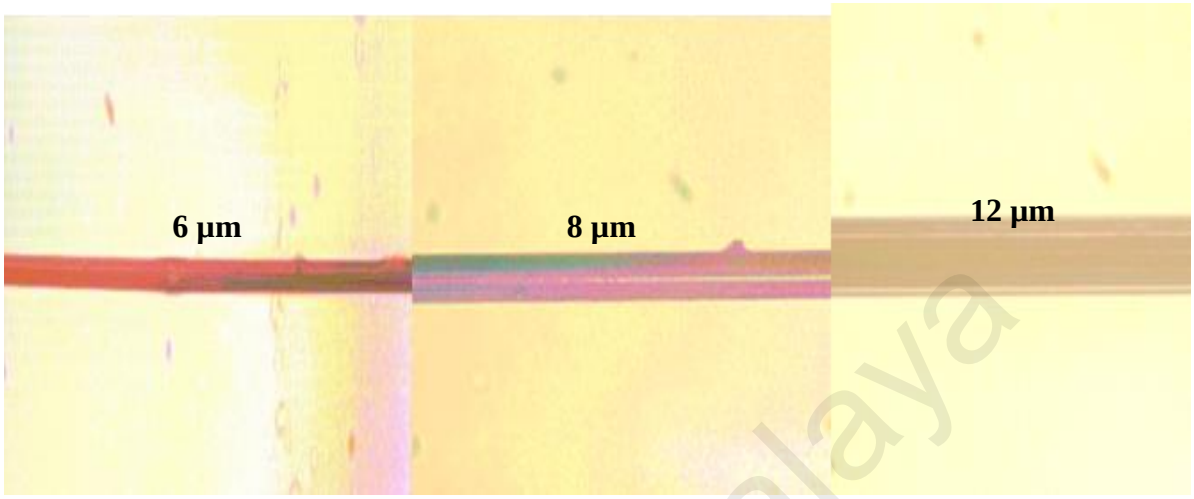

Figure 3.3: PMMA microfibers with three different waist diameter

Figure 3.4: Schematic diagram of an optical waveguiding in a single PMMA microfiber with two ends coupled with silica microfibers.

As shown in Figure 3.5, the transmitted power reduces linearly with the increase of the microfiber length. The microfiber loss is obtained at 0.37 dB/mm, 0.27 dB/mm and 0.19 dB/mm for the microfiber diameters of 6 µm, 8 µm and 12 µm, respectively. This shows that the microfiber loss increases with the reduction of its diameter. This is due to the amount of light travelling inside the cladding, which increases for smaller diameters. Some portion of the light leaks out the fiber as loss.

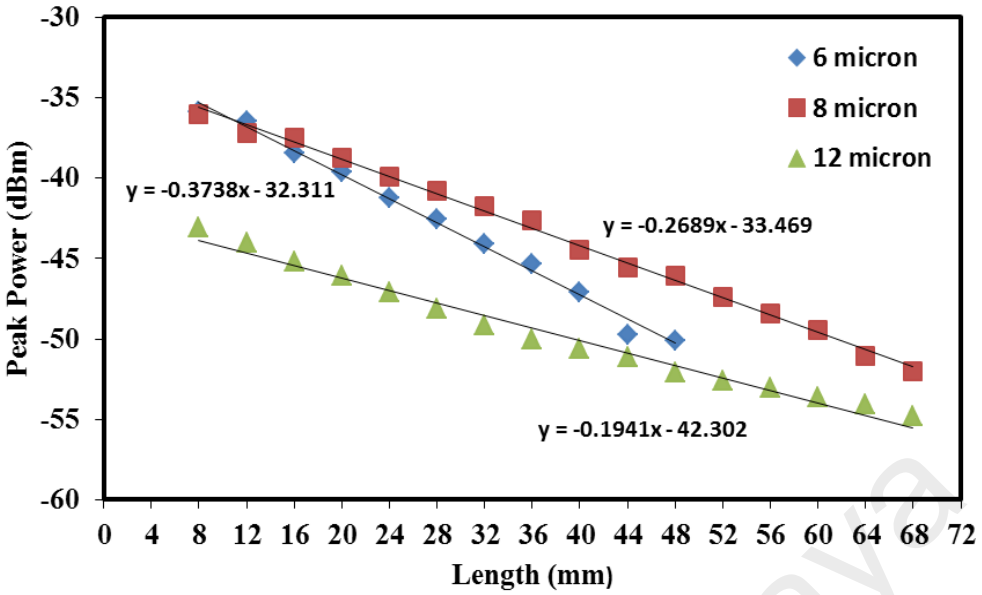

Figure 3.5: The transmitted output power from the PMMA microfiber against its length.

3.4 PMMA Microfiber for Potassium Permanganate (KMnO4) Sensing

Potassium Permanganate ($KMnO_4$), also known as permanganate of potash or Condy's crystals, is an inorganic chemical compound consisting of two ions which is a potassium ion and a permanganate ion. Potassium permanganate is one of the important chemical formulas because of its vast uses in various fields such as water treatment and disinfection, organic chemistry, analytical chemistry, and even in survival situations. Potassium permanganate also treats many skin infections, including eczema, canker sores, dermatitis, acne, and fungal infections of the hands or feet. The detection of the potassium permanganate solution is very important especially in the health, medical and clinical applications as high concentrations of potassium permanganate can become toxic and hence can harm the human body.

In the previous work, the $KMnO_4$ has been detected by using a newly synthesized squaraine dye in PVC matrix (Ertekin, Tepe, Yenigül, Akkaya, & Henden, 2002). The method that was introduced is very complicated in terms of the preparation of the cocktail protocols by using optode membranes and also the acquisition of the

spectra by preparing thin films. In this section, the developed PMMA microfiber is proposed for $KMnO_4$ detection. The PMMA is used due to its many advantageous properties such as having good flexibility and low melting temperature which eases the fabrication process. The performance of the PMMA microfiber in sensing the $KMnO_4$ concentrations was evaluated in terms of its linearity and sensitivity.

The schematic illustration setup used to detect the potassium using the fabricated PMMA microfiber is shown in Figure 3.6. A 1550 nm ASE light source was injected into the one end of the fiber, and travels to the other end to the OSA and the power meter via 3dB coupler. These two pieces of equipment were used to analyze the spectrum of the wavelength and the output power of the sensor, respectively. Throughout the experiment, the sensor probe was immersed into the potassium permanganate solutions with varied concentrations from 1% to 6%. The PMMA microfiber has a diameter of 12 μm.

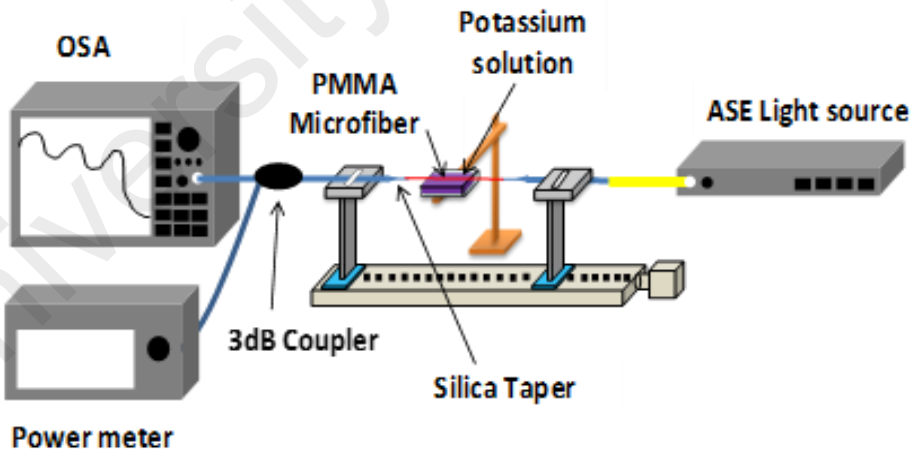

Figure 3.6: Schematic illustration of the employment of PMMA microfiber for $KMnO_4$ concentration measurements

Figure 3.7(a) shows the output power against various concentrations of $KMnO_4$ for the proposed sensor. It is observed that the output power reduces from 250μW to 80μW as the $KMnO_4$ concentration is increased from 1% to 6% for the silica and PMMA microfiber, respectively. Figure 3.7(b) shows the refractive index of the $KMnO_4$ (as measured by using METTLER Toledo RE40D refractometer) against the $KMnO_4$ concentration. As the concentration $KMnO_4$ increases from 1% to 6% , the refractive index of the solution also increases from 1.3330 to 1.3483. A digital refractometer can measure the refractive index within a short time with high precision. As shown in the figure, the output power from the power meter, which corresponds to the transmitted light intensity, linearly decreases with the concentration of the $KMnO_4$ solution.

The sensitivity of the microfiber sensor is obtained at 32.57μW/% with a slope linearity of more than 91.61% and a resolution of 0.0064%. The standard deviation for the PMMA microfiber sensor is calculated to be 0.656. Since the cladding area of the sensor was in the micrometer range, the surrounding medium works as a passive cladding and its refractive index can influence the amount of power loss as the signal propagates through the microfiber region (Figure 3.8). The evanescent field penetration of guided modes will increase with the reduction of the fiber size (Beres, de Nazaré, de Souza, Miguel, & Werneck, 2011; Wu & Tong, 2013). When immersing the microfiber sensor into the $KMnO_4$ solution with various concentrations ranging from 1% to 6%, the refractive index of the surrounding medium increases since the refractive index of $KMnO_4$ is larger than water (1.333). The reduction of the output power is due to the reduction of the core and cladding index contrast, since the refractive index of the microfiber sensor increases as the concentration of $KMnO_4$ increases. Therefore, it will reduce the light guiding capability of the structure and thus allows more photons to escape from the microfiber. The sensitivity of the fiber is influenced by the interaction

length, bending effect, and electrostatic interaction between different concentrations of the $KMnO_4$ solution and the fiber.

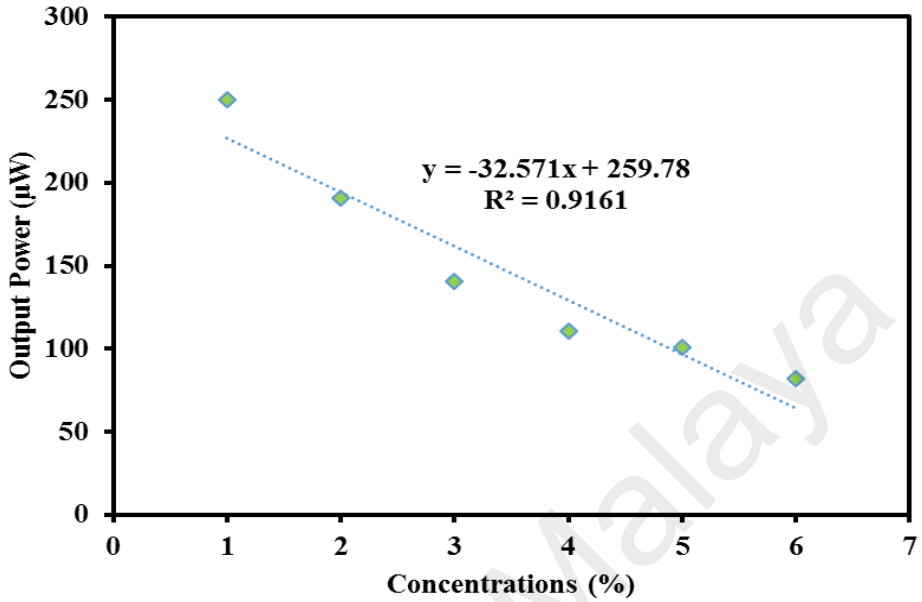

(a)

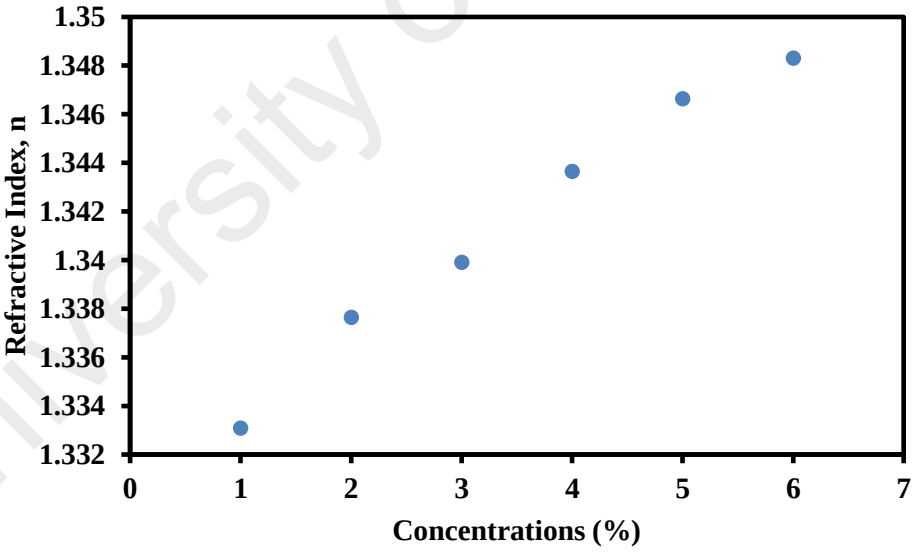

(b)

Figure 3.7: (a) Output power and (b) refractive index against $KMnO_4$ solution concentration for the PMMA microfiber sensor.

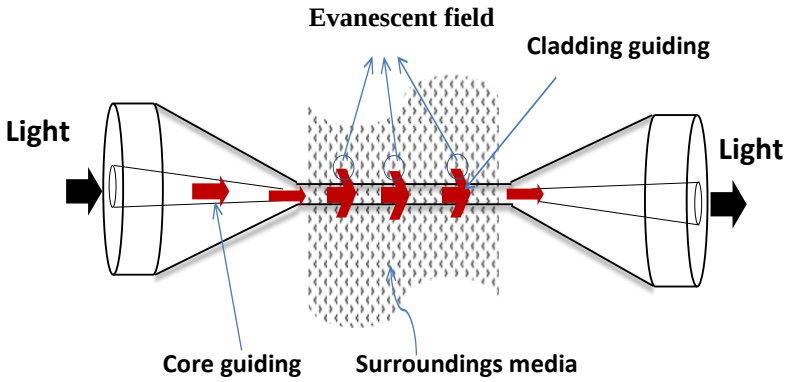

Figure 3.8: Schematic diagram of the propagation of light inside the microfiber

Figure 3.9 shows the output spectra recorded by using the OSA for 1 %, 5 % and 6% concentrations of the $KMnO_4$. Referring to the peak power of the spectra, it is easy to determine the 21.23 dB excess loss that the PMMA microfiber had suffered after being immersed in the $KMnO_4$ solutions of concentration 1% to 6%. The drop in the output power is possibly due to the change in the index contrast and the disturbance on the structure of the microfiber sensor when the $KMnO_4$ solutions were introduced. Figure. 3.10 shows the wavelength against the $KMnO_4$ solution for the proposed PMMA microfiber sensor. By referring to the figure the wavelength decreases as the concentration of the $KMnO_4$ increases. For the 1% concentration, the refractive index is 1.33309 at the wavelength of 1558 nm. The resonant peak shifts to a shorter wavelength as the index of the solution increases when the concentration of $KMnO_4$ solution is increased. The temperature was kept almost constant around 25°C during the measurement.

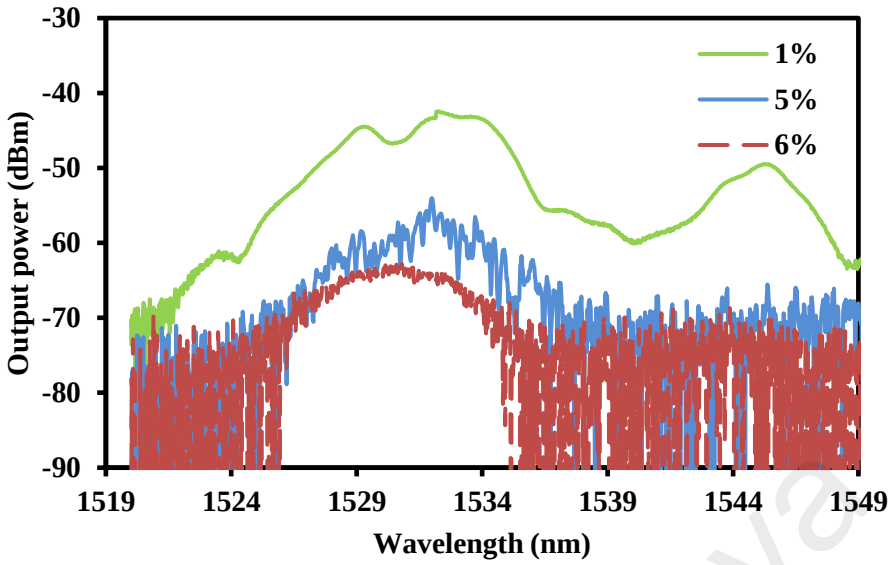

Figure 3.9: Transmission spectrum of the PMMA microfiber.

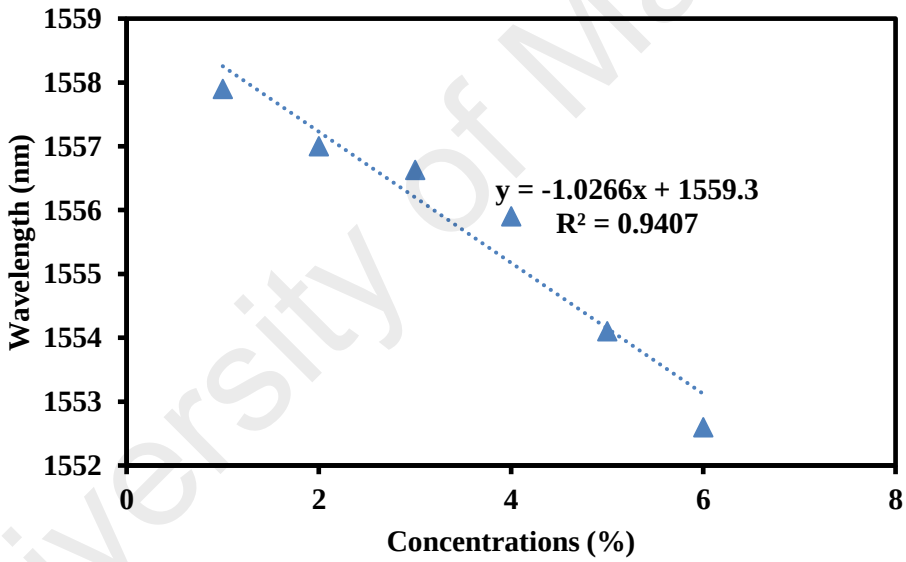

Figure 3.10: Resonance wavelength against $KMnO_4$ solution for the PMMA microfiber sensor. The resonant peak shifts to shorter wavelengths as the index of the $KMnO_4$ solution increases when the concentration of the $KMnO_4$ solution is increased.

The performance of the proposed $KMnO_4$ detection sensor is summarized in Table 3.1. Overall, the sensor is observed to be sufficiently stable with standard deviations of 0.211 μW. Lastly, the stability was obtained by measuring the output power for every 10 seconds for a total period of 10 minutes. Figure. 3.11 depicts the graph between the output power against time for the PMMA microfiber sensor. The results show that the output power obtained is stable.

Table 3.1: Performance of the $KMnO_4$ detection sensor

Parameters	Performance
Resolution (%)	0.0064
Standard Deviation (µW)	0.211
Linearity	More than 91%
Sensitivity (µW/%)	32.57
Linear Range (%)	1%-6%

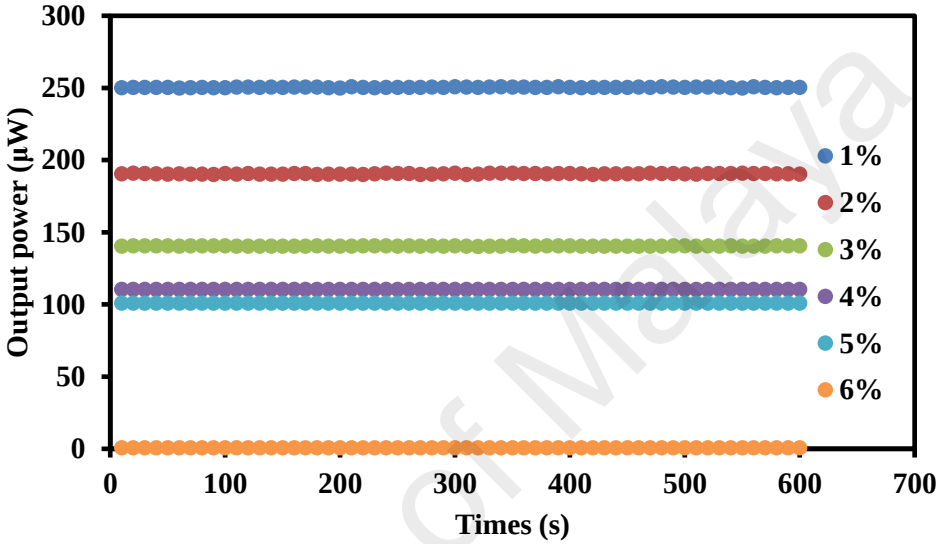

Figure 3.11: Stability of the PMMA microfiber for $KMnO_4$ detection.

3.5 PMMA Optical Microfiber Sensing of Adulterated Honey

Consumption of the honey product grew considerably during the last few decades. Adulteration of pure honey with synthetic honey has become much more prevalent in recent years. All food products targeted for adulteration are high-value commercial products, including honey. The quality of honey is mainly determined by its sensorial, chemical, physical and microbiological characteristic (Pilizota & Tiban, 2009). The preparation of an overall review of the applied procedures by researchers in detecting honey adulteration would be useful and serve as a good source in oncoming works (Mehryar & Esmaiili, 2011). The importance of honey adulteration detection has recently increased owing to the limited production levels in recent years and the relative

high price of honey; therefore, this illegal practice has become more and more attractive to producers. Hence, the need has arisen for more effective analytical methods aiming at detecting honey adulteration (Bertelli et al., 2010).

Recently, many optical sensors have been proposed and demonstrated for honey adulteration measurement. For instance, Sivakesava et al. proposed a combination of fourier transform infrared spectroscopy with multivariate procedures was used for determining the level of sugar addition to honey (Sivakesava & Irudayaraj, 2001). Bertelli et al. proposed the technique of one dimensional and two dimensional high resolution nuclear magnetic resonance to detect adulterated honey (Bertelli et al., 2010). Hida et al. demonstrated honey purity detection in distilled water based on intensity modulated fiber optic displacement sensor (Hida, Bidin, Abdullah, & Yasin, 2013). Bidin et al. (Bidin et al., 2016) demonstrated a similar honey adulteration based on a transmission technique of the fiber optic displacement sensor. The advantage of this scheme is that the sensing element can be fabricated using inexpensive components.

As previously discussed, microfiber offers many unique characteristics such as strong evanescent field in which a fraction of the transmitted power propagates outside the microfiber and that leads to its use in sensing application. Optical microfibers have emerged as a novel platform for exploring fiber optic technology in the micro or nanoscale. Based on optical fiber microfibers, a variety of physical, chemical or biological optical sensors have been demonstrated so far (Brambilla, 2010; Brambilla et al., 2009; Kou et al., 2012; Tong & Sumetsky, 2011; Tong et al., 2012). The present research is an effective method to detect adulteration in honey by using the newly developed PMMA microfiber.

In this section, microfiber based sensor is proposed and demonstrated for the measurement of different concentrations of added glucose in the honey sample which were varied from 1 % to 6 %. This particular range of glucose concentration was chosen

in order to observe the capability of the sensor to detect small changes of adulteration in honey samples. The microfiber area was immersed in adulterated honey solution and the performance of the sensor was investigated in terms of its linearity and sensitivity.

Figure 3.12 shows the experimental setup for the detection of adulterated honey solutions using a microfiber. A 1550 nm ASE light source was injected into the microfiber and transmitted to the optical spectrum analyzer (OSA) and the output power meter via a 3dB coupler. The OSA was used to display the output spectrum and the power meter was used to obtain the value of the output power. Both microfibers were immersed in the adulterated honey solutions with concentrations of 1%, 2%, 3%, 4%, 5% and 6%.

In this work, the honey samples were obtained from the faculty of pharmacy, UiTM Puncak Alam. Pure Acacia honey samples were used as a standard for non-adulterated honey. Honey gets its sweetness from the monosaccharides glucose and fructose that compose the honey. The composition of honey depends on the type of flower forged by the bees. Here, the adulterated honey was realized by the addition of glucose solution. A 50 ml of honey sample was measured by using six different beakers. The glucose solution was prepared by weighing the glucose powder and diluted with distilled water. Initially, a 25% glucose solution was prepared and then added individually into the six different beakers of non-adulterated honey with various volumes of glucose solutions ranging from 1% to 6%. The mixture was stirred for 15 minutes to homogenize the mixed solutions. The sugar content was measured using an in-house method based on AOAC 962.14 (HPLC) as listed in Table 3.2.

Table 3.2: Sugar contents in adulterated honey

Adulterated honey concentration	Total Sugar Glucose
1%	45.3
2%	45.5
3%	45.6
4%	45.8
5%	46.1
6%	46.4

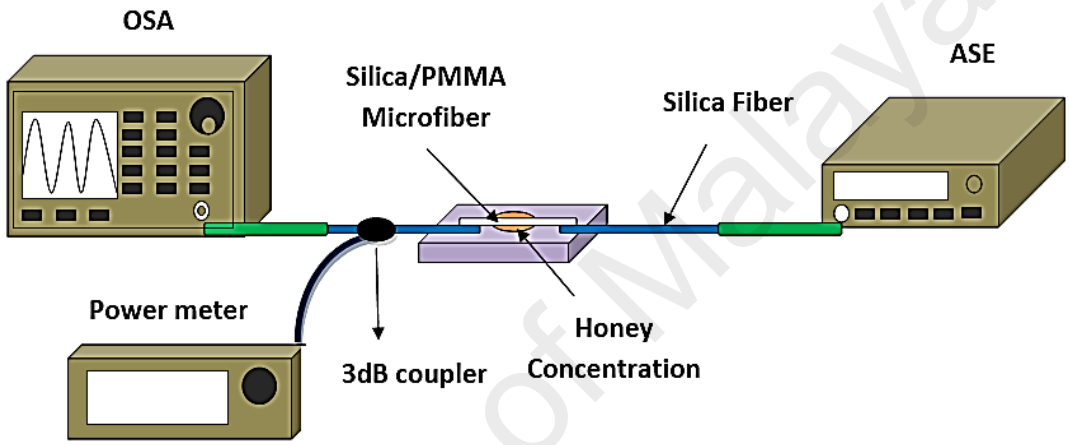

Figure 3.12. Experimental setup for the detection of adulterated honey solution using microfibers.

Figure 3.13 shows the refractive index of the adulterated honey solution (as measured by using METTLER Toledo RE0D refractometer) against the adulterated honey concentration. As the concentration of honey adulterated increases from 1% to 6%, the refractive index of the solution also increases from 1.4776 to 1.4832.

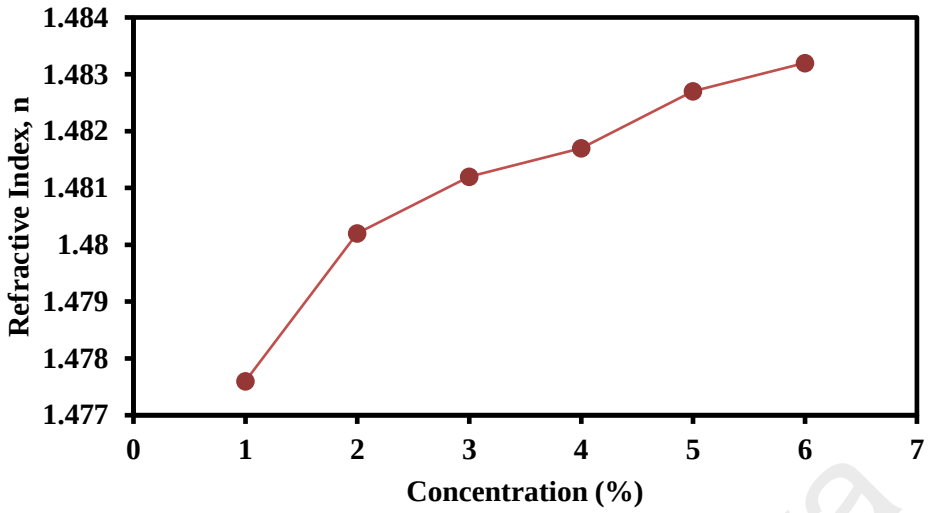

Figure. 3.13. The refractive index of the adulterated honey solution

Figure 3.14 shows the output spectra of the microfiber based sensor when the sensor probe is exposed to air and when it is immersed in the adulterated honey solution (6%). It can be seen that there is an interferometer pattern especially when the probe is exposed to air with a refractive index of 1.0. When the ASE light is injected into the honey solution, the reflection occurs on both sides of the coupling region mainly from the nonadiabatic structure of the transition region. The Fresnel reflection, which is caused by the high contrast between the refractive index of PMMA and silica or air also contribute for the reflection in the cavity. The reflection causes light to oscillate and interfere inside the microfiber. The interference produces an optical comb due to the phase difference as two beams propagate with two different path length. However, the extinction ratio of the interference comb is significantly reduced as the probe is immersed in the adulterated honey solution as shown in Figure 3.14.

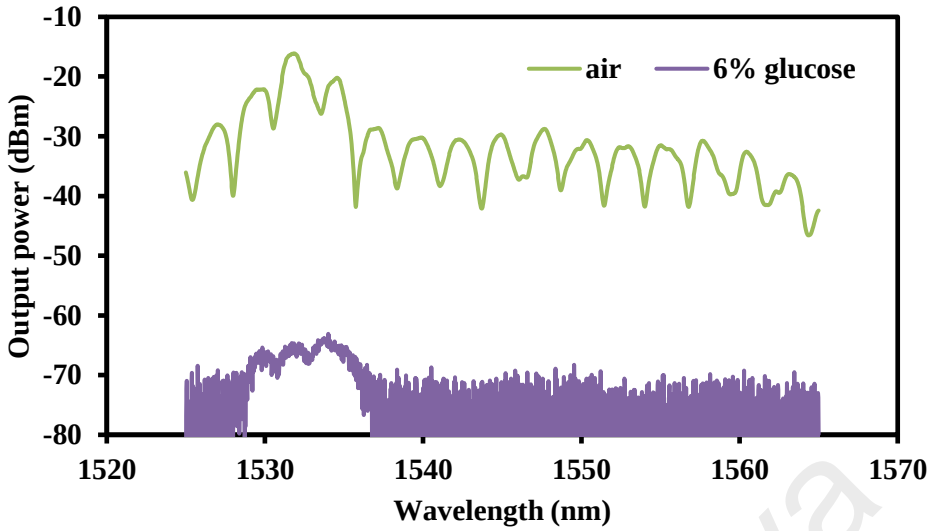

Figure 3.14: Output spectra for the immersion of microfiber in the air and adulterated honey solution.

Figure 3.15 (a) shows the transmitted light intensity from the PMMA microfiber based sensor with an increase in the adulterated honey concentration. It is observed that the light power linearly reduces from 3.51 µW to 1.15 µ as the adulterant is increased from 1% to 6%. The sensitivity and resolution are obtained at 0.49 µW and 0.03% respectively, with a standard deviation of 0.015 µW. The repeatability of a sensor is another important factor in the operation of any sensor system. The output power for each adulterated solution was measured three times to obtain the average value. Figure 3.15 (b) depicts the repeatability of the results by using error bars. The performance of the PMMA microfiber based adulterated honey sensor is summarized in Table 3.3. The resolution of the sensor was obtained by dividing the standard deviation of the readings with the sensitivity of the sensor. The sensitivity of the sensor is obtained from the slope of the output response graph (Figure 3.15 (a)). Hence, a smaller resolution signifies a better performance of the sensor. The resolution of the sensor can be improved by decreasing the value of the standard deviation or increasing the sensitivity of the sensor. The small diameter and high index contrast between the fiber core and its surrounding of an optical microfiber enables it to exhibit interesting waveguiding properties, including tight optical

confinement, large evanescent fields and waveguide dispersion (Brambilla, 2010; Brambilla et al., 2009; Tong et al., 2012).

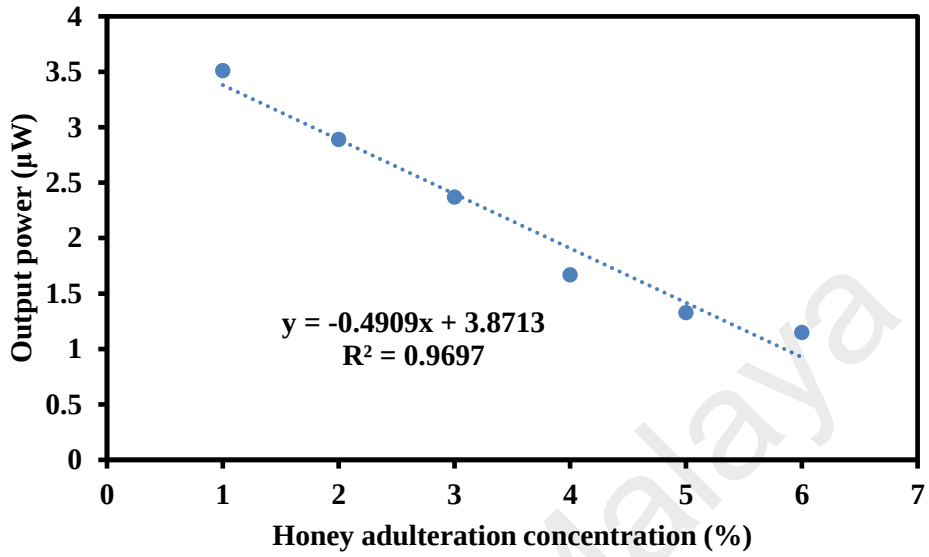

(a)

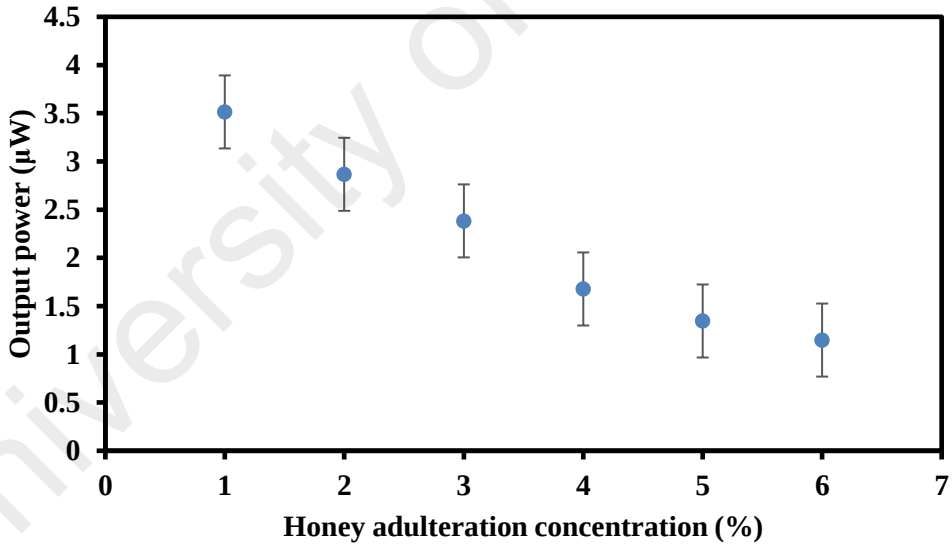

(b)

Figure 3.15. (a) Output power of the PMMA microfiber for different adulterated honey concentrations, (b) The repeatability of the sensor.

Table 3.3: The performance of the PMMA microfiber based honey adulterated sensor

Parameters	PERFORMANCE
Resolution (%)	0.03
Standard Deviation (μW)	0.015
Linearity (%)	96.97
Sensitivity (μW/%)	0.49
Linear Range (%)	1% - 6%

Figure 3.16 shows the shift of the output wavelength against the concentrations of the adulterated honey solutions for the PMMA microfiber sensor. By referring to the figure, the wavelength decreases as the concentration of adulterated honey increases. For the 1% concentration, the refractive index is 1.4776 at the wavelength of 1542.56 nm. The resonant peak shifts to a shorter wavelength as the index of the solution increases when the concentration of adulterated honey solution is increased. The temperature was kept almost constant around 25°C during the measurement. Lastly, the stability was obtained by measuring the output power for every 10 seconds for a total period of 10 minutes (see Figure 3.17). The results show that the output power obtained is stable.

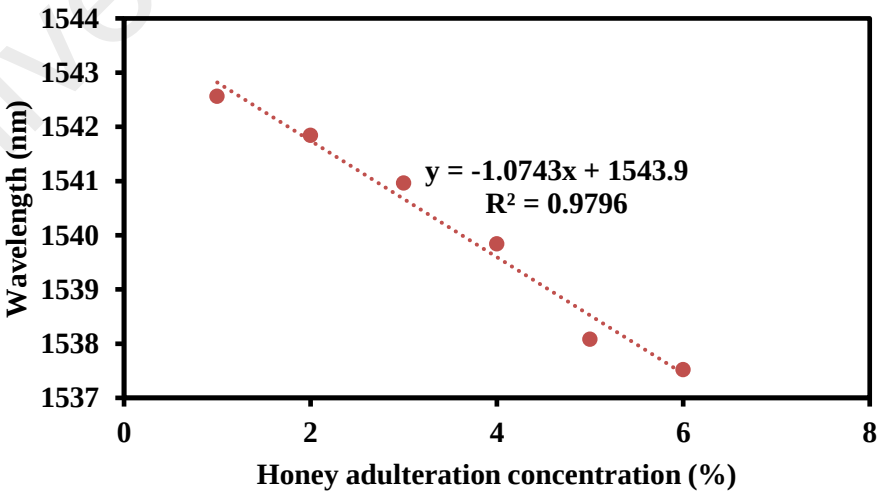

Figure. 3.16: Resonance wavelength against adulterated honey solution for the PMMA microfiber sensor. The resonant peak shifts to shorter wavelengths as the index of the adulterated honey solution increases with the increase in the concentration of the adulterated honey solutions.

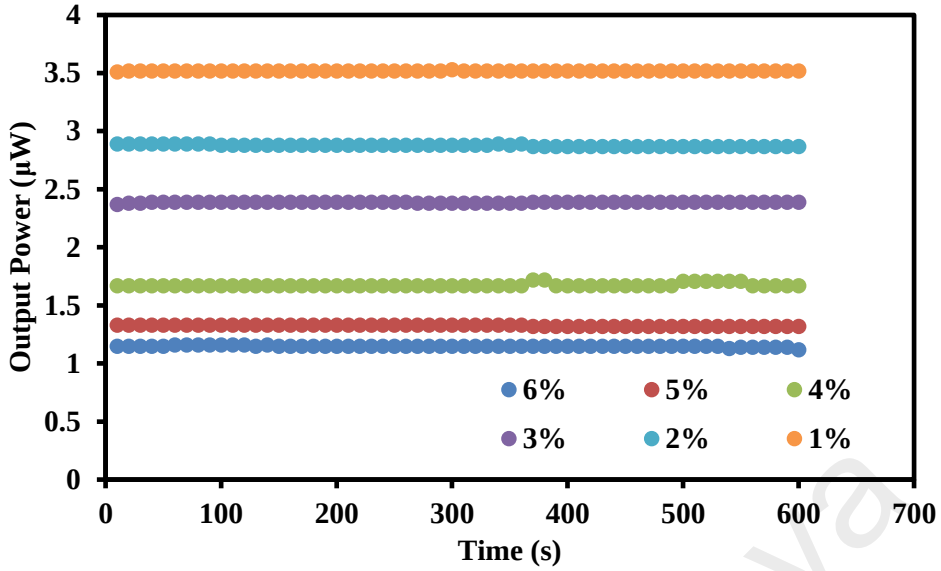

Figure 3.17: Stability of the PMMA microfiber sensor for adulterated honey detection.

3.6 Uric Acid Biosensor Using PMMA Microfiber Coated with ZnO

Zinc Oxide (ZnO) is a semiconductor with a bandgap of 3.3 eV with a wide range of properties including a metallic to insulator conductivity range (including n-type and p-type conductivity), high transparency, piezoelectricity, wide-band gap semi-conductivity, room-temperature ferromagnetism, and huge magneto-optic and chemical-sensing effects (Schmidt-Mende & MacManus-Driscoll, 2007). It has been the subject of intense interest in recent years for various applications such as communication, biosensor etc. (Yano et al., 2012). The advantages of ZnO are that it can be easily processed by wet chemical etching and has shown an excellent stability under high-energy radiation. In addition, it can be grown in a variety of nanostructured morphologies by various low cost and low temperature methods (Djurišić, Ng, & Chen, 2010). These nanostructures have many unique advantages such as high surface area and high sensitivity even at room temperature (Schmidt-Mende & MacManus-Driscoll, 2007). Besides, in combination with immobilized enzymes, it can also enhance the direct electron transfer between the enzyme's active sites and the electrons (Cui et al.,

2006). Therefore, many new sensors have been developed based on the ZnO nanostructure.

Uric acid (UA), the primary end product of purine metabolism, is present in biological fluids such as blood or urine. Abnormal levels of UA are symptoms of several diseases such as gout and hyperuricemia. High levels of serum uric acid is also considered as a risk factor for myocardial infarction and stroke (Ivekovic et al., 2012). In order to avoid these diseases the monitoring of uric acid is essential. So far, various uric acid detection methods have been proposed and demonstrated in literatures (Batumalay et al., 2014; Fu et al., 2016; Wang & Wolfbeis, 2015).

On the other hand, many methods have been employed to synthesize ZnO nanostructures, including sol–gel synthesis methods (Wang, Li, & Fan, 2011), electrochemistry depositions (Zheng et al., 2002), chemical vapor deposition (Liu et al., 2004), solution-grown methods (Wang, 2004), physical vapor depositions (Wang et al., 2005), metal–organic chemical vapor depositions (Tan et al., 2005), and laser-assisted growth methods (Zhang, Russo, & Mao, 2005). Although there were a mass of literatures concerning the fabrication of ZnO nanostructures, few reports were about the synthesis of Al-ZnO nanostructures. In fact, Al-ZnO nano-structures have many good physical properties, such as high electron concentration and electron mobility, which can be employed as a transparent conduction oxide electrode (TCO). In this section, a uric acid sensor is demonstrated using a PMMA microfiber coated with an Al doped ZnO nanostructure as a probe. In this work, we report a simple sol-gel process to synthesize Al-ZnO nanostructures on PMMA microfiber.

3.6.1 Preparation of the PMMA Microfiber Sensor Probe

The PMMA microfiber is prepared based on the direct drawing technique using a heating plate to melt the PMMA as discussed in the previous section. The temperature is kept constant during the fiber drawing process. A PMMA microfiber with a uniform

waist diameter of 6 µm was obtained by controlling the pulling speed and the viscosity of the PMMA. This microfiber is then coated with Al-doped ZnO nanostructures for the uric acid detection. In the coating process, the 1mol% Al-doped ZnO nanostructure was synthesized using the sol–gel method. Aqueous solution of zinc nitrate hexaydrate (Zn(NO3)2.6H2O (0.01 M), hexamethylenetetramine (HMTA; C6H12N4] (0.01 M) and aluminum nitrate nonahydrate (Al(NO3)3.9H2O) are prepared using deionized (DI) water. The solution was stirred until the solution temperature rose to 60 °C for 2 hours to obtain a clear homogeneous solution and then the solution was kept for aging for 24 hours prior to the fiber coating process. The fiber was put in the solution for 15 hours. Finally the fibers were taken out of the solution and cleaned with DI water and dried at 25°C. Figures 3.18 (a) and (b) show the microscope images of the original un-coated and the coated PMMA microfiber, respectively.

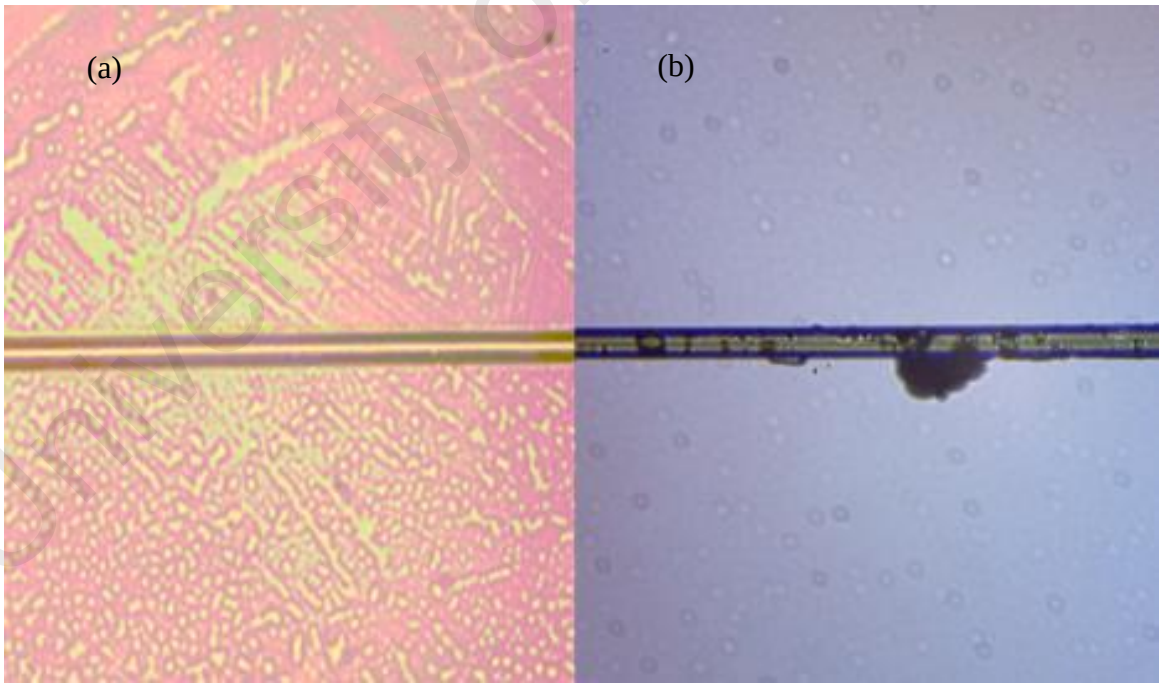

Figure 3.18: Microscopic images of (a) PMMA microfiber (with a diameter of 6 µm) and (b) PMMA microfiber coated with Al-doped ZnO growth solution

3.6.2 Experimental Setup of the Uric Acid Sensor

The setup used to measure uric acid concentration using the fabricated PMMA microfiber coated with Al-doped ZnO nanostructures is shown in Figure. 3.19. ASE light from the Erbium-doped fiber amplifier (EDFA) is launched into the microfiber probe, which is immersed in an uric acid homogeneous solution with different concentrations. The transmitted light is measured by the OSA. In the experiment, the performance of the proposed sensor was investigated for various uric acid concentrations. The uric acid concentration in DI water is varied from 0 to 500 ppm. During the experiment, the errors caused by the temperature were considered negligible and the temperature was kept constant at 25^{o}C.

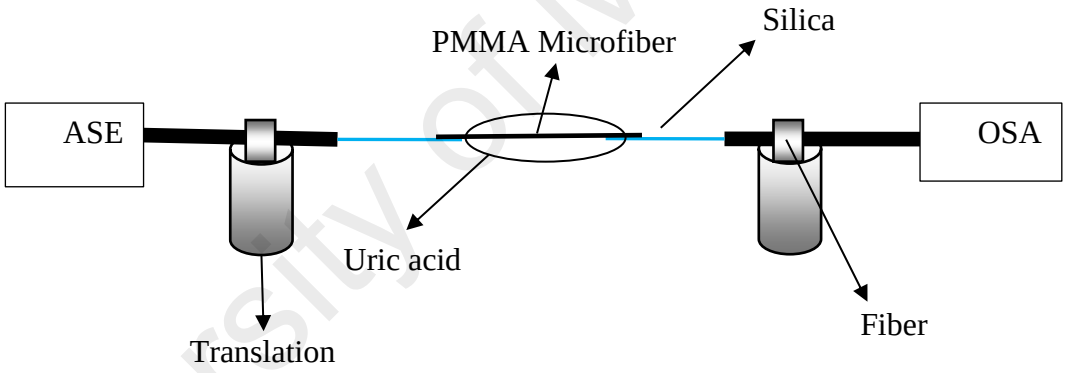

Figure 3.19: Experimental setup for detecting various uric acid concentrations

3.6.3 Results and Discussion

Figure 3.20 shows the output spectra of the PMMA microfiber based sensor when the sensor probe coated with Al-doped ZnO is exposed to air and when it is immersed in the uric acid solution (500 ppm). It can be seen that there is an interference pattern especially when the probe is exposed to air with a refractive index of around 1.0. When the ASE light is launched into the liquid medium through the input port of the sensor, the reflection occurs on both sides of the coupling region mainly from the Fresnel reflection, which is caused by the high index contrast between the PMMA

microfiber and the air. The reflections cause light to oscillate and interfere inside the microfiber. The interference produces optical comb due to the phase difference as two beams propagate with two different path length. However, the extinction ratio of the interference comb is significantly reduced as the probe is immersed in the uric acid solution as shown in Figure 3.20. This is attributed to the decrease in the reflection at the tip of the PMMA microfiber due to the decrease in the index contrast between two media. The intensity of the overall output spectrum is also slightly improved as shown in Figure. 3.20 due to the same reason.

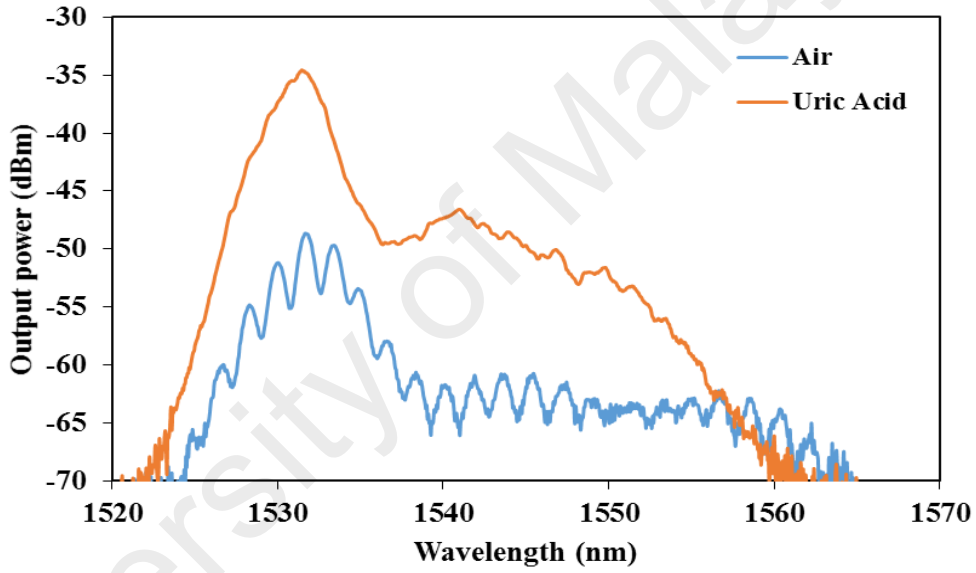

Figure 3.20: Output spectra for the immersion of PMMA microfiber with Al-doped ZnO growth solution in air and uric acid

The change in the transmitted light intensity from the PMMA microfiber based sensor with the increase in uric acid concentration is depicted in Figure. 3.21. It is observed that the light power linearly decreases with the increase in uric acid concentration. The adjusted R-square value or the coefficient of determination is the measure of the goodness of fit which is 0.9999. The considerably high values of the adjusted R-square allow the prediction of unknown concentration by the linear curve. As the uric acid concentration increases from 0 to 500 ppm, the reflected light intensity reduces from -31.54 dBm to -36.54 dBm. It is found that the sensor has a sensitivity of

0.010 dB/ppm with a good linearity of more than 99 %.

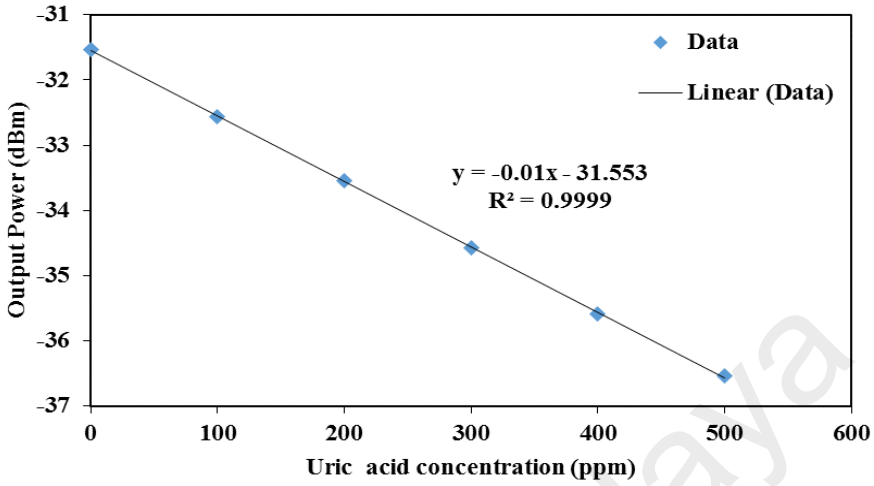

Figure 3.21: Output power of the PMMA microfiber with AlZnO growth solution for different uric acid concentrations.

3.7 Summary

Three types of optical sensors have been successfully demonstrated based on a PMMA microfiber. The microfiber sensor probe was fabricated using the simple direct drawing technique from molten PMMA. The probe was immersed in various solutions to be sensed and the sensor operates based on both intensity modulation and interfeometric techniques. At first, the microfiber sensor was proposed and demonstrated for the detection of various concentrations of $KMnO_4$ solution. The results show that sensitivity of the polymer microfiber is obtained at 32.57 µW/% with a resolution of 0.0064%. The second experiment used the fabricated PMMA microfiber to sense the relative honey adulteration using intensity modulation technique. As the solution concentration of the adulterated honey solution varies from 1% to 6%, the output power of the polymer microfiber decreases from 3.51 to 1.15 µW with a sensitivity of 0.49 µW/% and a linearity of more than 96.97%. Finally, an uric acid biosensor was also demonstrated using a PMMA microfiber coated with an Al doped ZnO nanostructure as a probe. The PMMA microfiber is coated with Al-doped ZnO

nanostructure using a sol-gel process. The sensor has a sensitivity of 0.010 dB/ppm with a good linearity of more than 99 %. Our results show that the PMMA microfiber are promising for these sensing applications with high sensitivity, stability, and repeatability.

CHAPTER 4

DEVELOPMENT OF SENSITIVE COATING AND DOPING MATERIAL BASED POLYMER MICROFIBER SENSORS FOR RELATIVE HUMIDITY MEASUREMENT

4.1 Introduction

Over the last two decades, fiber optic sensors have been gaining popularity among research institutions and industries. The fiber optic sensor technology offers the ability to accomplish multiplexing capabilities, remote sensing, versatility, improved performance, high sensitivity and can easily operate under strong electromagnetic field conditions. They also offer multiple possibilities for combining a large number of different sensors (e.g., those used for detecting temperature, pH, humidity, high magnetic field, displacement, pressure and acceleration) into the same optical fiber, thus eliminating the need for multiple cables as required in traditional electronic sensing (Yeo, Sun, & Grattan, 2008).

Sensor technology based on fiber-optic has historically achieved many developments and, continues to be driven to a large extent due to a reduction of the price of associated components (Grattan & Meggitt, 1995), coupled with integrated spatial miniaturized devices (Brambilla et al., 2009; Grattan & Meggitt, 1995; Kou et al., 2012; Lou, Wang, & Tong, 2014; Tong & Sumetsky, 2011). The combination of fiber optic and nanotechnology, called microfiber has opened up new possibilities of sensing systems, fitted for a new range of applications. Their tiny size (diameter of hundreds of nanometers to several micrometers) (Lou et al., 2014), accompanied by high-fractional evanescent fields and high flexibilities, makes them superior as a micro

scale waveguide that has higher sensitivity, faster responses and lower power consumption (Chen et al., 2013; Lou et al., 2014) over conventional optical fiber. In addition, the light propagating in the microfiber shows low optical loss and high mechanical strength, owing to the diameter uniformity and smoothness of the atomic-level sidewall of the fiber (Brambilla et al., 2004; Bures & Ghosh, 1999; Chen et al., 2013).

Recently, optical microfibers have been demonstrated to be useful in sensor applications including temperature, pH, concentration of molecules and humidity due to its interesting optical properties. An evanescent field is created around the decreased microfiber diameter of several micrometers, enabling 50% of the power guided through it to propagate outside the physical microfiber. This evanescent field is able to offer high light intensity due to strong confinement and is especially beneficial for sensing the surroundings that comes into contact with it. By exploiting these properties, low-cost, miniaturized and all-fiber based optical devices for various applications (Bilodeau, Hill, Faucher, & Johnson, 1988) could be developed. Furthermore, these optical microfibers have shown to be promising for the development of various kinds of micro- and nanophotonic components and devices (Brambilla et al., 2009; Tong et al., 2012). Typical microfiber-based sensing structures, including the simple, straight microfiber and the microfiber loop resonator have been widely used. The former can be directly fabricated by using the heat pulling method while the latter can be easily maintained by van der Waals or electrostatic forces at the joint area (Lou et al., 2014). Embedding the microfiber loop inside a polymer is another possible route to fabricate a robust micro-resonator for sensing applications (Vienne, Li, & Tong, 2007; Xiao et al., 2009; Xu & Brambilla, 2007).

Polymer microfibers have excellent merits over other waveguiding counterparts such as their ultrahigh optical confinement, strong evanescent fields, hospitality to many

functional dopants, capability of light modulation, mechanical flexibility and low cost. In recent years, several functionalized polymers, such as PMMA (Poly Methyl Methacrylate), PAM (Polyacrylamide), PVA (Poly Vinyl Alcohol), PEO (Poly Ethylene Oxide), PS (Polystyrene), and PANI (Polyaniline), have been proposed for sensors, waveguides or light source applications (Gu et al., 2008; Wang, et al., 2013).

Several techniques have been used to fabricate polymer microwires or nanowires including chemical synthesis, nano-lithography, electro-spinning and direct physical drawing. In this work, the physical drawing is used. It is a simple and cheap technique where a hot plate is used to melt the polymer. Then, the tip of a silica fiber is used to be immersed into the polymer droplet and drawn up quickly, forming a polymer microfiber as described in the previous chapter. The resulting polymer microfiber has an excellent uniformity and smooth surface which is required to decrease the loss in optical sensors (Ong et al., 2015)

The term humidity refers to the presence of water in gaseous form, but it is often used to refer to expressions which are related to water vapor characteristics and in the field of measurement, there are various terms associated with such water vapor measurements (Yeo et al., 2008). Humidity sensors are based on reversible absorption of water (H_2O) from the ambient atmosphere into a porous thin-film interferometer that sits on the tapered fiber and changes the refractive index of the thin films and subsequently transforms the lossy fiber into a light guide. Various relative humidity sensors have been explored using a glass silica fiber. For instance, (Arregui, Ciaurriz, Oneca, & Matıas, 2003) uses a tapered silica fiber coated with hydrogels while (Bariain, et al., 2000) uses the tapered fiber coated with agarose gel for humidity sensing based on refractive index change. Agarose has a high porosity which allows the gel to absorb moisture and function as a humidity sensor. Using the same approach, humidity sensors were also proposed based on a tapered silica fiber coated with nanostructured films

using the ionic self-assembled monolayer (ISAM) deposition technique (Corres et al., 2006; Corres, Arregui, & Matías, 2007). Many works have also been reported on using a side-polished silica optical fiber coated with a humidity sensitive layer for humidity sensing.

Polymer-based humidity sensors have been receiving greater attention due to polymer lattice hospitality to many functional dopants. Thus, it is easy to be functionalized by solvating the dopants into the polymer mixture. For instance, a PAM (polyacrylamide) 2-3 μm diameter micro-ring was reported in (Wang et al., 2011) for high-sensitivity (0.49 nm/%RH) optical humidity sensing. PAM absorbs H2O molecules, causing resonant wavelength shifts as humidity rate increases. A higher sensitivity (0.088 nm/10%RH) was achieved (Wu et al., 2011) by using a polymer microfiber 2.1 μm knot resonator. The functional doping material is able to enhance its capabilities of generating, propagating, converting and modulating light at the micro-nanoscale (Wang, et al., 2013).

In this chapter, the development of sensitive coating and doping material based polymer microfiber sensors for relative humidity measurement is presented. A PMMA microfiber was selected due to its smooth morphology, which makes it suitable for low loss optical wave guiding and sensing. Furthermore, it can be easily fabricated by directly drawing the solvated polymer. Compared to silica optical fibers, PMMA optical fibers are lower in cost and are generally more physically robust (Lye et al., 2005). In this chapter, ZnO nanostructures are used as the sensitive coating; whereas the doping material is agarose. The ZnO nanostructure coating and agarose doping on the microfibers induces changes to the optical properties in response to an external stimulus.

4.2 Fabrication of ZnO Nanostructure

Zinc oxide (ZnO) is an attractive, relevant and biosafe material and can be used as a sensing element. It has a wide band gap of 3.3eV at room temperature and may be integrated into a wide range of nanoscale devices such as optoelectronic devices, surface acoustic wave devices, piezoelectric devices, transparent conducting materials, solar cell and field emitters. In addition, ZnO nanorods are one of the most promising materials for the fabrication of chemical and biosensors due to its exotic and versatile properties including biocompatibility, nontoxicity, chemical and photochemical stability, high specific surface area, optical transparency, electrochemical activities, high electron communicating features and so on (Kang et al., 2005; Wan et al., 2004; Zhang et al., 2004). Growing ZnO nanostructure on flat substrates has been extensively demonstrated in various platforms such as glass, silica and aluminium foil (Lee et al., 2006; Umar et al., 2007; Wei, Zhi, & MacManus-Driscoll, 2005).

ZnO nanorods are a biosafe and sensitive material that changes its refractive index, subsequently enhances the guided light in the fiber. In this section, the PMMA microfiber loop and knot resonator was demonstrated where ZnO is used as deposited layer onto the PMMA fiber for detecting relative humidity (RH) changes. Their apparent difference with and without the deposition of ZnO was investigated, in term of output power and sensitivity Recently, it has been reported that ZnO nanostructure enhances the interaction of fiber guided light for humidity sensor (Batumalay et al., 2015). Two major steps were carried out for the preparation for ZnO nanorods. First, the seed layer was deposited on the fiber to grow the ZnO nanorods using a simple manual dip coating technique. The seeded solution was prepared by dissolving zinc acetate dehydrate ($Zn(CH_3COO)_2 \cdot 2H_2O$) as a precursor in isopropanol with a molarity of 0.025 M. The solution was stirred at 60° C for 2 hours at ambient temperature to yield a clear and homogenous solution. Then, the solution was cooled down to room temperature for

the coating process. The fiber was manually dipped into the seeding solution and dried at 30°C to evaporate the solvent. This coating and drying procedure was repeated 5 times to increase the thickness of the fibers. Following this, the growing solution was prepared by dissolving 0.01M zinc nitrate hexahydrate (Zn(NO3)2.6H2O and 0.01M hexamethylenetetramine (HMTA) in 100ml deionized water. The deposition process of ZnO nanorods on the PMMA microfiber was performed using the sol-gel immersion method by suspending the fiber in the growing solution at 30°C for 2 hours. Fig. 4.1 (a) shows the FESEM images of the sensor probe coated with ZnO; Fig 4.1 (b) shows the FESEM images of the ZnO nanorods; and Fig. 4.1 (c) shows the ZnO growing solution. The ZnO nanorods coating is expected to enhance the ability of the probe for sensing applications.

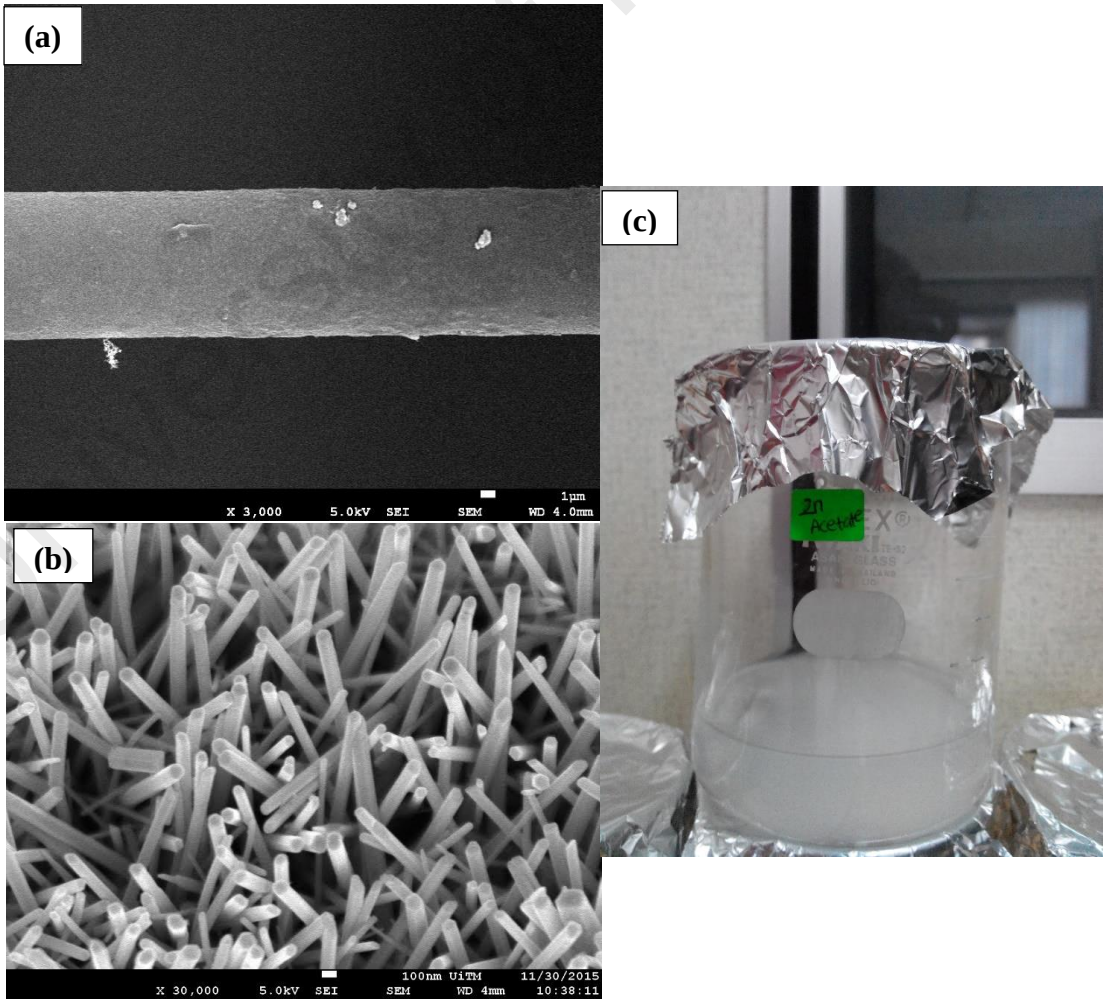

Figure 4.1: (a) FESEM images of the sensor probe coated with ZnO (b) FESEM images of ZnO nanorods (c) The ZnO growing solution.

4.3 Fabrication of Agarose gel

As mentioned by Stellan et al. (Stellan & Yao, 1981), the porosity of agarose gels decreases as the concentration of agarose increases. The agarose gel used is based on the swelling nature of hydrophilic materials which causes refractive index changes in accordance with humidity and modulates the light propagating through the fiber. Batumalay et al. reported that fiber coated with an agarose gel of 0.5% weight content shows higher sensitivity in comparison with 1% and 1.5% due to the effect of pore size (Batumalay et al., 2014). The PMMA doped agarose gel microfiber was fabricated by using the direct drawing method as follows: Poly (methyl methacrylate) (PMMA) was first dissolved in acetone to form a homogeneous solution with wt% 3. Agarose gel was then dissolved in water in a proportion of 1% in weight. The mixture was heated to 50°C. A small portion of the mixture was combined with PMMA solution and stirred at 35°C for 1.45 hours and then exposed to ultrasonic for 20 minutes to form a uniform solution with appropriate viscosity for drawing. Figure 4.2 (a) shows the photographic image of the 1% agarose weight content. Figure 4.2 (b) and (c) show the microscopic images of the 1% agarose gel weight content and the PMMA microfiber doped agarose gel with a diameter of 6µm, respectively.

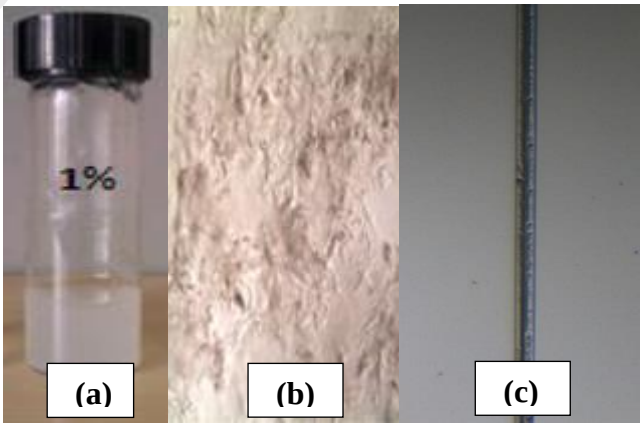

Figure 4.2: (a) Photographic image of agarose 1% weight content. Microscopic images of (b) agarose gel of 1% weight content. (c) PMMA microfiber doped agarose gel with diameter 6µm.

4.4 Relative Humidity (RH) Sensor Based on Loop PMMA Microfiber with ZnO Nanorods Coating

Microfiber resonators have attracted much attention because of its high sensitivity, simple structures and good refractive index sensing. The microfiber loop resonator is easy to be fabricated as the loop structure is maintained by van der Waals or electrostatic forces at the joint area (Lou et al., 2014). Embedding a microfiber loop inside a polymer is another possible route to fabricate a robust micro-resonator for sensing applications (Vienne et al., 2007; Xiao et al., 2009; Xu & Brambilla, 2007).

Recently, it has been reported that ZnO enhances the interaction of the fiber guided light for humidity sensing (Batumalay et al., 2015). A previous paper by Zheng et. al reported a novel coating-free RH fiber sensor by using a microfiber loop resonator (MLR) (Zheng et al., 2013). Wang et al. reported polymer microfiber rings for high sensitivity optical humidity sensing (Wang et al., 2011). Here, a PMMA microfiber loop resonator (PMLR) was fabricated by directly drawing the solvated polymer.

In this section, the performance of loop PMMA microfibers, before and after being coated with ZnO nanorods is presented. The PMLR was coated with ZnO nanorods for detecting the changes in relative humidity. The ZnO nanorods coating on the PMLR induces changes to the optical properties in response to an external stimulus.

4.4.1 Preparation of the Sensor Probe and Experimental Setup

A PMMA microfiber was fabricated using a molten PMMA in conjunction with the direct drawing technique (Figure 4.3). The fabricated PMMA with a diameter of 8 μm has a high surface smoothness and 7 mm fiber length uniformity. PMMA was selected as the polymer wave-guiding material due to its high mechanical strength, good dimensional stability, good weather resistance, and its natural transparency above the deep ultraviolet region. A heating plate was used to melt the PMMA and keep the temperature constant during the fiber drawing process. First, the tip of a tapered silica

fiber with a diameter of about 125 μm was immersed into the molten PMMA. Then the fiber tip was retracted from the molten polymer with a drawing speed of 0.1−1 m s^{-1}, leaving a PMMA microfiber extending between the molten PMMA and the tip. The extended PMMA microfiber was quickly quenched in air and subsequently formed a bare PMMA microfiber. The microfiber diameter can be controlled by the pulling speed and the viscosity of the polymer (which depends on the hot plate temperature).

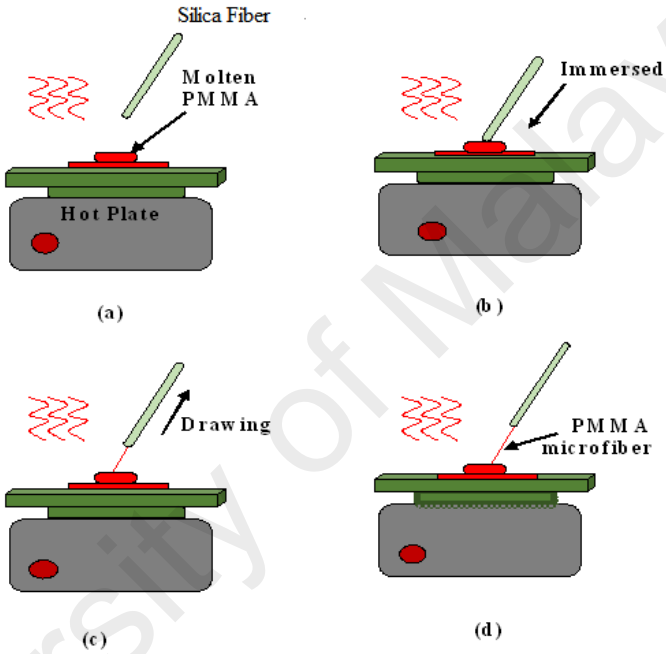

Figure 4.3: Schematic diagram of the PMMA microfiber fabrication setup

As for the ZnO nanorods, the seed layer was deposited onto the fiber to grow the ZnO nanorods using a simple manual dip coating technique. The seeded solution was prepared by dissolving zinc acetate dehydrate (Zn(CH3COO)2·2H2O) as a precursor in isopropanol with a molarity of 0.025 M. The solution was stirred at 60° C for 2 hours at ambient temperature to yield a clear and homogenous solution. Then, the solution was cooled down to room temperature for the coating process. The fiber was manually dipped into the seeding solution and dried at 30°C to evaporate the solvent. This process was repeated 5 times until the desired thickness of the fiber was achieved. Subsequently, the growing solution was prepared by dissolving 0.01M zinc nitrate

hexahydrate (Zn(NO3)2.6H2O and 0.01M hexamethylenetetramine (HMTA) in 100ml deionized water. The deposition process of ZnO nanorods on the PMMA microfiber was performed using the sol-gel immersion method by suspending the fiber in the growing solution at 30°C for 2 hours. The PMMA microfiber was then characterized using Field Emission Scanning Electron Microscope (FESEM) to investigate the morphology of the coated ZnO nanorods as shown in Figure 4.4 (a) displays the microscopic image of the PMMA microfiber coated with ZnO nanorods at magnification 7000x; and Figure 4.4 (b) displays the ZnO nanorods at a magnification of 4500x. It can be observed that although the ZnO nanorods are dispersively distributed, but their diameters and lengths are rather uniform.

The setup used to measure relative humidity using the fabricated PMMA microfiber coated with ZnO nanorods is displayed in Figure 4.5. The amplified spontaneous emission (ASE) light from the Erbium-doped fiber amplifier (EDFA) was launched onto the microfiber probe placed in a sealed chamber with a dish filled with a saturated salt solution. Relative humidity depends on the amount of moisture of the surrounding; therefore, salt solution was placed in the sealed chamber in order to simulate the different value of relative humidity until the equilibrium relative solution of the salt solution is achieved which is around 80% RH. The transmitted light and wavelength shift is measured by the optical spectrum analyzer (OSA, Anritsu MS9710C). In the experiment, the performance of the proposed sensor was investigated for various relative humidity levels, ranging from 50% RH to 80% RH. The humidity was measured using the Omega RH-21C temperature-relative humidity meter with a resolution of 0.1% RH.

The two important parameters that define the performance of the PMLR is the finesse, F and Q-factor. The finesse is defined as the free spectral range (FSR) of the resonator divided by $\Delta\lambda$.

$$F = \frac{FSR}{\Delta\lambda} \tag{4.1}$$

The Q-factor is defined as the ratio of the resonance wavelength to the bandwidth of the resonance, the full wave at half maximum (FWHM).

$$\text{Q-factor} = \frac{\lambda}{\Delta\lambda} \tag{4.2}$$

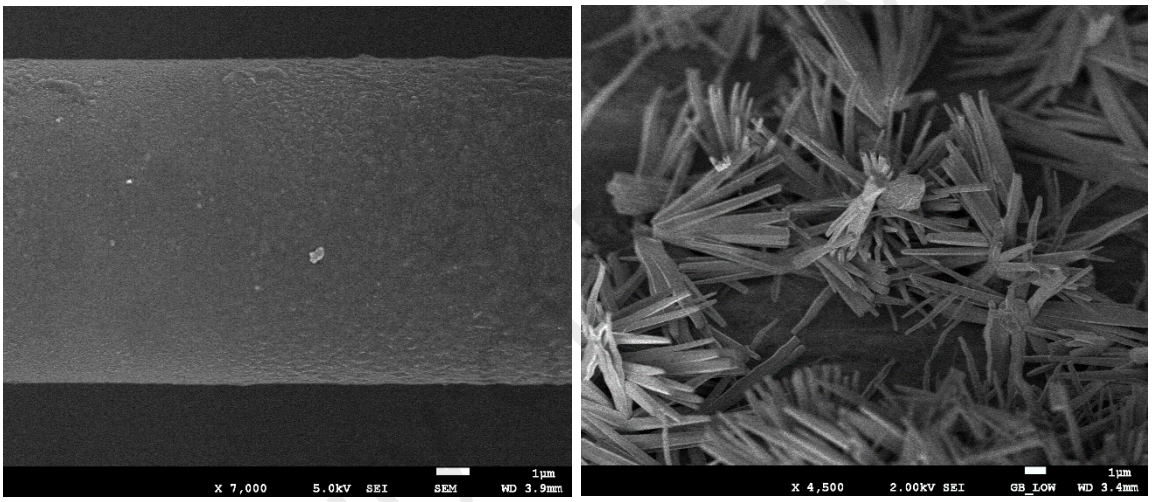

(a) (b)

Figure 4.4: FESEM images of (a) the 7000x magnified image of the PMMA microfiber coated with ZnO nanorods; and (b) the 4500x magnified image of the ZnO nanorods.

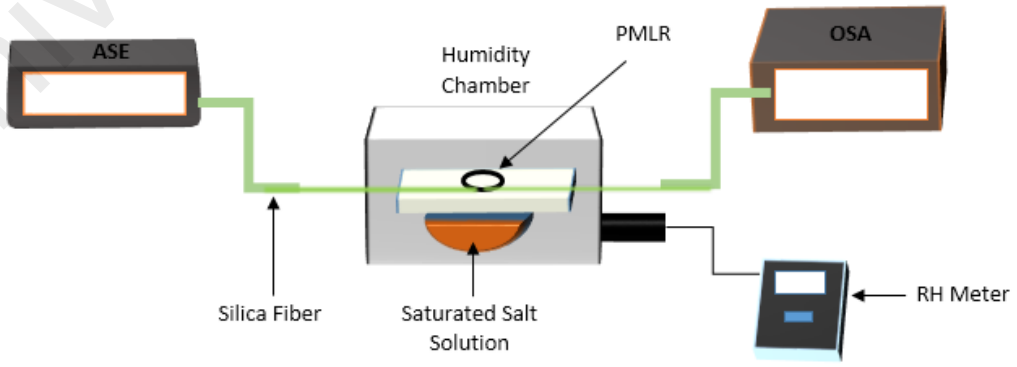

Figure 4.5: Experimental setup for the PMMA microfiber based humidity sensor

4.4.2 The Performance of the PMMA Microfiber Coated with ZnO Nanorods based RH sensor

Figure 4.6 depicts the 400x magnified microscopic image of the PMLR and the loop diameter of 8 µm and 42 µm, respectively. The microscopic image was taken by an optical digital microscope. The surface attraction force of the electrostatic and Van der Waals kept the ends of the PMMA microfiber to stick to each other. The van der Waals attraction force between the two adjacent PMMA microfiber is strong enough to withstand the elastic force from the bent microfiber and maintain the microfiber loop structure. Figure 4.7 displays the comb transmission spectrum of the uncoated PMLR, which was obtained by using an ASE source in conjunction with an OSA. The extinction ratio is about 4.0 dBm and 7.0 dBm, before and after the coating of the ZnO nanorods, respectively.

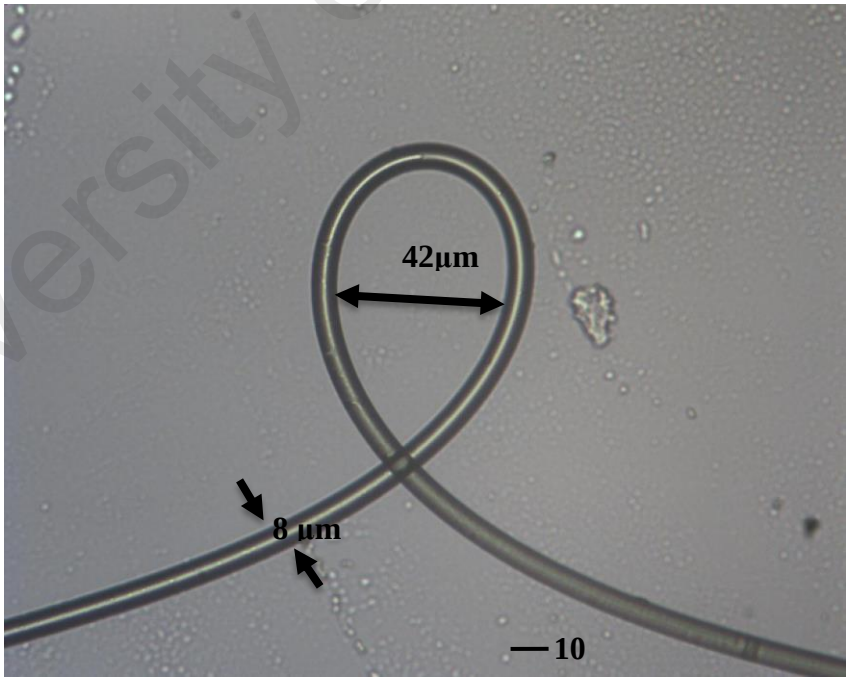

Figure 4.6: The optical microscopic image of the PMLR.

The values of the finesse and Q-factor of the uncoated and coated PMLR as extracted from Figure 4.7 (a) are 4988.54 and ~6.13 and Figure 4.7(b) are 3854.125 and ~2.75, respectively.

The resonance of the PMLR can be maintained by exploiting the Van der Waals attraction force between the two microfiber ends in the coupling region. A smaller loop diameter will result in a greater elastic force, hence, making it more difficult for the microfiber loop to maintain its shape and resonance condition.

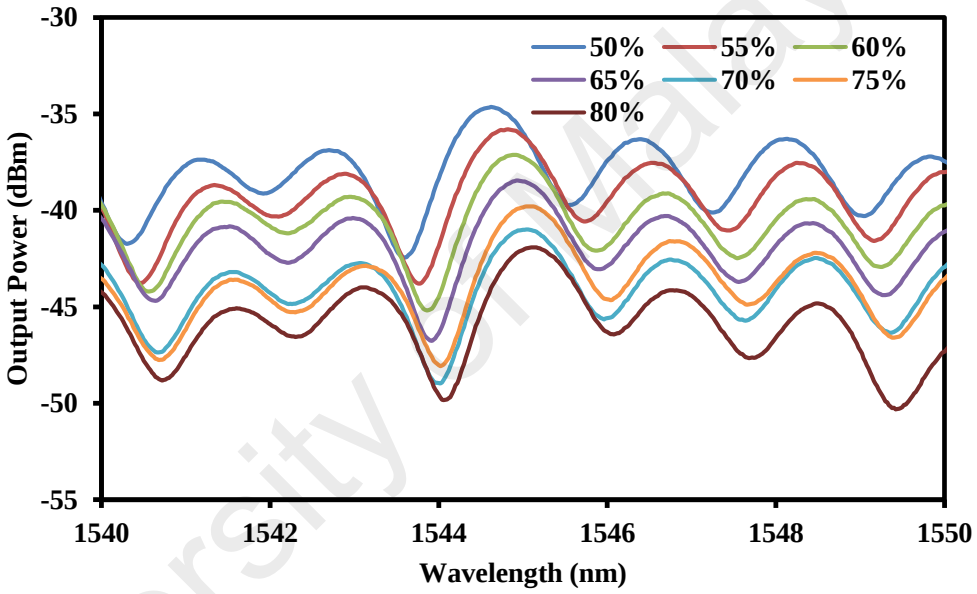

(a)

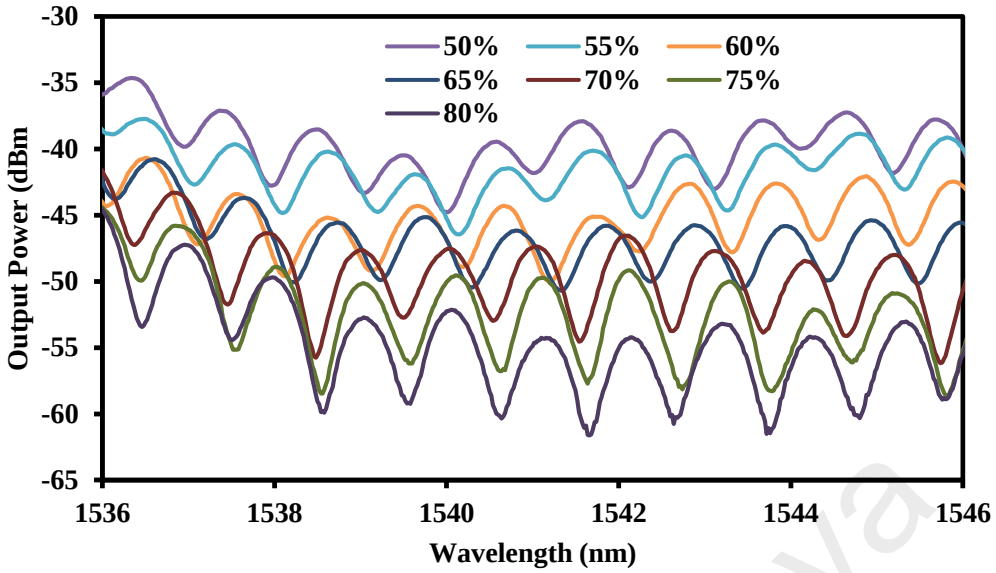

(b)

Figure 4.7**:** Transmission spectra of the RH-sensor measured at different relative humidity percentages (50, 60 and 70) for the cases of (a) an uncoated PMLR and (b) a PMLR coated with ZnO nanorods.

Figure 4.8 depicts the relative humidity (%) against resonant wavelength shift for the PMLR, with and without the ZnO nanorods coating. The gradual shifting of the wavelength is observed to occur starting from the 50% RH value up to its saturated value of 80%. The data set was measured two times and can be well fitted with a linear regression line, indicating a linearity and sensitivity of 99% and 0.0091 nm/%; and 97% and 0.0224 nm/% for the uncoated and ZnO nanorods coated PMLR, respectively. Further analysis of the variation of the transmitted light from the PMLR against the relative humidity is displayed in Figure 4.9 (a). The change in the intensity of the transmitted light of the ZnO nanorods coated PMLR decreases with relative humidity with a linearity and sensitivity of 99% and 0.5221 dBm/%.

Throughout the experiment, it is evident that the performance of the sensor is enhanced after being coated with ZnO nanorods. These ZnO nanorods absorb more water and increase the sensitivity of the sensor. The ZnO nanorods is a hydrophilic material and water molecules can be easily absorbed by the ZnO layer of the PMLR in a humid environment. A lot of factors come into play during the growth of the ZnO, like

the concentration of the chemical bath, temperature, duration of growth, pH, etc. (Baruah & Dutta, 2009; Pál et al., 2009; Zhao, Li, & Lou, 2014), which directly affect the final morphology of the rods grown using the hydrothermal method. According to Liu et al., the effective refractive index (RI) of ZnO composite varies from 1.698 to 1.718 as the relative humidity changes from 10-95%. The increasment in water molecules being absorbed by ZnO layer increases the RI of the effective coating of the fiber which leads to a larger leakage of light (He et al., 2013; Liu et al., 2012). This induce an additional mass on the surface which influences the transmission characteristics of the PMLR. The increase in the water molecules in higher humidity levels increases both from effective index of the surrounding medium and the absorption coefficient of the ZnO composite, justifying the improved performance of the PMLR coated with ZnO nanorods. Relative humidity depends on the amount of moisture; therefore, saturated (sodium chloride) was placed in the sealed receptacle in order to simulate the different values of relative humidity. When the water vapour from the salt solution increases, the relative humidity increases. Greenspan (Greenspan, 1977) reported the equilibrium relative humidity of saturated sodium chloride solution at 25^0C to be 75.29. During the experiment, we observed the increase in the relative humidity level from 50% to 80% within the time span of 47 minutes when the temperature was fixed at 25^0C. No further increase in the relative humidity was observed beyond 80%. Other ranges of relative humidity could be investigated by using other types of saturated salt solutions with different equilibrium relative humidity values.

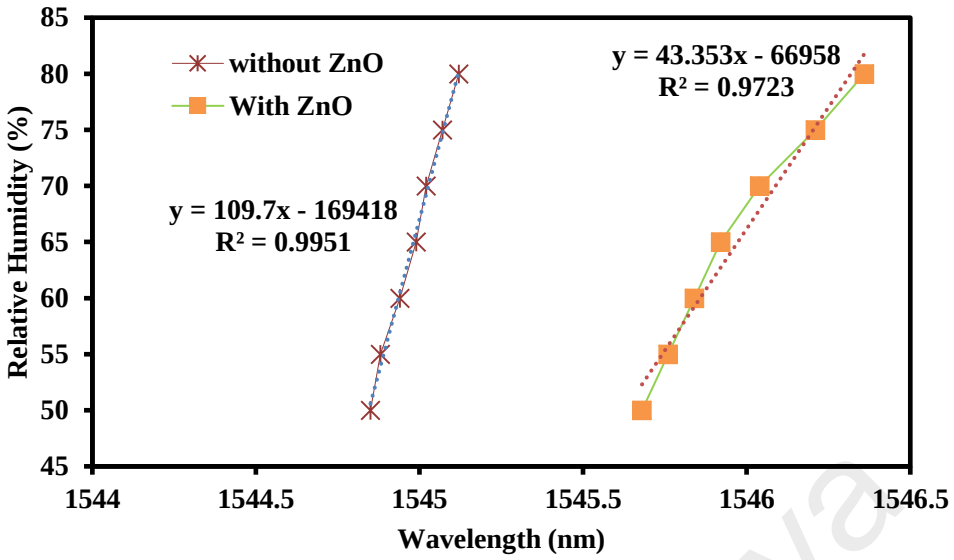

Figure 4.8: Relative humidity response of the bare PMLR and coated PMLR with ZnO nanorods

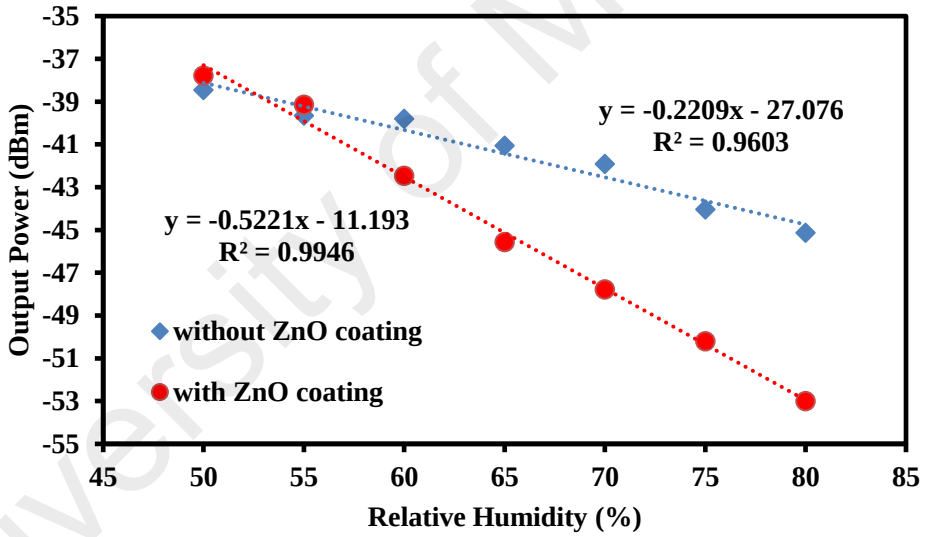

(a)

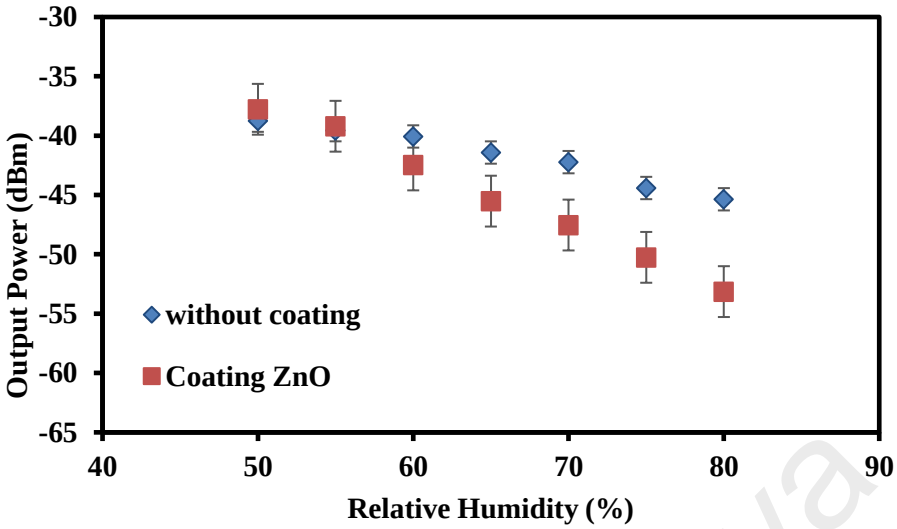

(b)

Figure 4.9: (a) Output power against relative humidity for the proposed PMLR based sensor with and without ZnO nanorods (b) The repeatability of the sensors.

The performance characteristic of the humidity sensor using PMLR is summarized in Table 4.1. Overall, the sensor is observed to be sufficiently stable with standard deviations of 0.61 dBm and 0.213 dBm for the uncoated and ZnO nanorods coated PMLR, respectively. The repeatability of the results in this experiment is another crucial factor in the operation of a sensor system. Thus, it can also be used to validate the results obtained as the relative humidity was varied from 80% to 50%. Figure 4.9 (b) shows the repeatability of the sensors.

A ZnO nanorod sensor exploits enhanced surface area and thus surface activity. Absorption of molecules on the nanorods can be detected through variation of the nanorods' properties, such as photoluminescence, electrical conductivity, vibration frequency, mass, etc. Throughout the experiment, it is evident that the performance of the sensor is enhanced after being coated with ZnO nanorods due to its ability to absorb more water. The same observation was made by Wang et al (Wang et al., 2008).

Table 4.1. The performance of the relative humidity sensor using PMLR

Parameter	Before Coating	After Coating
Resolution (%)	2.74	0.4094
Standard Deviation (dBm)	0.61	0.213
Linearity (%)	More than 96	More than 99
Sensitivity (dBm/%)	0.2209	0.5221
Linear Range (%)	50-80	50-80

4.5 The Humidity Sensor Performance of the Poly (Methyl Methacrylate) Microfiber Knot Resonator Coated with ZnO Nanorods

Besides the straight forward, loop structure of a microfiber resonator sensor, other structures such as knot and coil are also possible. Non-resonator microfiber employ intensity-dependent scheme, while optical sensor based-resonator depends on optical path or phase (Tong & Sumetsky, 2010). Resonator-type sensors allow light to recirculate at resonant, overlap and couple, thereby effectively increase the optical path, thus creating compact sensors with high Q-factors which is predicted to be as high as ~10^9 (Chen et al., 2013; Tong & Sumetsky, 2010). Microfiber loop resonators (MLR) were among the configurations that have been widely reported and its development as optical sensors have attracted much interest (Guo & Tong, 2008; Lim, Harun, Jasim, & Ahmad, 2011; Rahman et al., 2015; Shi, Xu, Tan, & Chen, 2007; Xu et al., 2008). However, it suffers from limited stability since the MLR geometry shape depends only on electrostatic and Van der Waals forces at the joint point of the fiber (Sumetsky et al., 2006; Sumetsky et al., 2005). This means that small environmental changes such as vibration or heat can break the bond. Therefore, researchers come out with an idea of forming a knot to couple adjacent microfibers called a microfiber knot resonator (MKR). This design requires less precision of the microfiber alignment, improved stability, and enhanced Q-factor and finesse. Moreover, the Q-factor and spectral

properties can be varied by changing the knot radius and wire diameter (Wang, Zhu, & Li, 2011).

Many techniques to produce the sensor-based fiber optic for different sensory purposes have been reported (Ali et al., 2012; Allsop et al., 2006; Batumalay et al., 2014; Batumalay et al., 2013; Ding et al., 2005; Liang et al., 2005; Wo et al., 2012). Long period gating (Liang et al., 2005) and fiber Bragg gratings (Allsop et al., 2006) are inscribed on microfibers where their responses to a change in ambient condition are in the form of spectral shifts. Wo et al., proposed a refractive index sensor using a Mach Zehnder interferometer (MZI) which is formed by manipulating two strands of microfibers (Wo et al., 2012). Alternatively, simpler fabrication of the sensor by coating grown material (Batumalay et al., 2014; Batumalay et al., 2013; Yao, Wu, Gong, & Rao, 2012) onto the fiber have received much attention for sensing application (Lim et al., 2011; Zibaii et al., 2010). Here, the performance of PMMA microfiber knot resonators (PMKR) before and after being coated with ZnO nanorods is presented.

4.5.1 Preparation of the Sensor Probe and Experimental setup

The same PMMA fabrication setup and ZnO nanorods fabrication process as in section 4.4.1 was used. Figure 4.10(a) displays the microscopic image of the PMMA microfiber coated with ZnO nanorods at a magnification 8000x; and Figure 4.10(b) displays the ZnO nanorods at a magnification of 30000x. It can be observed that although the ZnO nanorods are dispersively distributed, their diameters and lengths are rather uniform.

A similar setup as in Figure 4.5 was used to measure relative humidity using the fabricated knot PMMA microfiber coated with ZnO nanorods, with the exception of replacing the PMLR with a PMKR, as displayed in Figure 4.11. In the experiment, the performance of the proposed sensor was investigated for various relative humidity levels, ranging from 50% RH to 80% RH. The humidity was measured using the Omega RH-21C temperature-relative humidity meter with a resolution of 0.1% RH.

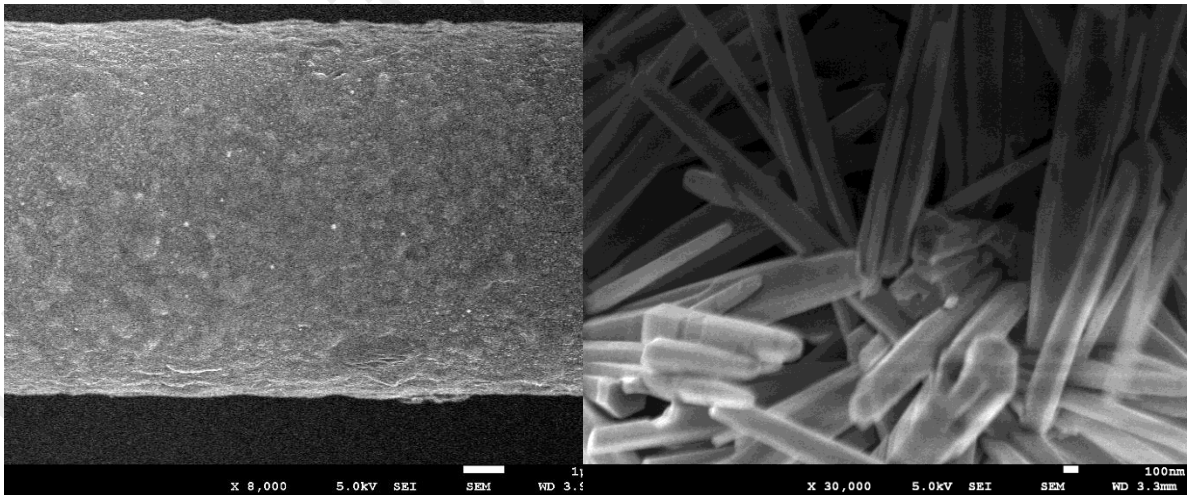

(a) (b)

Figure 4.10: FESEM images of (a) the 8000x magnified image of the PMMA microfiber coated with ZnO nanorods; and (b) the 30000x magnified image of the ZnO nanorods.

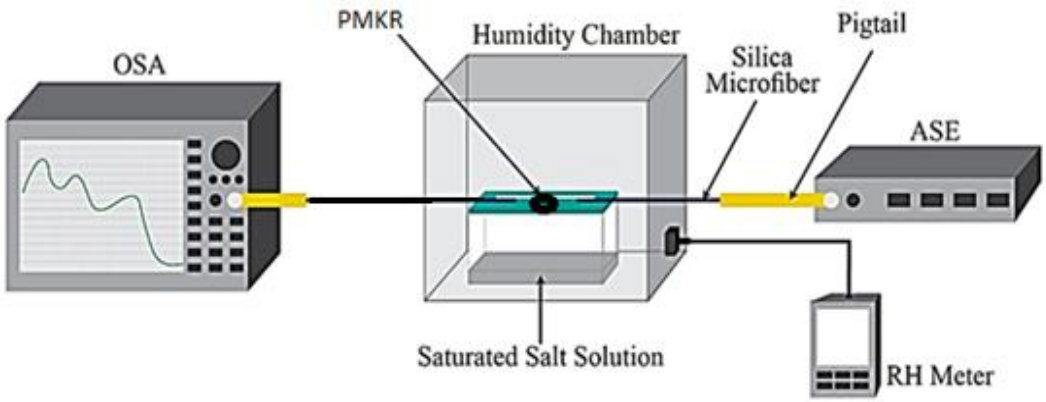

Figure 4.11: Experimental setup for the PMMA microfiber based humidity sensor

4.5.2 Results and Discussions

Figure 4.12 shows the 100x magnified microscopic image of the PMKR and the knot diameter of 7 µm and 133 µm, respectively. The diameter of 133 µm was obtained by the axial tension from the pulling force at the two sides of the PMMA fiber. The PMMA microfiber was tied into the knot structure under an optical microscope using a micromanipulation process. Precise alignment can be easily achieved by naturally overlapping the fiber with itself, which attributes to the high robustness and high stability of the MKR structure. As reported by Zubia *et. al.*, (Zubia & Arrue, 2001) and Magi *et. al*. (Mägi, Nguyen, & Eggleton, 2005), the bending loss of a knot structure is very low. Figure 4.12 shows that no surface scratch is found after the tightening process.

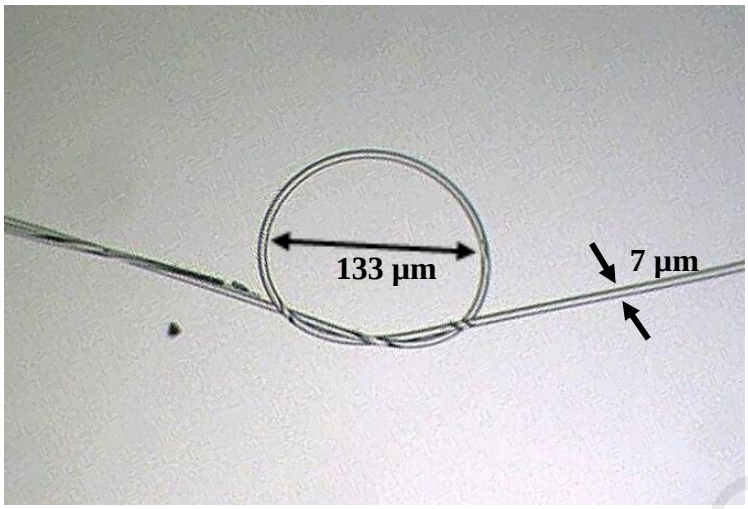

Figure 4.12: The optical microscopic image of the PMKR

Figure 4.13 shows the transmission spectra of the microfiber knot with different relative humidity (RH) percentages. Figure 4.13(a) shows the transmission spectra of the uncoated PMKR while Figure 4.13(b) shows the transmission spectra for the PMKR coated with ZnO. The comb spectra was obtained by using an ASE source at the input ports of the PMMA microfiber and an OSA was connected at the output ports. The RH was varied by controlling the saturated salt solution as mentioned above.

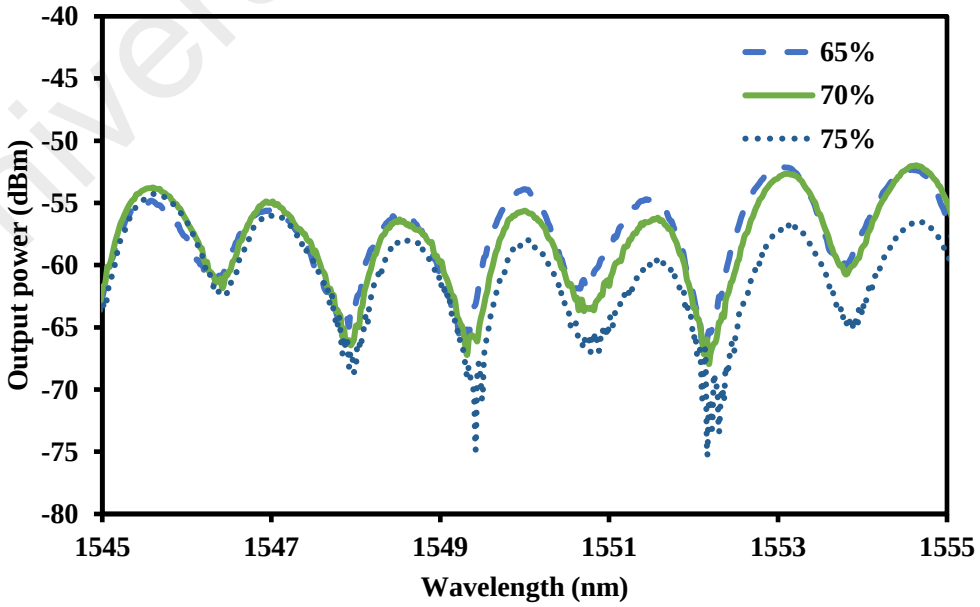

(a)

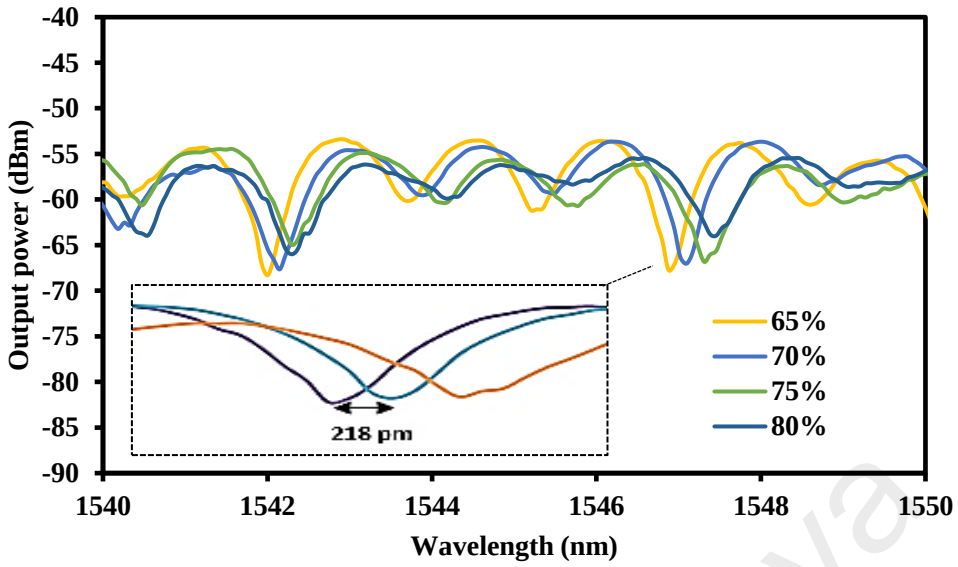

(b)

Figure 4.13: Transmission spectrum of the RH-sensor measured with different relative humidity percentages using (a) an uncoated PMKR, (b) a ZnO nanorod coated PMKR

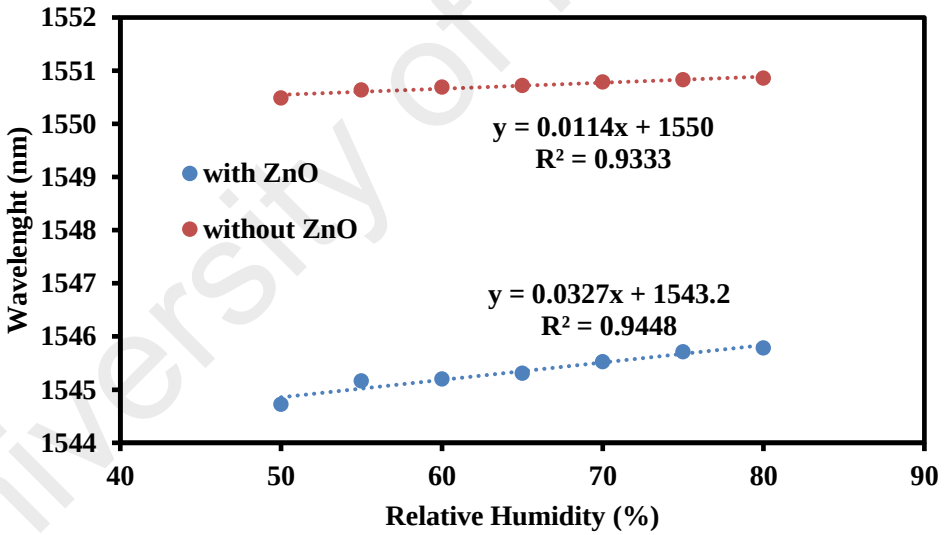

Figure 4.14: Resonant wavelength shift against relative humidity for the PMKR, with and without ZnO

Based on Figure 4.14, it was observed for the uncoated PMKR that as the RH increased, there are slight increments in the wavelengths ranging from 1550.49-1550.86 nm (for the RH-50% to RH-80%) by 370 pm. This might be caused by the polymer microfiber's sensitivity towards the RH itself. The shift of resonance in the uncoated PMKR can be explained by the enhanced molecular state adsorption of water on the

PMMA surface as the PMMA consist of larger molecule and hydrophilic material compared with other polymer materials. The retention of water on the surface of the PMMA occurs through a process of physical adsorption without possible swelling effect being ruled out. The water will keep its molecular state and will always remain in solid, liquid or vapor and will only be a charge in the hydrogen bonds between molecules (Zhang et al., 2008). However, from the observation of Figure 4.14, there is a significant 1055 pm shift of the resonant for the microfiber coated with ZnO within the relative humidity range of 50% to 80%. This phenomenon can be due to the porous matrix of the ZnO which enables the trapping of water molecules on its interior surface, and increases the average density of the ZnO composite (Wu et al., 2011). This results in the increase of the refractive index medium (cladding) and the shifting of resonant wavelength. Thus, the sensor exhibit a high sensitivity of 437 pm wavelength shifting for a 5% humidity change as a function of RH for approximately 1055 pm change of resonant wavelength for RH range from 50% to 80%. The extinction ratio is about 10.0 dBm and 7.0 dBm, before and after the ZnO is being coated onto the PMKR, respectively. The values of the finesse and Q-factor of the uncoated and coated PMKR as extracted from Figure 4.13 (a) are 1985.12 and ~1.82; and Figure 4.13 (b) is 1247.14 and ~1.47, respectively.

Further analysis of the variation of the transmitted light from the PMKR against the relative humidity is displayed in Figure 4.15. The change in the intensity of the transmitted light of the PMKR coated with ZnO decreases with relative humidity with a standard deviation of 0.074 nm, slightly lower than that of the uncoated PMKR which is 0.208 nm. This shows that the computed results indicate low possibility of measurement error. Subsequently, the square regression coefficient (R^2) for the uncoated PMKR was 0.9333 while for the coated PMKR was 0.9448.

The repeatability of the results in this experiment is another crucial factor in the operation of a sensor system. Thus, it can also be used to validate the results obtained as the relative humidity was varied from 50% to 80%. Figure 4.15 shows the repeatability of the sensors. From Figure 4.15, it can be observed that the ZnO coated PMKR has a higher stability than the uncoated PMKR. Thus, our proposed PMKR coated with ZnO is suitable to be implemented in sensor applications.

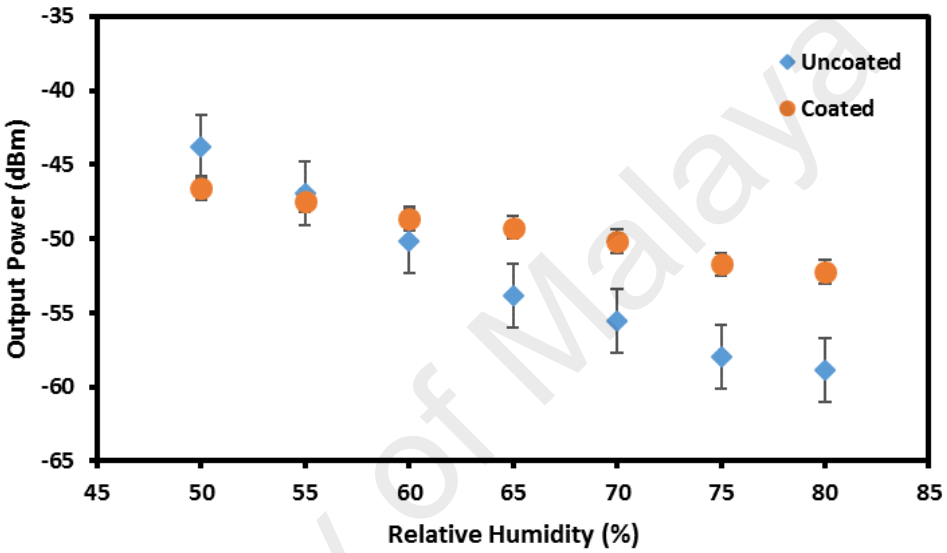

Figure 4.15: The repeatability of the PMKR sensor

The performance characteristic of the humidity sensor using PMLR is summarized in Table 4.2. Overall, the sensor is observed to be sufficiently stable with standard deviations of 0.11 dBm and 0.05 dBm for the uncoated and PMKR coated with ZnO, respectively.

Table 4.2: Comparison of the PMKR microfiber performance with and without ZnO as the coating layer

Parameter	Without ZnO	With ZnO
Resolution (%)	18.26	2.28
Standard Deviation (nm)	0.208	0.07
Linearity (%)	More than 93	More than 94
Sensitivity (pm/%)	11.4	32.7
Linear Range (%)	50-80	50-80

In comparison, when the PMKR is used instead of the PMLR, an improvement in the sensitivity and resolution of the sensor was observed. This is because the PMKR induces more portion of the evanescent wave outside of the microfiber, enabling more interaction with the relative humidity. It is observed that the coating of the ZnO nanostructure onto the microfiber is able to further increase the sensitivity of the sensor hence improving the sensor's resolution. The coating of sensitive material onto the tapered fiber has successfully enhanced the performance of the microfiber as a humidity sensor.

4.6 Relative Humidity Sensing Using A PMMA Doped Agarose Gel Microfiber

Humidity refers to the existence of water in vapor form. Due to their advantages over their electrical counterparts, optical humidity sensors have attracted photonic researchers to investigate different fibers, coatings and functionalizing materials to fabricate and implement a sensor. However, most of them have the same working principle by which, the surrounding humidity variations are detected as changes of the effective refractive index (Batumalay et al., 2015).

In previous works, a single mode glass tapered fiber coated with different humidity sensitive materials, such as: polymeric nano-assembled composites (Corres et al., 2006; Corres et al., 2006), gelatin (Zhang et al., 2008), Al-doped ZnO (Zuraidah Harith et al., 2015) and agarose gel (Bariain et al., 2000) were reported. Multimode

optical fiber probe coated by three porous oxide films was also used (Huang et al., 2015) as a humidity sensor with an average sensitivity of 0.7 nm/%RH. A hollow core fiber is another possible structure of humidity sensors where the central air gap cladded by fiber is spliced between two standard multimode fibers and coated by a nano-film (Matias., 2007). Besides glass optical fibers, photonic crystal fiber (PCF) (Li et al., 2010), plastic optical fiber (POF) (Batumalay et al., 2015) and polymer optical fiber (Rodriguez-Rodriguez et al., 2008) were also utilized as RH sensors.

In this work, an optical based humidity sensor at a low manufacturing cost is demonstrated; this sensor is based on the doping of PMMA with agarose gel which was directly drawn using a silica SMF. Basically, the proposed humidity sensor relies on a humidity-induced refractive index change in the agarose gel. As a result, the transmitted optical power through the PMMA doped agarose gel microfiber varies as a function of the RH. The overall low fabrication cost of the sensor and the wide use of agarose gel in biological research applications (Bariain et al., 2000; Harith et al., 2015; Huang et al., 2015; Li et al., 2010; Matias et al., 2007; Zhang et al., 2008) make our sensor very attractive for laboratory and industrial applications. To our knowledge, this is the first time that the agarose gel is used as the sensitive material of a PMMA microfiber.

4.6.1 Sensor Fabrication and Experimental Set-up

The PMMA doped agarose gel microfiber was fabricated using the direct drawing method as follows: Poly (methyl methacrylate) (PMMA) was first dissolved in acetone to form a homogeneous solution with wt% 3. Agarose gel was then dissolved in water in a proportion of 1% in weight. The mixture was heated to 50°C. A small portion of the mixture was combined with PMMA solution and stirred at 35°C for 1.45 hours and then exposed to ultrasonic for 20 minutes to form a uniform solution with appropriate viscosity for drawing. In the fabrication process, first, the buffer of the silica fiber (SMF corning 28) was removed and then cleaned with alcohol. Later on, the tip of

the 125 μm diameter was immersed into the solution. Then the fiber tip was retracted from the molten polymer with a speed of 0.1−1 m/s, leaving a PMMA microfiber extending between the molten PMMA and the tip. The extended PMMA microfiber was quickly quenched in air and subsequently forming a bare PMMA microfiber. The microfiber diameter can be controlled by the pulling speed and the viscosity of the polymer (which depends on the hot plate temperature). Microfibers produced by this technique are uniform in diameter over a long length with good flexibility. In this work, the PMMA with Mw ~15.000 by GPC and agarose powder (no. A6013) were purchased from Sigma Aldrich. Figure 4.16(a) shows the microscopic image of the PMMA doped agarose gel microfiber, while Figure 4.16(b) shows the microscopic image of the un-doped PMMA microfiber (both having a diameter of 6μm). The total length of the polymer microfiber section was fixed at around 10mm.

In order to connect the polymer microfiber into our system, one of the ends of a pair of silica fiber were tapered forming a microfiber and utilized as an interface between our polymer microfiber and the laboratory apparatuses, as shown in Figure 4.17 Both microstructures (polymer and silica microfibers) were linked electrostatically by allowing one of them to overlap the other in the two ends of the polymer microfiber. Light waveguiding along the microfiber is employed by an evanescent coupling method where light is able to be launched from the fiber taper and collected by the polymer microfiber within the overlapping area (Gu et al., 2008). As can be seen in the arrangement of Figure 4.17, the light is coupled from the laser source and is guided until the sensor head, where the light interacts with the humidity sensing material. The signal is then transmitted to the optical detector.

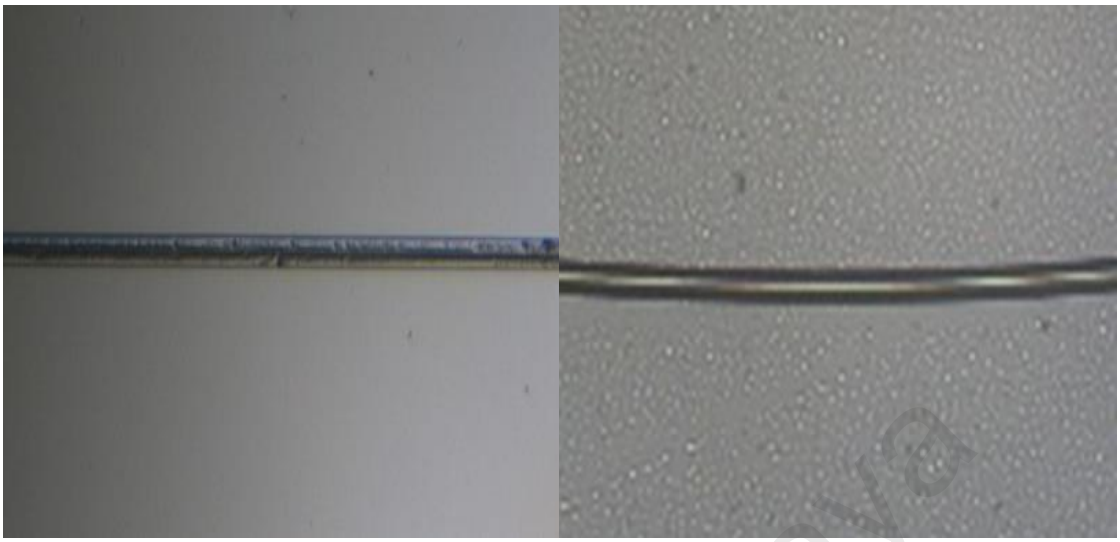

(a) (b)

Figure 4.16: The microscopic image of the (a) PMMA doped agarose gel microfiber; (b) Un-doped PMMA microfiber

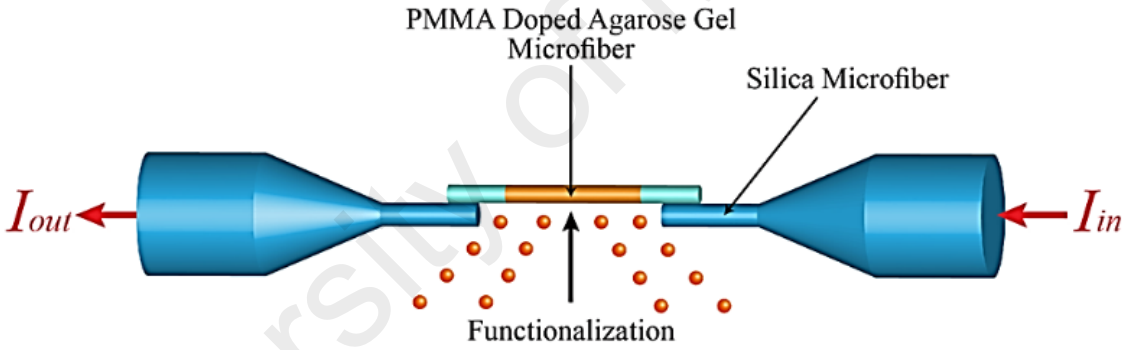

Figure 4.17: Linking the polymer microfiber into our system

The experimental setup used for the relative humidity measurement is shown in Figure 4.18. An amplified spontaneous emission (ASE) light source operating at a wavelength of 1550 nm is launched into the silica microfiber. The light is guided through the lead in the silica microfiber then passes through the PMMA microfiber doped agarose gel, which is placed in a sealed chamber with a dish filled with a saturated salt solution. Salt solution was placed in the sealed receptacle in order to simulate the different value of relative humidity. The humidity will increase as a result of the increase in the water vapour from the salt solution. The end of the output from the

other side of the silica fiber (untapered end) is coupled into a 3dB coupler and sent to an optical spectrum analyzer (OSA) and power meter for data recording. The relative humidity is detected by the change in the output power recorded by the power meter and also the wavelength shifting recorded by the OSA. The sealed chamber is constructed with a hole and the PMMA microfiber is introduced through it into the sealed receptacle and suspended in the air above different saturated salt solutions in order to measure different values of relative humidity (Corres et al., 2006). In the experiment, the performance of the sensor was investigated for a series of changes in relative humidity ranging from 50% to 80% in steps of 5% using the omega RH-21 C temperature-relative humidity meter.

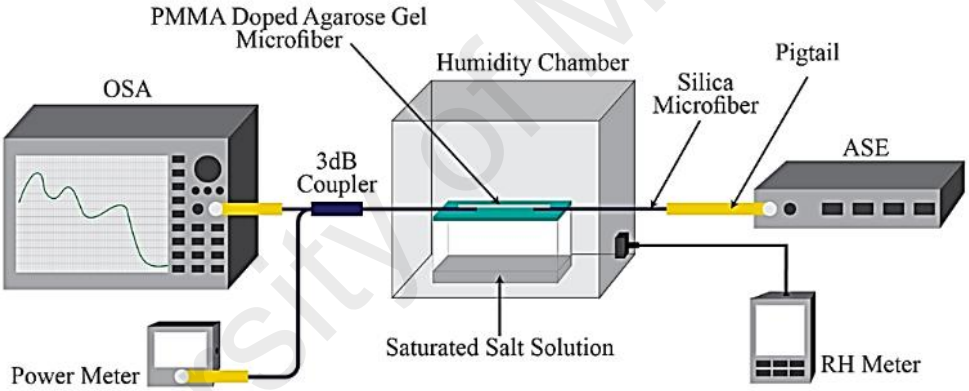

Figure 4.18: Experimental setup for the measurement of relative humidity using a PMMA doped agarose gel microfiber

4.6.2 The Performance of the Proposed Relative Humidity Sensing Using A PMMA Doped Agarose Gel Microfiber

The changes in the transmission spectrum corresponding to the increase in relative humidity using an undoped PMMA microfiber is presented in Figure 4.19 (a) for the resonance peak at λ~1544 nm. It was found that the peak wavelength shifts from 1544.1 nm to 1544.51nm as the relative humidity increases from 50 % to 80 % for the undoped PMMA microfiber. Subsequently, the change in the transmission spectrum with

increasing relative humidity of the PMMA doped agarose gel microfiber is shown in Figure 4.19 (b). The resonant peak is at λ~1546 nm. It was found that the peak wavelength shifts from 1546.87 nm to 1547.67 nm as the relative humidity increases from 50 % to 80 % for the PMMA doped microfiber..

Relative humidity monitoring can be carried out either by evaluating the wavelength shift at a fixed output power or by evaluating the power change at a fixed wavelength. Figure 5.20 displays the relative humidity variation against output power, which shows that the linear trend line can be fitted to the experimental data with a correlation coefficient value, r of more than 0.98 and 0.97 for the undoped PMMA and PMMA doped agarose gel microfiber, respectively. Correspondingly, the linear fitting of the experimental data indicate that the relative humidity sensitivity of the device is 0.068μW/% and 0.1μW/%. The fixed wavelength to monitor the output power in Figure 5 is 1550 nm. Based on Figure 5.21, the linear fitting of the experimental data indicates that the peak wavelength is shifted against relative humidity in a rate of 13.3 pm/% and 20.9 pm/% and with a linearity of 96.7% and 70.17% for undoped PMMA and PMMA doped agarose, respectively. When the relative humidity increases, the diffusion of water molecules into the sensor probe causes reduction in the refractive index of the sensor probe. Agarose is a hydrophilic material with high porosity which allows the absorption of moisture and displays good sensitivity as a humidity sensor.

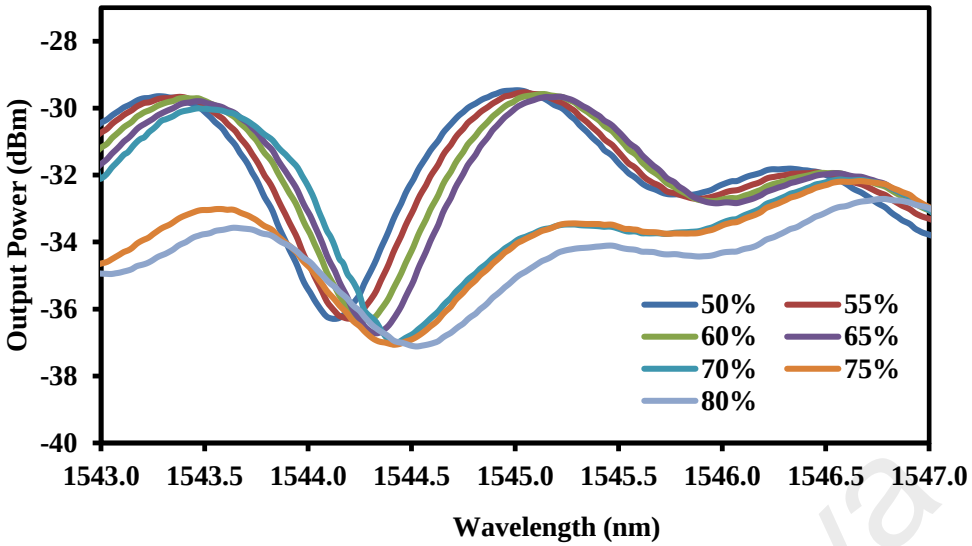

(a)

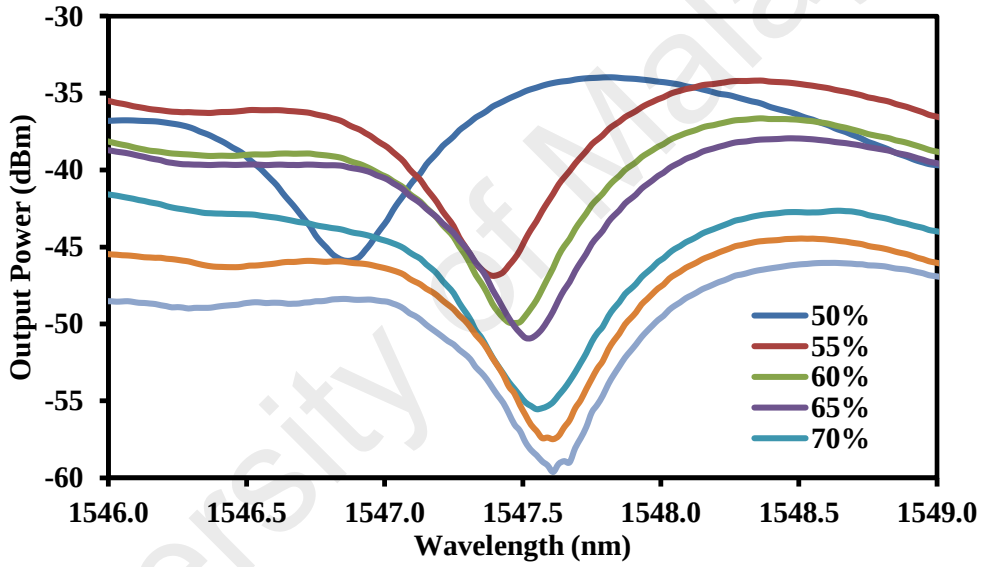

(b)

Figure 4.19: The transmission spectra of the (a) undoped PMMA microfiber when the relative humidity increases; (b) PMMA doped agarose gel microfiber when the relative humidity increases.

According to Batumalay (Batumalay et al, 2015), the fiber with an agarose gel of 0.5% weight content shows higher sensitivity in comparison with 1% and 1.5% due to the effect of the pore size. Furthermore, Stellan and Yao (Stellan & Yao, 1981) mentioned that the porosity of agarose decreases as the concentration of agarose increases. The agarose causes a refractive index change in accordance with humidity which affects the modulation of light propagating through the fiber. It is observed that

the output power is found to be decreasing, as the relative humidity increases. The higher refractive index on PMMA doped agarose creates a lossy waveguide which leads to a decrease in the output power. According to Lee (Lee et al, 2006) the refractive index value of agarose gel varies from 1.52 to 1.54 when RH changes from 20% to 80%

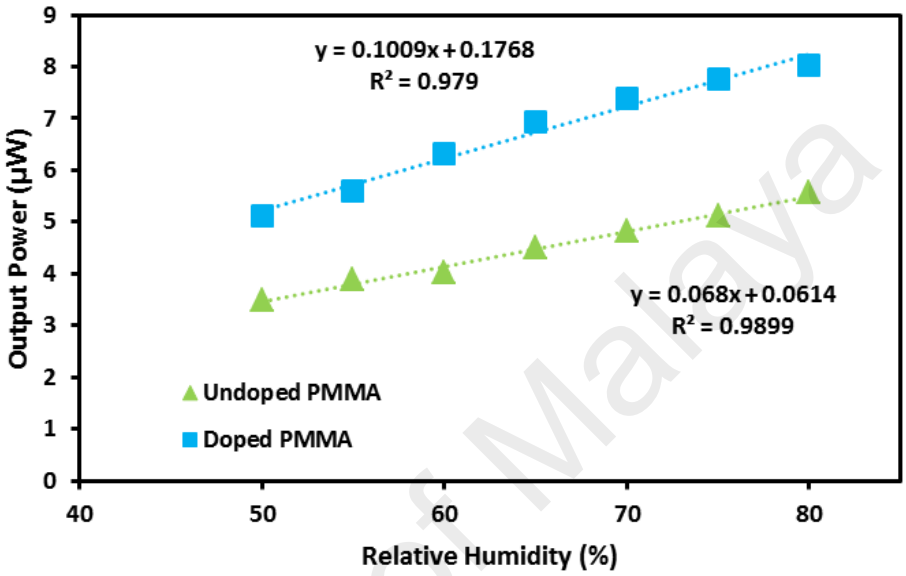

Figure 4.20: The output power variation against relative humidity.

Doping PMMA microwires with agarose offered an enhancement in power changes in response to RH variations with a sensitivity of about 0.1 µW/%RH and a linearity of more than 97%. Based on the standard deviation of 0.011µW, its resolution is obtained at 0.2%. Moreover, agarose-doped PMMA has a sensitivity of 20.9 pm/%RH comparing to the bare PMMA sensor proposed by Wu (Wu et al, 2011) which had a sensitivity of 8.8 pm/%RH. It is interesting to notice that although our proposed sensor has no resonating structure, it has achieved higher wavelength shifts comparing to the PMMA resonating knot structure reported by Wu.

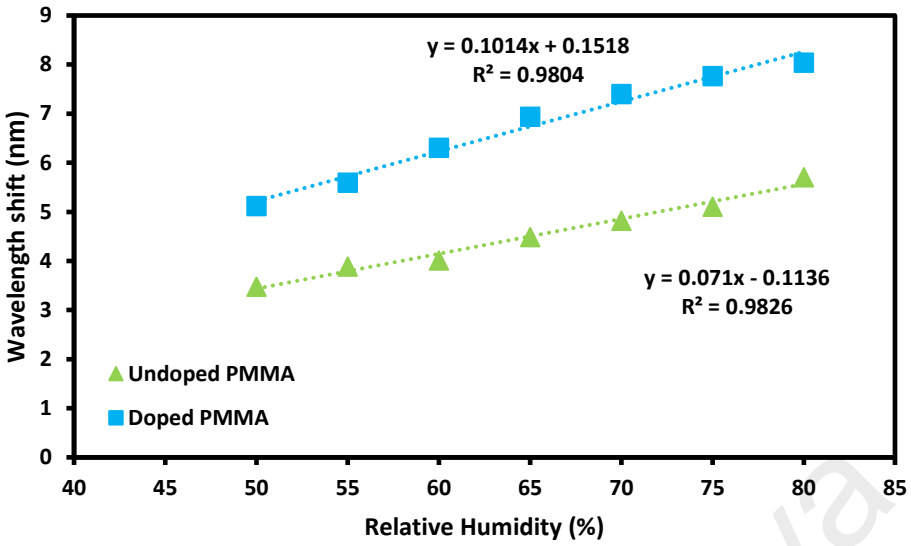

Figure 4.21: The wavelength shift against relative humidity

Table 4.3. Performance of the proposed relative humidity sensors for the undoped PMMA and PMMA doped agarose gel microfiber.

Parameters	PMMA doped agarose	Undoped PMMA
Resolution (%)	0.2	1.22
Standard Deviation (µW)	0.011	0.087
Linearity	More than 97%	More than 98%
Sensitivity (µW/%)	0.1	0.068
Linear Range (%)	50-80	50-80

The performance characteristic of the proposed sensor is summarized in Table 4.3 The PMMA doped agarose gel microfiber shows a sensitivity of 0.1µW/% and linearity of more than 97%. Based on the standard deviation of 0.011µW, its resolution is obtained at 0.2%. Since the PMMA doped agarose gel microfiber has a higher refractive index value than that of the undoped PMMA, it behaves as a lossy waveguide and allows more light to be transmitted. Our agarose-doped PMMA sensor is also benchmarked to some recent RH sensors reported in the literature. The comparison shows that our sensor's sensitivity is considerably high. In addition, the sensor has been

produced by a simple method and configured in a straight-fiber structure, which is the simplest microfiber structure.

Our agarose doped PMMA microfiber sensor is benchmarked to some recent RH sensors reported in the literature in Table 4.4. The comparison shows that our sensor's sensitivity is considerably high. In addition, the sensor has been produced by a simple method and configured in a straight fiber structure, which is the simplest microfiber structure.

Table 4.4 : Benchmarking Summary

Parameter	Our Sensor (2016)	Wu et al., (2011)	Correia et al., (2012)	Eryürek et al.,(2015)	Mehrabani et al.,(2013)
Sensitivity [pm/%RH]	20.9	8.8	22.2	26	12.98
Structure	Straight	MKR	FBGs	WGMR	WGMR

4.7 Summary

Simple PMMA microfiber probes in the form of uncoated and ZnO coated loop and knot; as well as a straight PMMA microfiber doped with agarose gel is proposed as sensors for RH measurements. The performance of both sensors is investigated for the probe, with and without ZnO nanorods coating; and with and without doping agarose gel. For both RH sensors, it can be seen that the output spectrum is shifted when the level of RH increases. It is found that the sensitivity of PMLR and PMKR based sensor significantly improves with the ZnO coating. The output intensity of the PMLR coated with ZnO nanorods decreases linearly with relative humidity. Its sensitivity, linearity and resolution are 0.5221 dBm/%, more than 99% and 0.4094%, respectively. The performance of the proposed PMKR sensor was investigated for various relative humidity levels, ranging from 50% to 80%. Different values of RH were simulated by controlling the moisture of the surrounding using salt solution. Resonant wavelength shift against relative humidity for PMKR with and without ZnO was compared. We

observed an increase of sensitivity level, approximately 1055 pm change of resonant wavelength for RH ranging from 50% to 80% (437 pm wavelength shifted for 5% humidity change). Compared to the uncoated PMKR, there is a slight resonant wavelength shifting of 370 pm that might be caused by the polymer microfiber's sensitivity towards RH itself. The extinction ratio is about 10.0 dBm and 7.0 dBm, before and after the PMKR was coated with ZnO, respectively. For the agarose gel doped PMMA, it is observed that the spectrum also shifted when the level of RH increases from 50% to 80%. The linear fitting of the experimental data indicates that the peak wavelength shifted against relative humidity at a rate of 21.4 pm/% and 28 pm/%, and with a linearity of 98.36% and 98.83% for the un-doped PMMA and PMMA doped agarose, respectively. Doping PMMA microwires with agarose offered an enhancement in power changes in response to RH variations with a sensitivity of about 0.1 μW/%RH and a linearity of more than 97%. Based on the standard deviation of 0.011μW, its resolution is obtained at 0.2%. When the relative humidity increases, the diffusion of water molecules into the sensor probe causes reduction in the refractive index of the sensor probe. Agarose is a hydrophilic material with high porosity which allows the absorption of moisture and displays good sensitivity as a humidity sensor.

CHAPTER 5

CdSe QUANTUM DOT DOPED PMMA MICROFIBER AND ITS APPLICATIONS

5.1 Introduction

The unique optical and electronic properties that are exhibited by quantum dot (QD) such as strong extinction coefficient, high quantum confinement effect, high optical gain, broad absorption profile, photochemical stability (Wang, et al., 2013), large Stokes shift (Jorge et al., 2007), enable them to be utilized in a wide variety of fields such as in the fabrication of electronic devices (Folarin, Sadiku, & Maity, 2011), gas sensors (Tatavarty et al., 2011; Zan et al., 2011), nonlinear optics (Liu et al., 2012), photovoltaic cells, lasers, thin film transistors and light emitting diodes (Yu et al., 2006). Their popularity is mainly due to the smaller bandgaps of the polymer/QD combination, perhaps due to bandgap narrowing that occurs due to high local electric fields between closely spaced quantum dots (Dickerson et al., 2005).

In comparison to other reinforcements, QD have an upperhand because of their small size distribution and high surface area to volume ratio of QD which allows better distribution within the microfibers (Mthethwa et al., 2011). Compared with dye doped polymer microfibers, QD polymer microfibers show higher resistance to photobleaching and high photoluminescence efficiency (Zhang, Yu, & Li, 2012), making them good candidates as sensors for applications requiring high stability and long term usage.

QD polymer microfiber have been drawn and demonstrated by electrospinning (Liu, Edel, Bellan, & Craighead, 2006; Mthethwa et al., 2011) and direct drawing method (Meng et al., 2011; Zhang et al., 2012). Electrospinning is quite expensive for fabrication and more complicated than the direct drawing method. Cheng et al.

successfully fabricated a PMMA doped with CdSe QD, prepared by organic synthesis. The narrow sized distribution of the QD exhibited an increase in the photoluminescence (PL) peak intensity 2.5 times (Cheng, Wang, & Cheng, 2012). Furthermore, Antonio et al. successfully fabricated active nanocomposite planar waveguides on colloidal QDs/ PMMA for the use of temperature sensing (Bueno et al., 2012).

In this chapter, CdSe quantum dot (QD) doped PMMA microfiber, which is obtained by using a previously demonstrated fabrication method of drawing from the solvated liquid polymer, is proposed and demonstrated for both sensor and laser applications. The CdSe QD can be well-dispersed throughout the PMMA microfiber without obvious aggregation, making the CdSe QD functionalized polymer microfibers as excellent active nanowaveguides (Meng et al., 2011). At first, the use of the QD doped PMMA microfiber, by virtue of their small sizes and favorable photostability, is demonstrated for temperature sensing. Then, a Q-switched and mode-locked fiber lasers are demonstrated using the CdSe doped PMMA microfiber as an SA.

5.2 Fabrication and Characterization of CdSe QD Doped PMMA Microfiber

In this work, the first stage of the process is fabrication of CdSe powder. The fabrication process is almost identical to the previous reported by Hamizi et. al where Cadmium oxide (CdO) (99.99% purity), selenium (Se) (99.99% purity), and manganese (Mn) acetate (98%) powders are used as a precursor (Hamizi & Johan, 2010). In this process, the solvent is prepared by mixing oleic acid and Paraffin oil in ratio of 3:5. Then, the CdO and Mn acetate powders are mixed with the prepared solvent under Argon gas flow at temperature of 160 ^{o}C by using a three-neck flask. The mixture was then stirred constantly until all the powders are completely dissolved before the solution was distilled in vacuum to eradicate any remaining acetone. Subsequently, the Se powder was dissolved in paraffin oil at 220°C temperature. Finally, the 5 ml Mn-Cd

solution was swiftly added into the Se-paraffin oil solution so that it exhibited rapid nucleation and allow a gradual growth of the CdSe in QD atomic structure. The CdSe solution was then underwent a few centrifugation process and washed in methanol to eradicate unreacted chemicals. It was then dried in a vacuum oven to form a CdSe powder.

Figure 5.1 (a), (b) and (c) show the results for material characterization of CdSe with transmission electron microscopy (TEM) and energy dispersive X-ray spectroscopy (EDS) and X-ray diffraction (XRD). The samples was prepared by placing a drop of a diluted methanol suspension of CdSe QD on the surface of a mesh copper film which then dried for several days. The TEM images were taken by using LEO LIBRA 120 kV Transmission electron microscopy. The CdSe particle diameter is approximately 10 nm, which complies with the QD size requirement as shown in Figure 5.1 (a). The elemental composition of the PMMA doped CdSe QDs was examined by energy dispersive X-ray spectroscopy (EDS) which was obtained by using a Siemens D500 X-ray diffractometer consisting of graphite monochromatized Cu Kα radiation (λ= 1.5418Å) irradiated with a scanning rate of 0.02 s^{-1} as shown in Figure 5.1 (b). The EDS analysis confirms the existence of Se (0.32 wt%) and Cd (0.24 wt%) elements which is within the range of normal doping concentration. The C and O in the other two peaks correspond to impurities. Figure 5.1 (c) depicts the typical XRD pattern of a PMMA doped CdSe QD which confirmed that all the reflections in the observed pattern indicate the characteristic peaks of the cubic crystal structure corresponding to (111), (220), (311) reflections (Mbese & Ajibade, 2014).The results showing peaks around of 25.5°, 42° and 49.7° correspond to (111), (220) and (311) planes, respectively. The broad peak of the XRD confirmed that the CdSe QD is nano-sized.

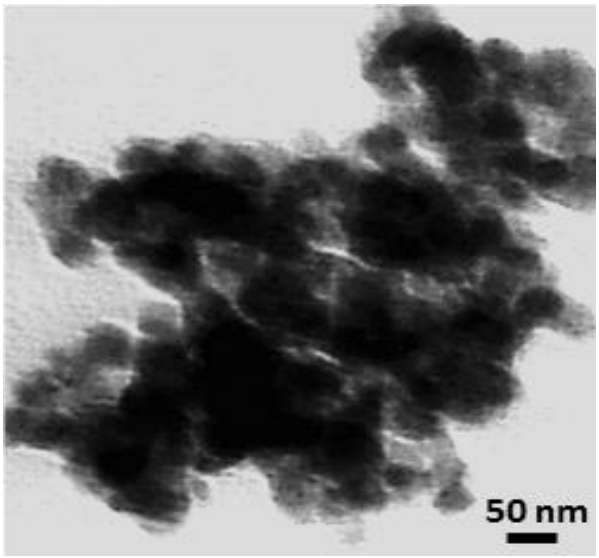

(a)

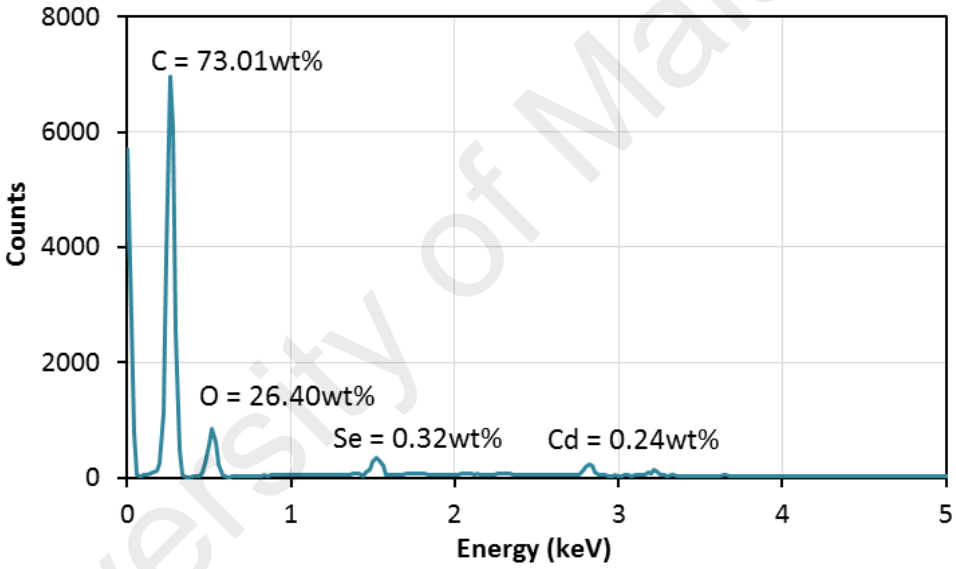

(b)

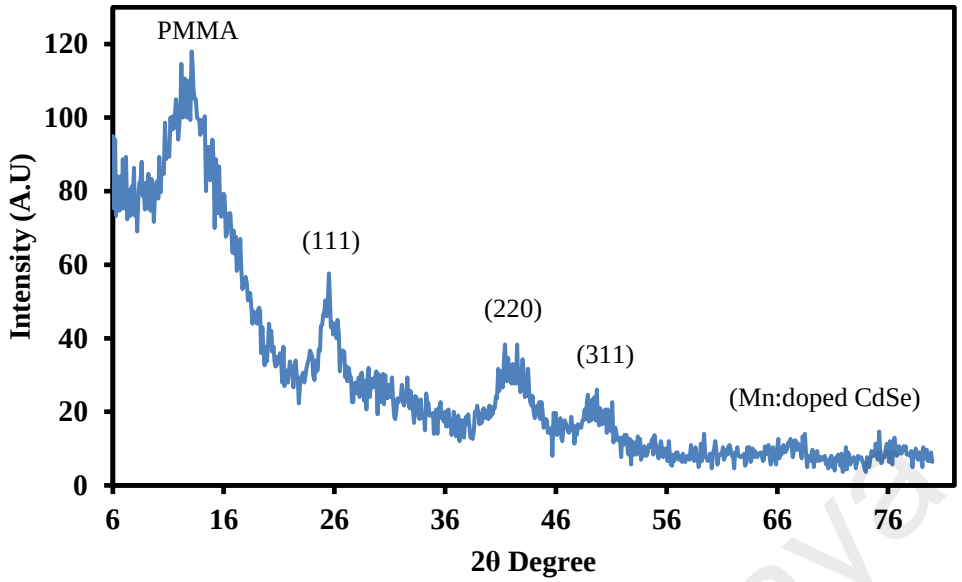

(c)

Figure 5.1: (a) The TEM micrograph and SAED pattern of the CdSe QD (b) the energy dispersive X-ray spectroscopy (EDS) measurement showing the existence of cadmium, zinc and sulfur. (c) the XRD patterns of PMMA doped CdSe QD.

In second stage, we prepare a molten CdSe-PMMA solution by mixing 1 ml of CdSe solution with a gram of PMMA powder as a based polymer. About 7 ml acetone was then added into the glass beaker that content the mixture of CdSe solution and PMMA powder. This acetone liquid was used to dissolve the mixture. Then, the acetone liquid was added continuously to overcome the evaporation issues of acetone. The mixture in the glass beaker was successfully dissolved by stirring with speed of 900 rpm and temperature of 30^{o}C, for about 1 hour and 30 minutes. Finally, the molten CdSe-PMMA solution was obtained. The PMMA microfiber doped CdSe QDs sensor was fabricated by directly drawing the solvated polymers doped with CdSe QDs as described in Chapter 3. PMMA doped CdSe QDs with diameters down to micrometers and lengths up to tens of millimeters with excellent structural uniformity are able to be produced through this process.

Optical waveguiding in a single PMMA microfiber was implemented by an evanescent coupling method as shown in Figure 5.2. A silica microfiber with a diameter

of about 4 µm was first fabricated using the flame brushing technique and later cut at the center, forming a pair of end tapered fibers. The polymer microfiber was then placed in parallel and in close contact between the two silica microfibers in order to tightly bound them via the electrostatic force and van der waals force. Due to the strong evanescent coupling between the polymer microfiber and the silica microfibers, light can be efficiently launched into and picked up from the polymer microfiber within a few micrometers' overlap.

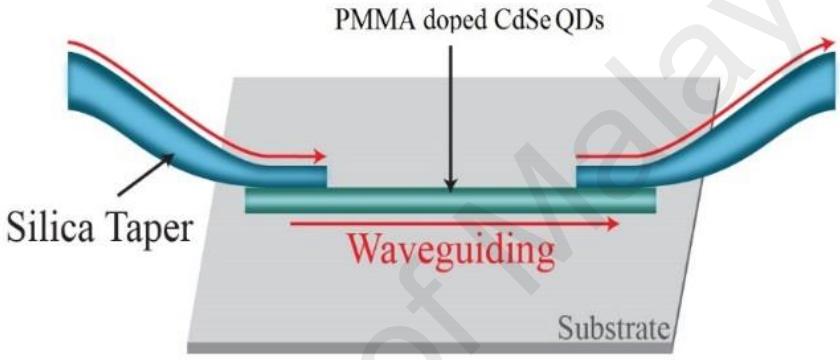

Figure 5.2: Illustration of an optical waveguiding in a single PMMA microfiber doped CdSe QDs with two ends coupled with silica microfibers.

The optical characterization of the PMMA doped CdSe QDs was then carried out using optical digital microscope. Figure 5.3 (a) displays the microscopic image of the 3µm diameter PMMA microfiber doped CdSe, indicating its smooth surface morphology. Subsequently, Figure 5.3 (b) shows the image of the same microfiber when excited by a 637 nm light source from the left side via a silica microfiber. The coupling length between the silica microfiber and the PMMA doped with CdSe QDs is 1 mm .

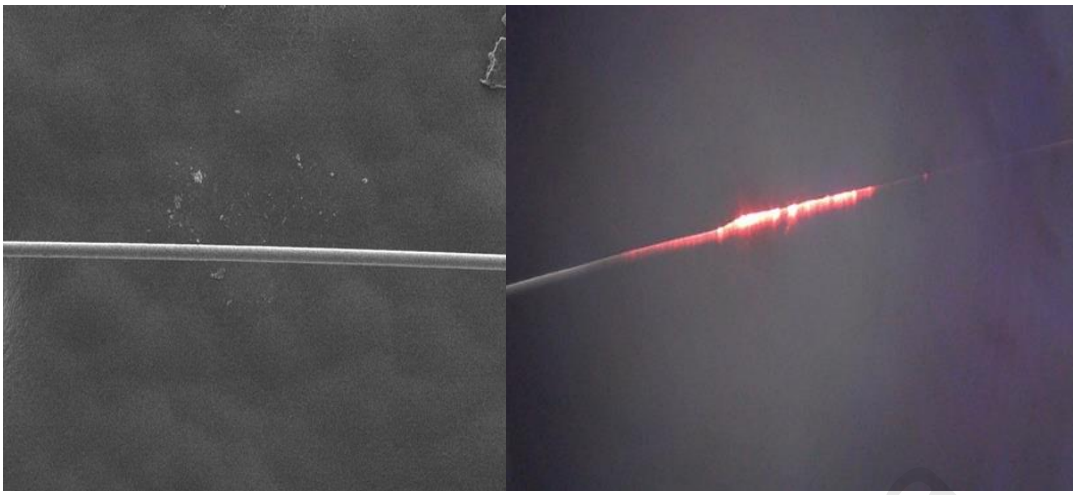

(a) (b)

Figure 5.3: Optical characterization of CdSe doped PMMA microfiber (a) Microscope image of PMMA microfiber doped with Cdse QD with a diameter of 3μm. (b) The PMMA microfiber doped with CdSe QD is excited by a 637 nm light source from the left side.

5.3 Temperature Sensing with CdSe Quantum Dot Doped PMMA Microfiber

One of the biggest challenges nowadays in temperature sensing is the measurement of temperature functional structures within the nanometric range. This is due to the insufficient spatial resolution of conventional techniques such as a thermocouple, which has a spatial resolution of approximately 100 μm. Hence, optical temperature sensors have recently attracted much attention. Recently, polymer microfibers have been promoted as a sensing element in various applications. Polymer microfiber lattice provide excellent hospitality to many functional dopants. These properties make polymer microfiber suitable for photonics devices. In this section, we propose the use CdSe quantum dot (QD) doped PMMA microfiber, by virtue of their small sizes and favorable photostability, for temperature sensing. This work describes non-contact, temperature measurements using both wavelength shifts and intensity modulation approaches.

Figure 5.4 shows schematically how CdSe QDs can be used to detect temperature changes. The input and output ports of the sensor were connected to the

Amplified Spontaneous Emission (ASE) and Optical Spectrum Analyzer (OSA) (ANRITSU MS9710C), respectively. The light from the ASE light source was guided until it reached the PMMA microfiber sensor head, where the light interacted with the temperature sensing material, before being transmitted to the OSA. Optical waveguiding in a single PMMA microfiber was implemented by an evanescent coupling method as described in the previous section (Figure 5.2). In the experiment, the performance of the proposed sensor was investigated for various changes in temperature ranging from 25 ºC to 48 ºC using a hot plate (Pyroceram PC-420D CORNING). The fiber shows slight distortion at 47 ºC and twisted at 69 ºC. However, the light propagating along the fiber maintains well within the selected range. To reduce the influence of any mechanical vibrations, the experimental setup was arranged on a vibration free table.

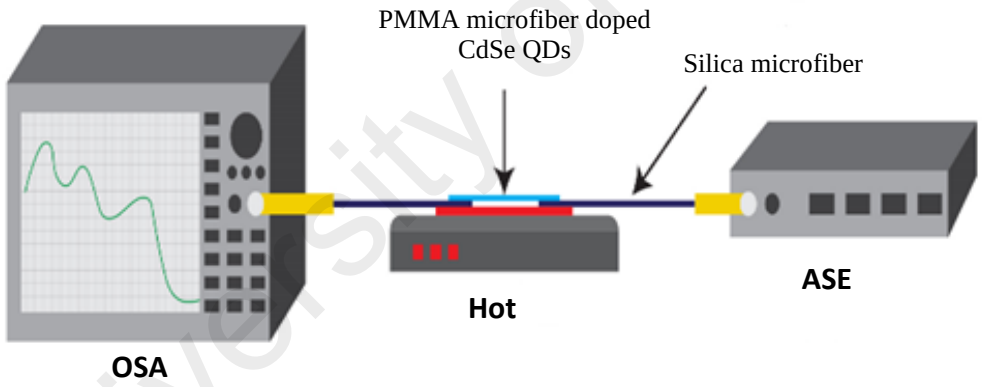

Figure 5.4: The schematic diagram of the experimental set to demonstrate of the use of PMMA doped CdSe QD for temperature sensing

Figure 5.5 displays the representative transmission spectra of the (a) undoped PMMA microfiber and (b) doped PMMA microfiber with an increase in the hotplate temperature. It is observed from Figure 5.5(a) that the peak wavelength exhibits shift to longer wavelengths as the temperature increases. The peak wavelength at 1553.4 nm shifted to 1553.52 nm as the temperature rises from 29ºC to 65ºC. Figure 5.5(b) displays the representative transmission spectra of the CdSe QD PMMA microfiber

with an increase in the hotplate temperature. Similarly, it is observed that the peak wavelength exhibits shift to longer wavelengths as the temperature increases. The peak wavelength at 1548.6 nm shifted to 1548.78nm as the temperature rises from 25 °C to 48 °C. The experiment was repeated several times and the results were quite reproducible.

According to Yuan et al and Sato et al, the PL intensity is enhanced in complex CdSe/PMMA compared with plain CdSe QD (Sato et al., 2007; Yuan et al., 2008). The PL intensity is determined by the competition between radiative and nonradiative processes. The surface of the QD is surrounded by the PMMA matrix after CdSe QD is added into PMMA. In addition, according to Cheng et al, the QD surface is photo-etched, decreasing the QD size and producing interspaces between the PMMA matrix and QD surface after under continuous lasing irradiation. Photo-oxidization desorption of nonradiative recombination centers can occur on the QD surface, making the number of nonradiative recombination centers to be reduced and the effective PL emission is enhanced (Cheng et al., 2012). The transmission light from the ASE may relax molecular chains of PMMA and oxidize the QD surface with photo-etching action, reducing the QD size and causing the peak wavelength shift due to the quantum size effect.

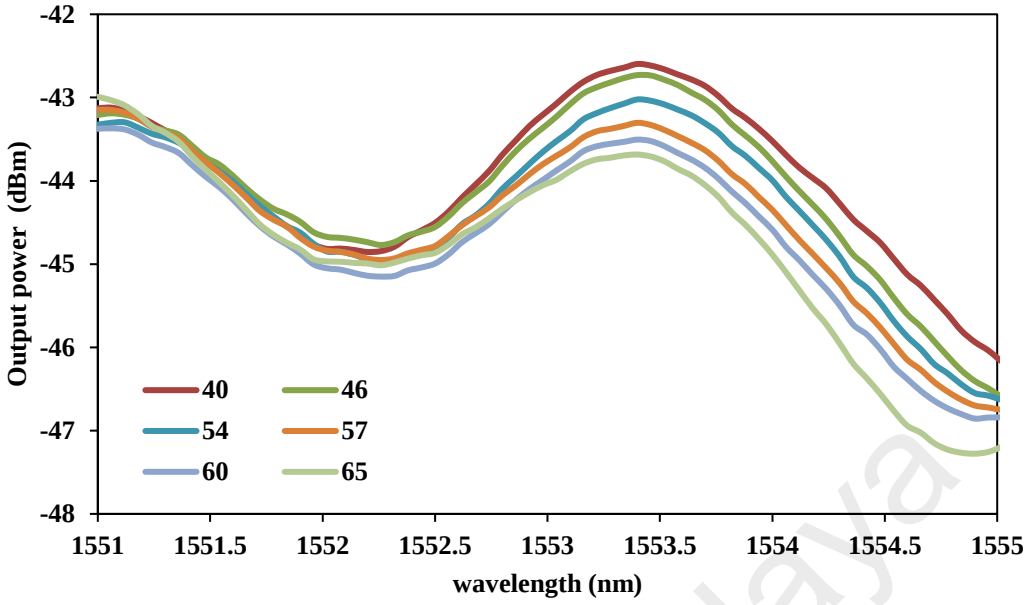

(a)

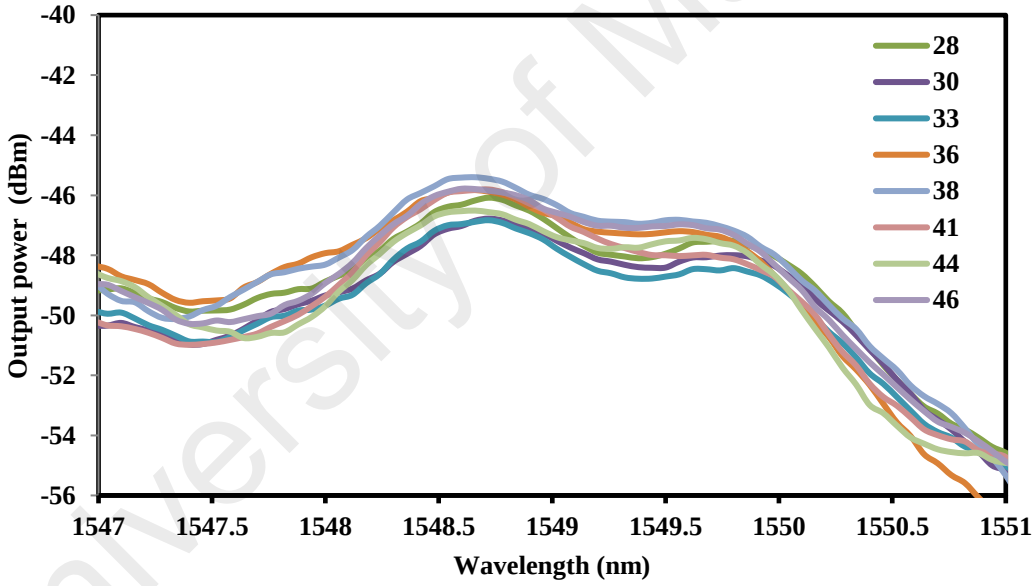

(b)

Figure 5.5: The transmission spectra of the (a) undoped PMMA microfiber (b) doped PMMA microfiber at different temperatures. The arrow indicates the peak wavelength at which its shifting is being analyzed

An alternative explanation is that the incorporation of QDs makes a microfiber with an effectively different index of refraction, which will make the fiber properties different. These transmission spectra are then a measure of the wavelength dependent coupling between all the fibers; as the temperature is changed, the sizes and index of

refraction will change, slightly altering the behavior. This occurs from the coefficient of thermal expansion (CTE) and dn/dT, which improves with the incorporation of QDs.

Figure 5.6 shows the linear function between temperature and output power for the undoped and doped PMMA microfiber. The temperature of the hot plate is then increased from 25 ºC to 48 ºC, resulting in an output signal ranging from-22.50 dBm to -23.04 dBm and -26.2 dBm to -33 dBm for undoped and doped PMMA microfiber respectively. The output signal starts to significantly increase with the rise in hotplate temperature, and at 47 ºC the fiber shows slight distortion and twisted at 69 ºC. The insertion loss of the device are 0.018 dBm and 0.26 dBm for undoped and doped PMMA microfiber, respectively. Figure 5.7 shows the shift of the output wavelength against the temperature for both undoped and doped PMMA microfiber. By referring to the figure, the wavelength increases as the temperature increases. The sensitivity and resolution are obtained at 2.8 pm and 12.34 pm, respectively, with a standard deviation of 34 pm for undoped PMMA microfiber. Meanwhile, the sensitivity of PMMA microfiber doped CdSe QDs is 8.1 pm, with resolution and standard deviation of 7.47 pm and 60 pm, respectively. Figure 5.8 shows the temperature sensor is observed to be very stable for undoped and doped PMMA microfiber. The output power is recorded for 112 seconds and the standard deviation obtained at 25º C for undoped and doped are 0.5% and 0.7%, respectively.

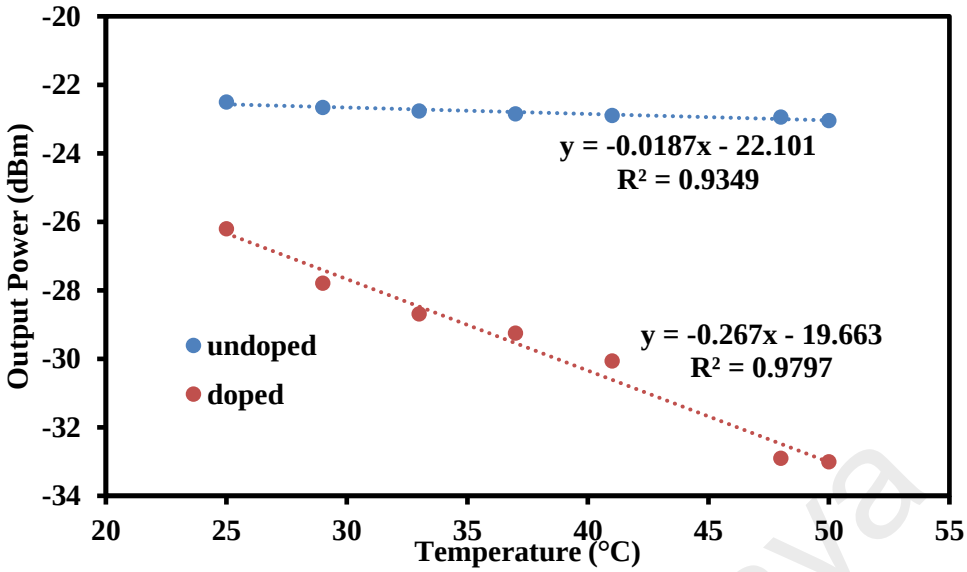

Figure 5.6: Linear relationship between temperature and output power for the undoped and doped PMMA microfiber.

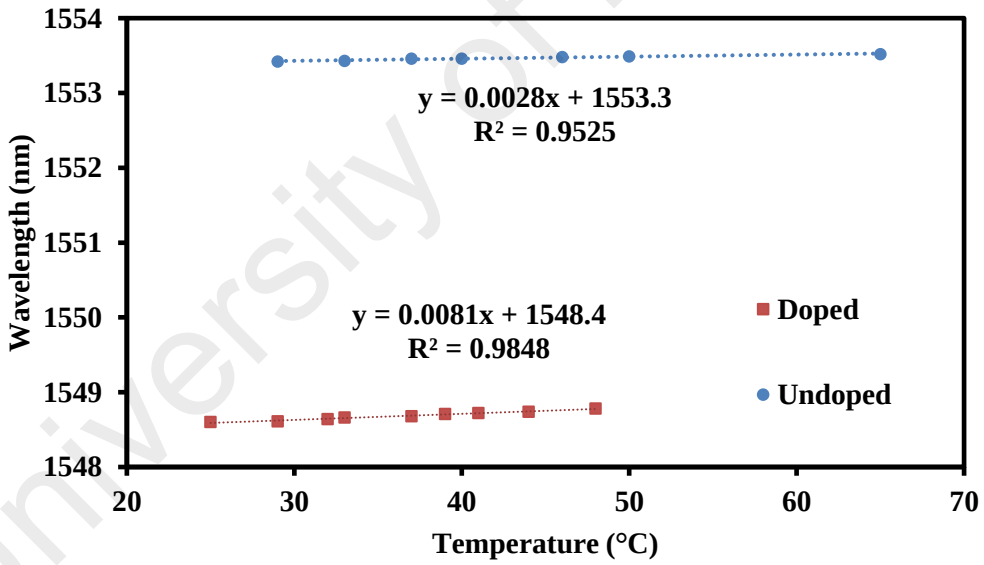

Figure 5.7: Resonance wavelength against temperature for the undoped and doped PMMA microfiber.

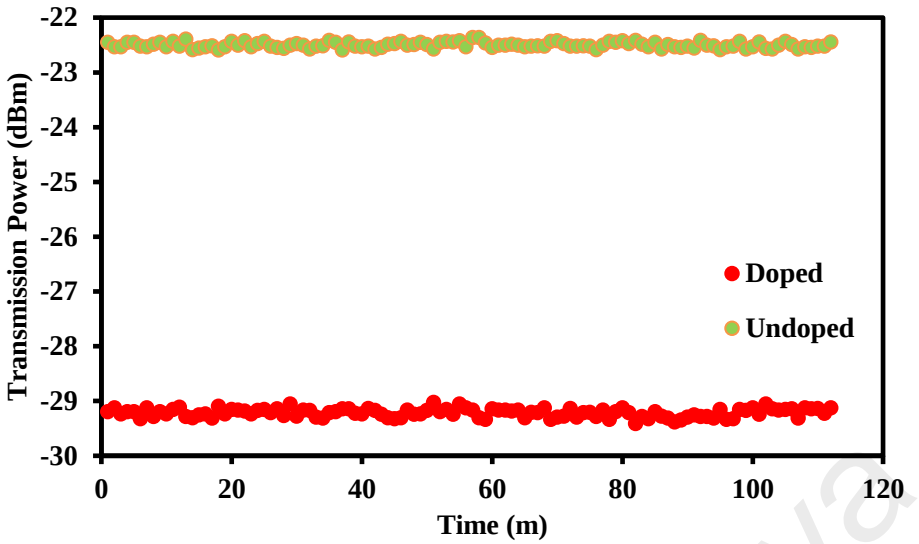

Figure 5.8: The stability characteristics of the sensor using the undoped and doped PMMA microfiber

The performance comparison of the undoped and doped CdSe QD PMMA microfiber based temperature sensor is summarized in Table 5.1. It is observed that the doping of the CdSe QD is able to increase the sensitivity of the sensor by a factor of 14, hence improving the sensor's resolution by 9.4 times. This experiment demonstrates that CdSe QD doped PMMA microfibers are capable of sensing temperature variations and reporting temperature changes remotely through optical readout of the transmission spectra for micro- and nanostructures.

Table 5.1: Performance comparison of the undoped and doped CdSe QDs PMMA microfiber based temperature sensor

Parameters	**Undoped**	**Doped**
Sensitivity (°C)	0.019	0.267
Linearity (%)	More than 93%	More than 97%
Linear Range (°C)	25-48	25-48
Resolution (°C)	2.771	0.292
Standard Deviation (dBm)	0.051826	0.077964

5.4 Q-switched Fiber Laser with CdSe QD Doped PMMA Microfiber as a Saturable Absorber

Fiber-optic technology has attracted many researcher and has been used in many applications. Optical fiber has been developed not only as a medium for communication purpose between two different locations but also for other applications such as sensing and lasers. Fiber laser is more popular to explore and develop because it is proven has more potential and benefits compared to other types of laser like; gas, chemical, dye, solid-state and semiconductor laser. Passive Q-switched fiber laser has been widely demonstrated compared to the active one due to their many advantages such as compactness, simplicity and flexibility of design. Recently, passively Q-switched fiber lasers were explored and reported in Erbium (Er) and Ytterbium (Yb) gain media by using various types of artificial or real saturable absorbers (SAs) (Latiff, Shamsudin, Ahmad, & Harun, 2016)

(Latiff et al., 2016; Tsai et al., 2010). The artificial SA is normally generated by nonlinear polarization rotation effect (NPR) and nonlinear optical loop mirror (NOLM) and it needs to utilize nonlinear fiber property similar to saturable absorption and it was difficult to optimize. Dye color glass was the first real SA and follow by semiconductor saturable absorber (SESAM) (Huang et al., 2009). SESAM required complex fabrication and need to be prepared by using an expensive packaging but it is widely used in the commercial fiber lasers. Lately, the many researchers were also explored other materials such as carbon nanotube (CNT) (Zhou, Wei, Dong, & Liu, 2010) and graphene (Liu, Wu, Yang, & Wang, 2011; Luo et al., 2010; Popa et al., 2010; Zhang, Zhuo, Wang, & Wang, 2012) to generate stable Q-switching pulse fiber laser. CNT was simple and low cost but it often required on broad wavelength range of saturable absorption (Sun, Hasan, & Ferrari, 2012). CNT also has poor stability, low damages threshold and the reliability in short term. Boa et al. (Bao et al., 2009) reported that graphene could provide an outstanding saturable absorption that could counter the drawback of CNT. The

graphene has several advantages such as large saturable absorption modulation depth, ultrafast recovery time and higher damage threshold (Song, Jang, Han, & Bae, 2010; Zhang et al., 2009).

Other two dimension (2D) materials such as transition metal dichalcogenides (TMDs) (Wang et al., 2012) (Woodward et al., 2014; Wu et al., 2015) and Black Phosphorus (BP) have also gained a tremendous interest in recent years for optoelectronics applications. For instance, BP has much attraction since it appears with narrow direct band gap which can fill the gap between graphene and the wide band gap of TMDs. Compared with TMDs and graphene SAs, they do not fit the band gap that required optical materials with the range of 0.8 eV for most optical device which operating at optical communication band but BP has band gap from 0.3 eV to 1.5 eV (Li et al., 2014; Liu et al., 2014). However, BP is hydrophilic material which the performance easily degrades as expose to oxygen and water (Island et al., 2015; Wood et al., 2014). Thus, the exploration of BP in the future may have a limitation.

More recently, quantum dots (QDs) semiconductor crystal, 0D material was also joining the group of nanocluster materials and have given interest by researchers to explore for plenty of applications including SA (Rafailov, Cataluna, Wilcox, & Zolotovskaya, 2009), synthesis of solar cell (Chang & Lee, 2007), as energy filtered electron microscopy (Nisman et al., 2004) and also for biological application (Gao et al., 2004; Jamieson et al., 2007). The QDs that grown on a semiconductor substrate can emit laser from 1.0 μm to 1.9 μm wavelength range (Rafailov, Cataluna, & Sibbett, 2007). Cadmium selenide (CdSe) is one of the promising materials in class of QDs which has unique properties like great photoelectrical characteristic and direct band gap which make it promising materials for photovoltaic and photodetector (Antohe, Ion, & Ruxandra, 2001). The CdSe also have a strong florescence in the visible region which is photon emission from molecule called electron goes from excited state to ground state (Trivedi & Hatch, 2013). The band gap energy of CdSe QDs depends on the size of the crystal, which make it a beneficial materials for biological and chemical sensor (Somers, Bawendi, & Nocera, 2007), and high density optical memory.

In this section, Q-switched Erbium-doped fiber laser (EDFL) is demonstrated by using a new SA based on CdSe QD doped PMMA microfiber. To our knowledge, this is the first demonstration of the Q-switching generation using a polymer microfiber based SA.

5.4.1 Experimental arrangement

At first, a CdSe QD doped PMMA microfiber was fabricated by using a simple drawing technique as described in section 5.2. Before that, a normal single mode fiber (Corning SMF-28) with core and cladding diameters of 0.8 μm and 125 μm, respectively, was tapered about 6 cm long with 3 μm diameter waist. The tapering process was based on a flame brushing technique where the bare fiber, which both sides were fixed onto a fiber holder was heated with a moving flame while pulling one side of the fiber. The tapering region diameter is uniformly decreased when the length of tapering region is increased. Then, we cut the tapered fiber in the middle of the tapered region with ~ 0.25 cm long separation.

Figure 5.8 illustrates the CdSe doped microfiber fabrication process by physically drawing from the composite solution. At first, a single mode fiber with perfectly cleaved fiber-end tip is vertically dropped down and immerse in the molten CdSe-PMMA solution as shown in Figure 5.9 (a). Then, the collected molten CdSe-PMMA droplet be vertically deposited onto one side of tapered fiber (Fig. 5.9 (b)). Finally, the SMF is moved horizontally about 0.25 cm long in slow speed of 0.1-1 ms^{-1} to another end of tapered fiber (Figure 5.9(c)). This process is repeated until the molten CdSe-PMMA droplet fully reconnected to another end of the tapered silica fiber via van der Waals and electrostatic force (Gilberto Brambilla, Xu, & Feng, 2006). The molten CdSe-PMMA droplet quickly quenched in air, and subsequently obtained the free-standing CdSe doped microfiber. The connection can be reformed depends on the diameter of the tapering region that related to the electrostatic force which allow the combination happened. The microfiber diameter can be controlled by the pulling speed and viscosity of the polymer (which depends on the hot plate temperature).

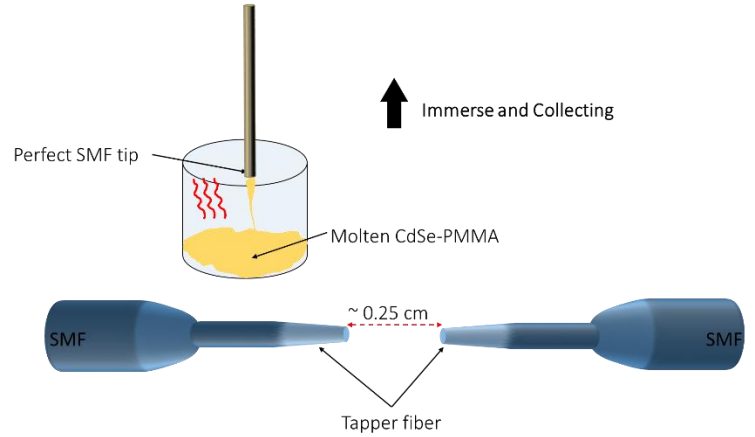

(a)

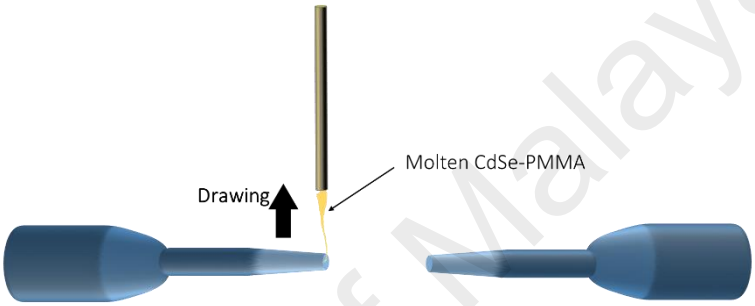

(b)

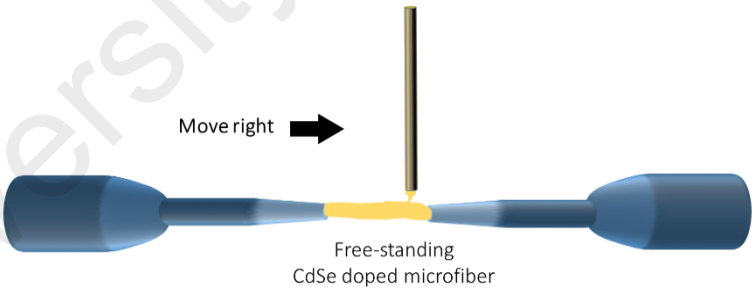

(c)

Figure 5.9: Illustration of free-standing CdSe doped PMMA microfiber fabrication process. (a) SMF tip is vertically immersed in the molten CdSe-PMMA solution (b) the molten polymer is transferred to the one side of tapered fiber and vertically drawn up (c) the polymer microfiber is horizontally moved to another side of the tapered silica fiber.

The nonlinear optical profile of the fabricated CdSe was also measured by using the twin-balanced detector measurement (I-scan). Figure 5.10 shows the result, which indicates that this CdSe has a modulation depth, a saturable intensity, and a non-saturable absorption of 11 %, 0.25 MW/cm^2, and 34 %, respectively. These obtained

parameters are capable to generate a pulse train in both Q-switched and mode-locked regimes. Here, the generation of Q-switching pulse train in EDFL is demonstrated by using the CdSe doped PMMA microfiber, which is placed between two cutting microfiber tips which are connected to an EDFL cavity.

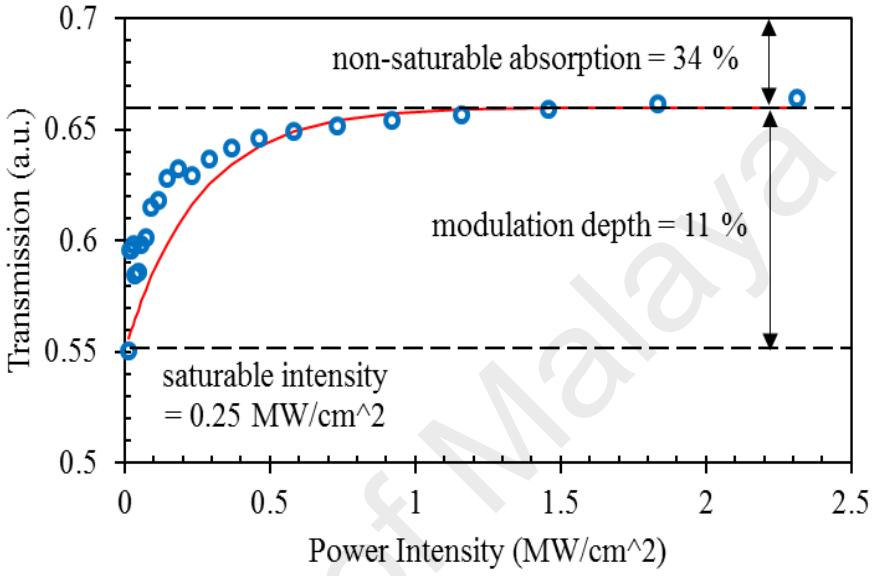

Figure 5.10: Nonlinear optical profile of the CdSe microfiber

Figure 5.11 (a) shows the experimental setup of the proposed Q-switched EDFL using a CdSe-doped PMMA microfiber as an SA. It employs a 2.4 m long Erbium-doped fiber (EDF), which was pumped by a 980 nm laser diode via wavelength division multiplexer (WDM) as the gain medium. The EDF used has an Erbium ion concentration of 2000 ppm, and numerical aperture (NA) of 0.24. An isolator was used to force the unidirectional direction of the laser operation. A 2.5 cm long CdSe-doped PMMA microfiber, which is placed two tapered silica fiber functions as a Q-switcher device. It was connected in between the 10 dB output coupler and isolator via fiber connector. The output from the laser cavity is extracted by the output coupler while allowing 90% of the photons to oscillate in the cavity. It was fed into an optical spectrum analyser (OSA) for optical spectral measurement and oscilloscope via a fast photodetector for pulse train measurement. Optical power meter was swapped with optical

spectrum analyzer (OSA) for average output power measurement while the radio frequency spectrum analyser (RFSA) was swapped with oscilloscope for RF spectrum measurement. The measured total cavity length was 9 m. Figure 5.10 (b) shows schematic diagram and actual image of the CdSe doped PMMA microfiber based SA device when the red light was injected via a taped silica fiber. As shown in the figure, the red light was well propagated through the CdSe microfiber via the tapered fiber with waist diameter of around 3 µm.

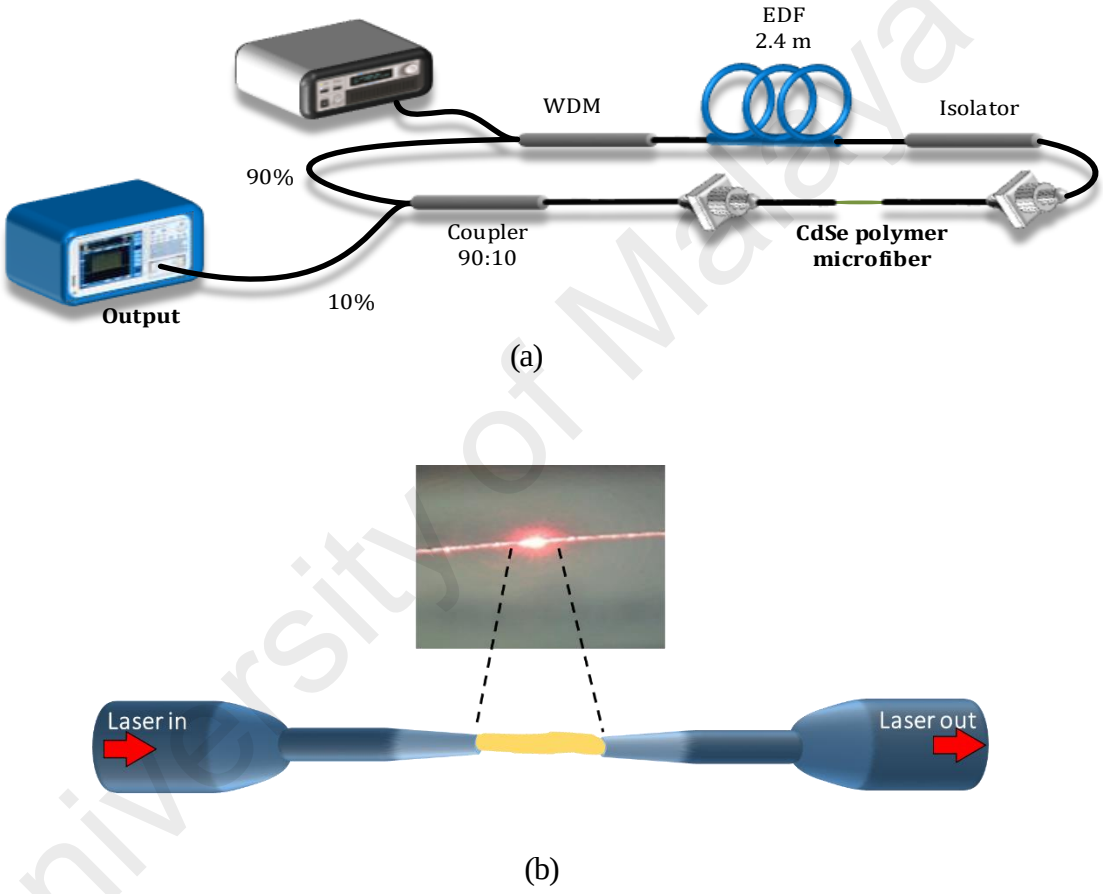

Figure 5.11: Experimental setup of Q-switched EDFL. (a) Ring cavity configuration. (b) Microfiber structure with molten CdSe-PMMA. Inset image is an actual image of CdSe microfiber when it is injected by red light via the tapered silica fiber.

5.4.2 Q-switching performance

As the pump power is increased, the EDFL starts to generate continuous wave (CW) laser at pump power 21 mW. The fiber laser changes its state of operation from CW to Q-switched regime when the pump power reaches 34 mW to generate pulse train at repetition rate

of 37 kHz. Such a low threshold power for Q-switching operation is attributed to the small intra-cavity loss performed by the SA device. The repetition rate increases as the pump power increases up to 74 mW. Figure 5.12 shows the output spectrum of the Q-switched EDFL at the pump power of 74 mW. It indicates that the laser operates at wavelength of 1533.5 nm. Figure 5.13 illustrates the typical oscilloscope trace of the Q-switched EDFL at the pump power of 74 mW. The distance between pulses is measured to be around 15.6 µs, which corresponds to the repetition rate of 64 kHz. The generated pulse has a constant shape, frequency and pulse width with no timing jitter presence. A single pulse profile at this pump power has full width half maximum (FWHM) of 4.84 µs.

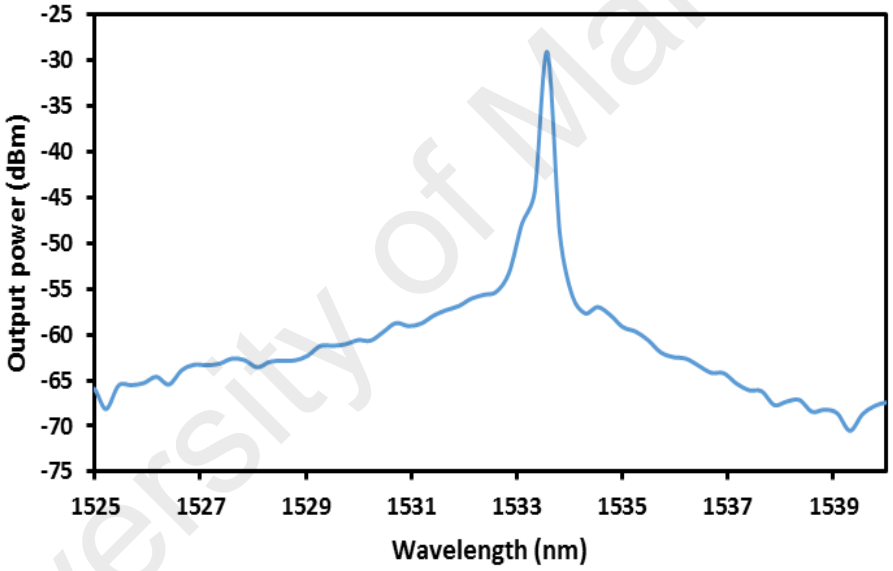

Figure 5.12: Output spectrum of the Q-switched EDFL at pump power of 74 mW

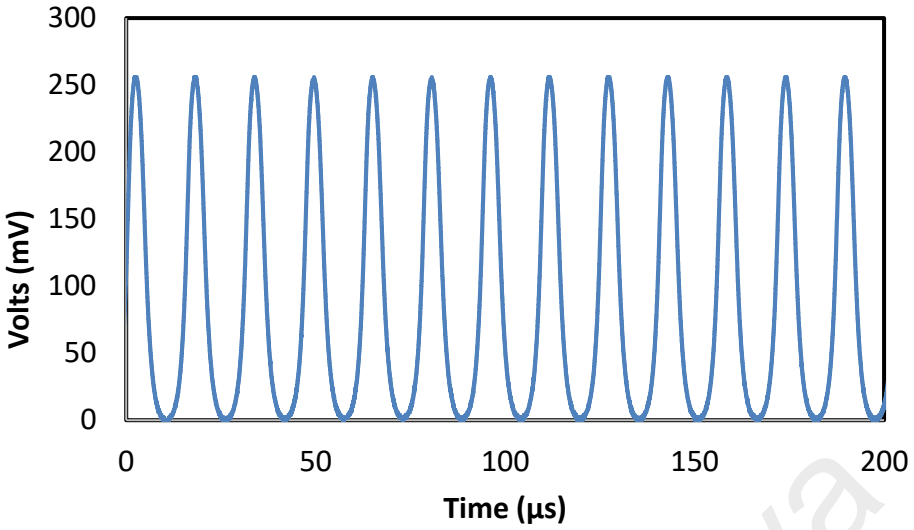

Figure 5.13: Typical pulse train of the Q-switched EDFL at pump power of 74 mW

Figure 5.14 depicts the relationship between pulse repetition rate and pulse width with input pump power. Stable output pulses train with monotonic increment of repetition rate from 37 kHz to 64 kHz was observed as the 980-nm pump power increased from 34 mW to 74 mW. This differ for pulse duration measurement as it narrowed and shortened from 7.96 µs to 4.84 µs which typical characteristic of Q-switching operation. As pump power increases, more power circulates inside the laser cavity, thus hasten the saturation of SA. It is also observed in Figure 5.14 that smaller changes of pulse width from 48-74 mW indicates the SA were almost saturated with continually increasing the light intensity (pump power). Furthermore, pulse operation was switched into CW mode as the pump increased above than 74 mW. As confirmation for contribution of CdSe based SAs to generate the Q-switching pulse fiber laser, the SAs was removed and the there is no pulse train on the oscilloscope and it operated under normal cavity condition.

Figure 5.15 shows the output power of EDF fiber laser and calculated energy pulse fiber laser correspond to the variation of pump power from 34 mW to 74 mW. It shows that output power of EDF linearly with increment input power. The maximum output power of about 0.21 mW is recorded at maximum pump power 74 mW. On the graph, the calculated slope efficiency of the Q-switch laser at 0.25% when the maximum pulse energy was calculated

at 22.35 nJ. The pulse energy shows the increment steadily with the increment of pump power. This can be realized from the strong modulation of the net gain. The increment of pump power leads to a raise of average output power and shorten the pulse width and hence higher pulse energy is extracted in the Q-switching process.

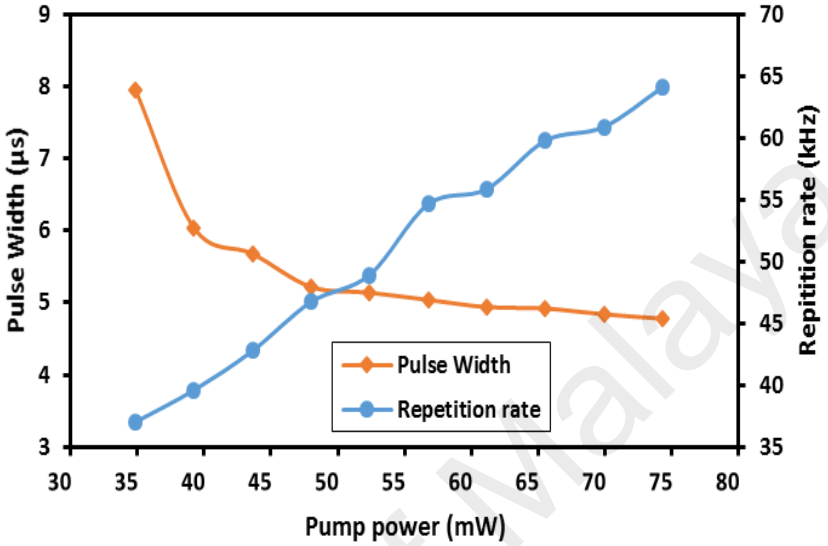

Figure 5.14: Repetition rate and pulse width within 34 mW to 74 mW pump power

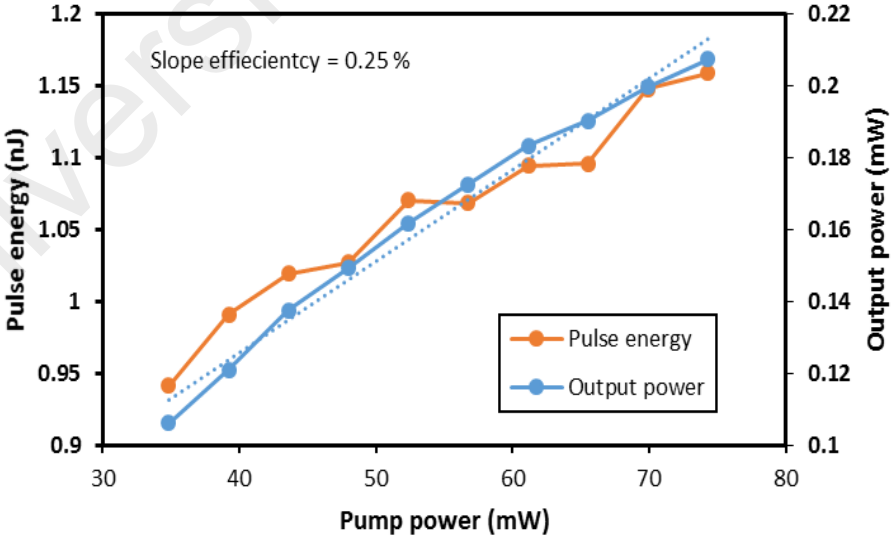

Figure 5.15: Output power and pulse energy within 34 mW to 74 mW pump.

Figure 5.16 shows the RF spectrum of the Q-switched EDFL at the maximum pump power at 74 mW. The RF spectrum are correspond to it time domain which is related with Fourier Transform. Signal to noise ratio (SNR) of the fundament frequency is obtained at 47 dB, which indicates the stability of the laser.

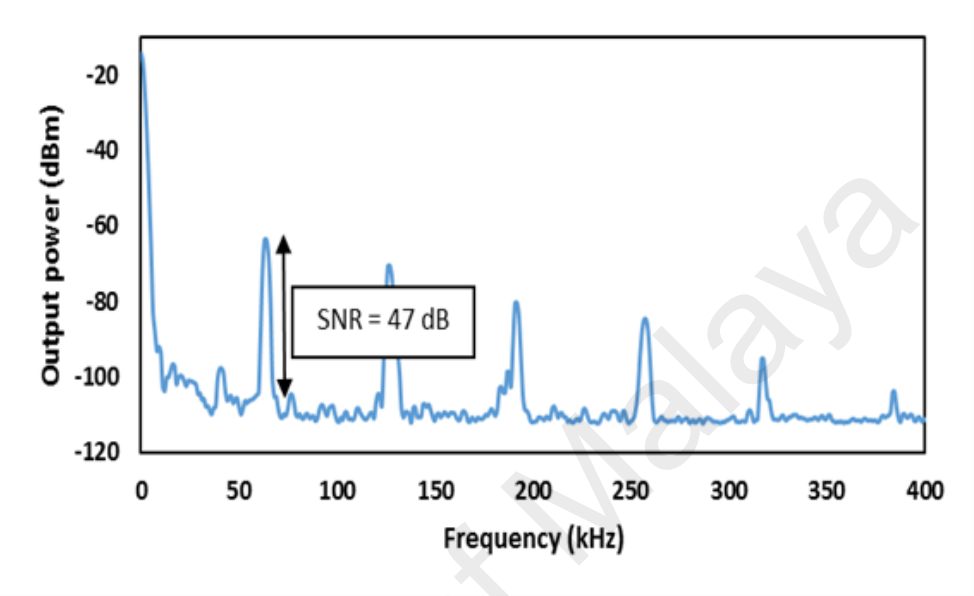

Figure 5.16: Typical RF spectrum of the Q-switched EDFL at pump power of 74 mW.

5.5 Mode-locked Fiber Laser with CdSe QD Doped PMMA Microfiber as a Saturable Absorber

Pulsed fiber laser have become one of the main research topic in photonic field since it would benefit a lot of application including industrial machining, medical surgery, spectroscopy, free-space imaging and distance ranging (Amann, Bosch, Lescure, Myllyla, & Rioux, 2001; Nelson et al., 1997; Schaffer, Brodeur, & Mazur, 2001). While the continuous wave (CW) laser output have reach 100 kW (Shcherbakov et al., 2013), the ultrashort pulsed laser still far way behind it with the maximum power achieved of only 100 W (Richardson, Nilsson, & Clarkson, 2010), a troubling percentage of only 0.001% compared to those of CW laser. Several pulse generation methods have been discovered, which passive methods using saturable absorber (SA) is most desired since it does not involve any externally controlled system to modulate the

pulse. Two classes of SA, categorized in either artificial or real SA, have been extensively studied where the artificial SA utilize non-linearity effect of optical fiber to mimic the real SA saturation absorption ability. However, despite of having low loss since it is based on all-fiber cavity, artificial SA mechanism such as nonlinear polarization rotation (NPR) (Matsas, Newson, Richardson, & Payne, 1992; Tang, Zhao, Zhao, & Liu, 2005), nonlinear optical loop mirror (NOLM) (Doran & Wood, 1988) and nonlinear amplifying loop mirror (NALM) (Fermann, Haberl, Hofer, & Hochreiter, 1990) are difficult to optimized and tend to be very sensitive to movement and heat imposed to the system. Therefore, high motivation shift towards the real SA which utilizing the saturation absorption of specific material to produce pulsed laser. The first material discovered in this class was the ion-doped crystal (Bret & Gires, 1964) and bleachable dye (Soffer, 1964), which several pulse generation abilities were successfully demonstrated on bulk laser. The success was followed by the discovery of quantum dots (QD) semiconductor where Q-switched pulse laser was demonstrated using PbS SA in ruby laser (Guerreiro et al., 1997). However, the use of QD semiconductor as SA diminished along with the obsolete bulk laser.

In early 90s, semiconductor saturable absorber mirror (SESAM) have been introduced where its popularity increased rapidly and remain as the most used SA device in commercial market until present day (Keller et al., 1992; Zirngibl et al., 1991). However, it was discovered later on that SESAM have a narrow operational bandwidth and low damage threshold, preventing it to be applied in high power laser and ultrashort pulse application (Keller, 2003). Therefore, continuous research is carried out to develop better SA which lead to the carbon nanotubes (CNT), a one-dimensional material wrapped into a hollow tube (Set et al, 2004). Despite of having ability to generate ultrashort mode-locked pulse, CNT induce high loss due to broad tube diameter to cover broad operational wavelength. Next discovery witness an important

milestone in photonic history, which is the emergence of graphene (Bao et al., 2009). This first two-dimensional material (Woodward & Kelleher, 2015) hold great promising to become best SA since it have zero bandgap, thus enabling operation in all wavelength spectrum (Geim & Novoselov, 2007). Even though that it has many special attribute that overcome many problem induced by previously developed SA, graphene eventually have a very low modulation depth, typically less than 1% per layer (Cafiso et al., 2013; Janulewicz et al., 2014). Transition metal dichalcogenides (TMD) is another promising material that having tunable bandgap by varying its number of layers (Q. H. Wang et al., 2012). However, its high bandgap energy preventing it to be used in near and mid-infrared application (Bonaccorso & Sun, 2014). Recently, a new material that have nearly similar features like graphene is discovered which is the black phosphorus (BP) (Xia, Wang, & Jia, 2014). This material successfully overcome the high bandgap problem which its bandgap can be tunable from 0.3 to 2.0 eV by varying its number of layer which correspond to 600 to 4000 nm operational wavelength (Tran, Soklaski, Liang, & Yang, 2014). However, BP is environmentally unstable and tend to get easily damaged when exposed to water molecule and oxygen, thus reduce its reliability and complicate its fabrication (Island et al., 2015).

Polymer optical fibers have generated much research interest in recent years because of its many attractive properties including biocompatibility, good processability, high flexibility, tunable properties, and low cost for integration (Jin & Granville, 2016b; Koike & Koike, 2011; Wang, et al., 2013). Therefore, it is often chosen as excellent hosts for functional dopants materials including quantum dots (Meng et al., 2011; Yu et al, 2011), enhancing their capabilities of generating and propagating light at the microscale. Incorporation of quantum dots (QD) material into PMMA microfibers can alter the optical properties of the microfibers (Tatavarty et al., 2011) since QD possess unique optical and electronic properties such as quantum

confinement effect, continuous absorption profiles, robust signal intensity and high photochemical stability (Alivisatos, 1996). In recent years, many studies focused on CdSe QDs because of its high luminescence quantum yield, narrow band gap and a variety of optoelectronic (Zhu et al., 2000). For instance, in the previous sections, a CdSe doped PMMA microfiber has been fabricated and demonstrated for temperature sensor and Q-switched fiber laser applications. However, so far there is no scientific report of using QD CdSe doped PMMA microfiber to produce mode-locked pulsed based on all-fiber laser. In this section, a mode-locked fiber laser is demonstrated using the fabricated QDs CdSe doped PMMA microfiber as SA.

5.5.1 Configuration of the Mode-locked Fiber Laser

Figure 5.17 shows the experimental setup of the proposed mode-locked laser using CdSe QDs doped PMMA microfiber. The cavity employed Ytterbium doped fiber (YDF) as a gain medium to generate a mode-locking pulse train operating at 1 μm region. The YDF has a group velocity dispersion (GVD) of -18 ps^2/km and cladding absorption coefficient of 3.95 dBm at 975 nm wavelength. It was pumped by a 980 nm multimode laser diode that provide sufficient input power gain through a multimode combiner (MMC). The YDF was then connected to a 10dB optical coupler with a splitting ratio of 90/10 where the 10% of the output was filtered out from the cavity and channeled to the measurement devices. The rest 90% of the remaining laser beam was maintained inside the cavity to allow it to oscillate along the line to improve the laser beam generation. A CdSe QDs doped PMMA microfiber was placed between two tapering silica fiber with diameter ~ 22 μm (SMF, Corning 28) and the tapering silica fiber were coupled by direct spliced to another fiber. In addition, a polarization controller (PC) was used to adjust the polarization state of the laser beam. The rest of the fibers inside the cavity were standard–single-mode fiber (SMF) with a GVD of 44.2 ps^2/km while the total cavity is measured at 15.8 m with a normal dispersion of ~ 0.076 ps^2. The laser output

was measured by the means of wavelength spectrum, pulse train characteristic, signal-to-noise ratio (SNR) and optical power. These data is well obtained by an optical spectrum analyser (OSA, Yokogawa AQ6370B), 500 MHz oscilloscope (OSC, GW Instek GDS-3352), and 7.8 GHz RF spectrum analyser (Anritsu MS2683A) via a 1.2 GHz InGaAs photodetector (Thorlabs DET01CFC).

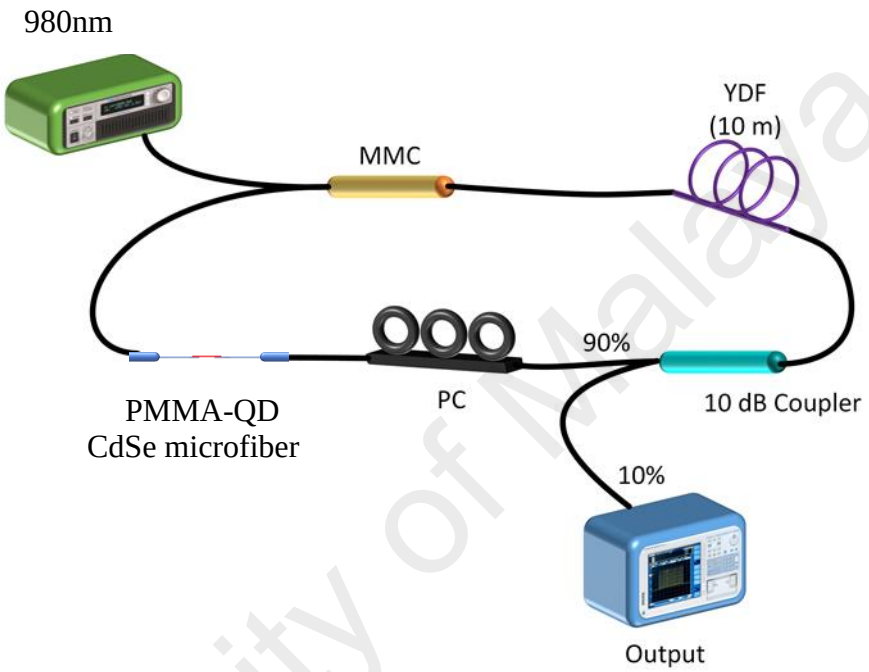

Figure 5.17: Configuration of the mode-locked Ytterbium-doped fiber laser

5.5.2 Performance of the Mode-locked Fiber Laser

The Ytterbium doped fiber laser (YDFL) starts to produce a CW narrow laser beam at pump power of 295 mW. As the pump power is slightly increased to 323 mW, mode-locked pulses emerge with a fundamental repetition rate of 12.6 MHz. The mode-locking operation remains stable until 481 mW and disappears as the pump power continue to increase. Figure 5.18 shows the output spectrum of the mode-locked YDFL which is obtained at the threshold pump power. As shown in the figure, the mode-locking operation exhibits single wavelength spectrum centered at 1087.5 nm with

narrow spectral bandwidth of 0.7 nm. The spectrum did not exhibit any trace of Kelly side band which confirming that the mode-locked operate in normal dispersion.

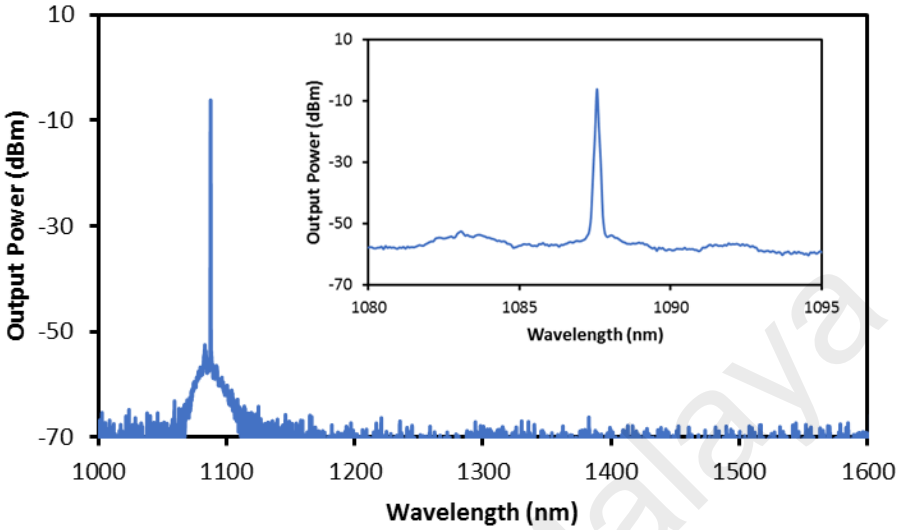

Figure 5.18: Output spectrum of the mode-locked YDFL. Inset shows the enlarged figure.

Figure 5.19 shows the pulse train of the mode-locked pulse with stable and constant frequency of 12.6 MHz with peak-to-peak duration of 79 ns, in agreement with the cavity length roundtrip of 15.8 m. Even though that the value of pulse width measured by oscilloscope was obtained at 33 ns, the actual pulse width should be very much smaller which this mismatch value occurs due to the limitation of oscilloscope resolution. However, the actual pulse width value can be obtained by either using an auto-correlator device or by using calculation method based on time bandwidth product (TBP). The TBP value was estimated at 0.441 based on the Gaussian profile, resulting minimum value of actual pulse width to be about 2.49 ps.

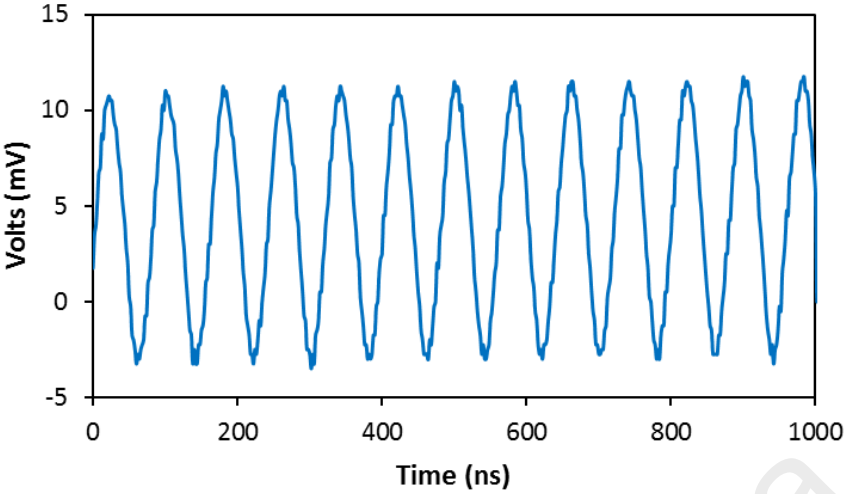

Figure 5.19: Typical pulse train of the mode-locked pulse

Figure 5.20 shows the RF spectrum of the mode-locked operation where fundamental repetition rate recorded at 12.6 MHz with significantly high signal-to-noise ratio (SNR) of 47 dB, indicating high stability of the pulse generated. The presence of several harmonic frequencies confirmed that the pulse is having narrow pulse width. For this experiment, it was verified that the QD CdSe SA solely contributes the mode-locked pulse where no pulse train was observed at all pump level when the SA is removed. Figure 5.21 shows the relationship between the output power and the input pump power where the output power is gradually increased from 5 to 14 mW with the increment pump power from 323 to 481 mW that lead to slope efficiency of 6.3 %. The graph also shows the increment of pulse energy where the maximum pulse energy obtained is 1.1 nJ. These overall results indicate that the QD CdSe SA embedded in microfiber have a promising potential to become a mode-locking device.

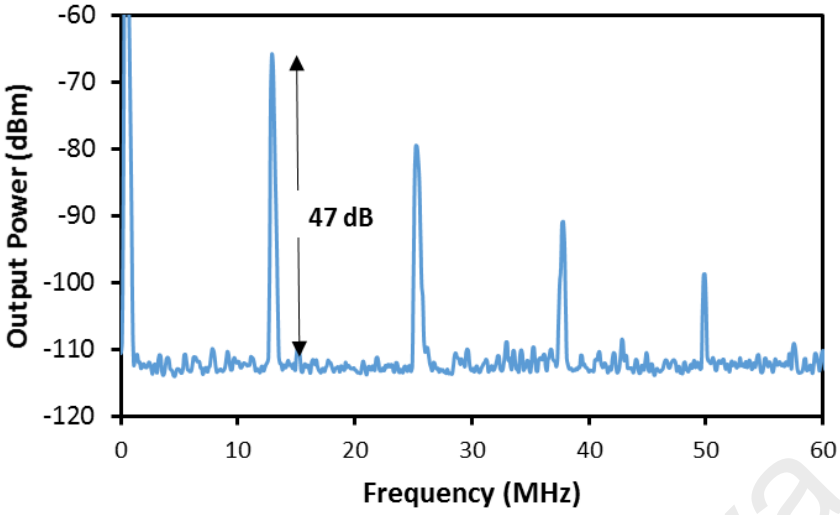

Figure 5.20: RF spectrum of the mode-locked pulse

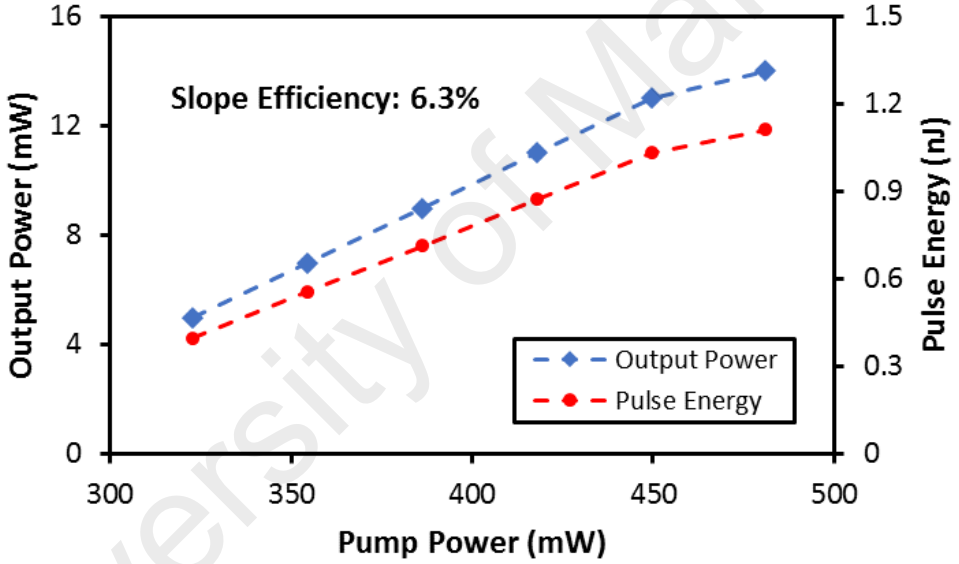

Figure 5.21: Output power and pulse energy against pump power of the mode-locked YDFL

5.6 Summary

A simple CdSe QD doped PMMA microfiber was fabricated using direct drawing technique for temperature sensing, Q-switched and mode-locked laser applications. The sensor probe was fabricated by bridging two tapered single mode fibers with the PMMA microfiber and its performance was investigated with and without the doping of the CdSe-ZnS core-shell quantum dot (QD). The experimental

results show that the doped PMF is able to achieve a higher performance with a reasonably good sensitivity of 58.5 pm/°C based on the wavelength shifting which is about eighteen times than that of the undoped PMMA microfiber temperature sensitivity. As such, this technique has the potential to be applied to non-contact micro- and nanotemperature measurements. Then, a Q-switched EDFL with a slope efficiency of 0.25 % was achieved using the fabricated CdSe doped PMMA microfiber as an SA. The SA has a modulation depth of 11 %. Variation of pump power within 34 mW to 74 mW generates the stable Q-switching operation with the repetition rate was tuned from 37 kHz to 64 kHz. The pulse width was decreased from 7.96 µs to 4.78 µs with the increment of pump power. At pump power of 74 mW, the maximum pulse energy was measured about 22.35 nJ. A passive mode-locked fiber laser operating at 1087.5 nm was also successfully demonstrated using a 10 m long double-clad YDF as a gain medium in conjunction with the CdSe doped PMMA microfiber as a SA. The stable mode-locked pulses were attained from threshold pump power of 323 mW to 481 mW. The consistent pulse repetition rate of 12.6 MHz was obtained with 47 dB SNR. At 481 mW pump power, the maximum pulse energy and output power were about 1.1 nJ and 14 mW, respectively.

CHAPTER 6

CONCLUSION AND FUTURE RESEARCH

6.1 Conclusion

Recently, optical polymer microfibers have attracted growing interests due to its vast potential as building blocks for photonics circuitry and integration. Compared with microfiber composed of inorganic material such as glasses or semiconductors, polymer microfiber shows many amazing characteristics such as a high fractional evanescent fields, tight optical confinement, an ultra-small allowable bending radius, fast evaporation and small foot print. Besides these characteristics, polymer microfiber also offers fascinating properties such as the polymer matrix is hospitable to a variety functional dopants, which can be readily employed to tailor the optical, electrical and magnetic properties of the host microfiber. Secondly, it exhibits excellent mechanical flexibility and biocompatibility. In addition, polymer microfiber offers more possibilities for sensing applications due to have a perm-selective nature with respect to gas molecule and high flexibility of surface functionalities.

In this work, polymer microfiber have been successfully fabricated using a one-step direct drawing technique. Polymer microfibers with diameters ranging from 6 to 12 μm and lengths up to few centimeters were fabricated by this technique. PMMA polymer is used in this work as it has many interesting properties such as high transmittivity for visible light and a refractive index of 1.49, which provides a good optical confinement. The microfiber exhibits high surface smoothness and length

uniformity. The microfiber losses were obtained at 0.37 dB/mm, 0.27 dB/mm and 0.19 dB/mm for the microfiber diameters of 6 μm, 8 μm and 12 μm, respectively.

Then, three types of optical sensors were demonstrated based on a PMMA microfiber. The probe was immersed in various solutions to be sensed and the sensor operated based on both intensity modulation and interferometric techniques. At first, the microfiber sensor was proposed and demonstrated for the detection of various concentrations of $KMnO_4$ solution. The proposed sensor has a sensitivity of 32.57 μW/% with a resolution of 0.0064%. The second PMMA microfiber sensor was used to sense the relative honey adulteration based on intensity modulation technique. As the solution concentration of the adulterated honey solution varies from 1% to 6%, the output power of the polymer microfiber has been decreased from 3.51 to 1.15 μW with a sensitivity of 0.49 μW/% and a linearity of more than 96.97%. Finally, an uric acid biosensor was also demonstrated using a PMMA microfiber coated with an Al doped ZnO nanostructure as a probe. The PMMA microfiber was coated with Al-doped ZnO nanostructure using a sol-gel process. The sensor has a sensitivity of 0.010 dB/ppm with a good linearity of more than 99 %. Our results show that the PMMA microfiber are promising for these sensing applications with high sensitivity, stability, and repeatability.

Later, various sensitive coating and doping materials have been investigated to develop polymer microfiber sensors for relative humidity (RH) measurement. At first, a RH sensor probe was developed using PMMA microfiber loop resonator (PMLR) structure coated with ZnO nanorods. It was observed that the output intensity of the sensor decreased linearly with RH with sensitivity of 0.5221 dBm/%, linearity of more than 99% and resolution of 0.4094%. Beside the loop structure, knot structure of polymer microfiber was also used in this work. Resonator-type sensors allow light to

recirculate at resonant, overlap and couple, thereby effectively increase the optical path, thus creating compact sensors with high Q-factors which is predicted to be as high as ~10^9. The performance of the PMMA microfiber knot resonator (PMKR) sensor was investigated for various RH levels, ranging from 50% to 80%. Different values of RH were simulated by controlling the moisture of the surrounding using salt solution. Resonant wavelength shift against relative humidity for PMKR with and without ZnO was compared. We observed an increase of sensitivity level, approximately 1055 pm change of resonant wavelength for RH changing from 50% to 80% (437 pm wavelength shifted for 5% humidity change). Compared to the uncoated PMKR, there is a slight resonant wavelength shifting of 370 pm that might be caused by the polymer microfiber's sensitivity towards RH itself. The extinction ratio is about 10.0 dB and 7.0 dB, before and after the PMKR was coated with ZnO, respectively. In comparison, when the PMKR is used instead of the PMLR, an improvement in the sensitivity and resolution of the sensor was observed. This is because the PMKR induces more portion of the evanescent wave outside of the microfiber, enabling more interaction with the relative humidity It is observed that the coating of the ZnO nanostructure onto the microfiber is able to further increase the sensitivity of the sensor hence improving the sensor's resolution. The ZnO nanorods is a hydrophilic material and water molecules can be easily absorbed by the ZnO layer of the PMLR in a humid environment. The increase in water molecules being absorbed by ZnO layer increases the RI of the effective coating of the fiber which leads to a larger leakage of light. This induces an additional mass on the surface which influences the transmission characteristics of the sensor. The increase in the water molecules in higher humidity levels increases both the effective index of the surrounding medium and the absorption coefficient of the ZnO composite, justifying the improved performance of the probe sensor coated with ZnO

nanorods. The coating of sensitive material onto the tapered fiber has successfully enhanced the performance of the microfiber as a humidity sensor.

In another approach, the PMMA microfiber was doped with agarose gel for RH sensing application. For instance, as the RH increases from 50% to 80%, the peak wavelength shifted against RH at a rate of 21.4 pm/% and 28 pm/%, and with a linearity of 98.36% and 98.83% for the un-doped PMMA and agarose doped PMMA microfiber, respectively. Doping PMMA microwires with agarose offered an enhancement in power changes in response to RH variations with a sensitivity of about 0.1 μW/%RH and a linearity of more than 97%. Based on the standard deviation of 0.011μW, its resolution is obtained at 0.2%. When the relative humidity increases, the diffusion of water molecules into the sensor probe causes reduction in the refractive index of the sensor probe. Agarose is a hydrophilic material with high porosity which allows the absorption of moisture and displays good sensitivity as a humidity sensor.

In this work, a simple CdSe QD doped PMMA microfiber was also developed and fabricated using direct drawing technique for temperature sensing, Q-switched and mode-locked laser applications. PMMA microfiber doped CdSe with diameter 3μm has been successfully fabricated by direct drawing technique. The experimental results show that the doped PMF is able to achieve a higher performance with a reasonably good sensitivity of 58.5 pm/℃ based on the wavelength shifting which is about eighteen times than that of the undoped PMMA microfiber temperature sensitivity. The insertion loss of the device are 0.018 dBm and 0.26 dBm for undoped and doped PMMA microfiber, respectively.The fiber shows slight distortion at 47 ºC and twisted at 69 ºC. However, the light propagating along the fiber maintains well within the selected range. the PL intensity is enhanced in complex CdSe/PMMA compared with plain CdSe QD. The PL intensity is determined by the competition between radiative and nonradiative processes. The surface of the QD is surrounded by the PMMA matrix after CdSe QD is

added into PMMA. In addition, the QD surface is photo-etched, decreasing the QD size and producing interspaces between the PMMA matrix and QD surface after under continuous lasing irradiation. The transmission light from the ASE may relax molecular chains of PMMA and oxidize the QD surface with photo-etching action, reducing the QD size and causing the peak wavelength shift due to the quantum size effect. As such, this technique has the potential to be applied to non-contact micro- and nanotemperature measurements.

Finally, a Q-switched EDFL with a slope efficiency of 0.25 % was achieved using the fabricated CdSe doped PMMA microfiber as an SA. The SA has a modulation depth of 11 %. Variation of pump power within 34 mW to 74 mW generates the stable Q-switching operation with the repetition rate was tuned from 37 kHz to 64 kHz. The pulse width was decreased from 7.96 μs to 4.78 μs with the increment of pump power. At pump power of 74 mW, the maximum pulse energy was measured about 22.35 nJ. A passive mode-locked fiber laser operating at 1087.5 nm was also successfully demonstrated using a 10 m long double-clad YDF as a gain medium in conjunction with the CdSe doped PMMA microfiber as a SA. The stable mode-locked pulses were attained from threshold pump power of 323 mW to 481 mW. The consistent pulse repetition rate of 12.6 MHz was obtained with 47 dB SNR. At 481 mW pump power, the maximum pulse energy and output power were about 1.1 nJ and 14 mW, respectively.

6.2 Future Work

The implementation of polymer microfiber doping with sensitive material in the laser applications is still in the early stages and need further research. Bearing this in mind, the system can be improved in the future via the use of doping with sensitive material, which will significantly enhancements their capabilities of generating,

propagating, converting and modulating light at the micro/nanoscale for laser applications. Future work should focus on a new doping sensitive material such as Polyanyline and nickel to enhance the sensitivity of the sensor and the most important thing is to find new applications for the polymer microfiber in laser generation.

REFERENCES

Adomavičiūtė, Erika, & Milašius, Rimvydas. (2007). The influence of applied voltage on poly (vinyl alcohol)(PVA) nanofibre diameter. *Fibres & Textiles in Eastern Europe, 15*(5-6), 63.

Agarwal, Seema, Greiner, Andreas, & Wendorff, Joachim H. (2013). Functional materials by electrospinning of polymers. *Progress in Polymer Science, 38*(6), 963-991.

Agrawal, Govind P. (2007). *Nonlinear fiber optics*: Academic press.

Ali, Syed M Usman, Ibupoto, Zafar Hussain, Kashif, Muhammad, Hashim, Uda, & Willander, Magnus. (2012). A potentiometric indirect uric acid sensor based on ZnO nanoflakes and immobilized uricase. *Sensors, 12*(3), 2787-2797.

Alivisatos, A Paul. (1996). Semiconductor clusters, nanocrystals, and quantum dots. *Science, 271*(5251), 933.

Allsop, T, Floreani, Filip, Jedrzejewski, KP, Marques, PVS, Romero, R, Webb, David J, & Bennion, Ian. (2006). Spectral characteristics of tapered LPG device as a sensing element for refractive index and temperature. *Journal of lightwave technology, 24*(2), 870.

Amann, Markus-Christian, Bosch, Thierry, Lescure, Marc, Myllyla, Risto, & Rioux, Marc. (2001). Laser ranging: a critical review of usual techniques for distance measurement. *Optical engineering, 40*(1), 10-19.

Antohe, S, Ion, L, & Ruxandra, V. (2001). Electrical properties of electron irradiated thin polycrystalline CdSe layers. *Journal of Applied Physics, 90*(12), 5928-5932.

Arregui, Francisco J, Ciaurriz, Zuri, Oneca, Maria, & Matıas, Ignacio R. (2003). An experimental study about hydrogels for the fabrication of optical fiber humidity sensors. *Sensors and Actuators B: Chemical, 96*(1), 165-172.

Aussawasathien, D, Dong, J-H, & Dai, L. (2005). Electrospun polymer nanofiber sensors. *Synthetic Metals, 154*(1), 37-40.

Bao, Qiaoliang, Zhang, Han, Wang, Yu, Ni, Zhenhua, Yan, Yongli, Shen, Ze Xiang, Tang, Ding Yuan. (2009). Atomic-layer graphene as a saturable absorber for ultrafast pulsed lasers. *Advanced Functional Materials, 19*(19), 3077-3083.

Bariain, Candido, Matías, Ignacio R, Arregui, Francisco J, & Lopez-Amo, Manuel. (2000). Optical fiber humidity sensor based on a tapered fiber coated with agarose gel. *Sensors and Actuators B: Chemical, 69*(1), 127-131.

Baruah, Sunandan, & Dutta, Joydeep. (2009). pH-dependent growth of zinc oxide nanorods. *Journal of Crystal Growth, 311*(8), 2549-2554.

Batumalay, M, Harith, Z, Rafaie, HA, Ahmad, F, Khasanah, M, Harun, SW, Ahmad, H. (2014). Tapered plastic optical fiber coated with ZnO nanostructures for the measurement of uric acid concentrations and changes in relative humidity. *Sensors and Actuators A: Physical, 210*, 190-196.

Batumalay, M, Harun, SW, Ahmad, F, Nor, RM, Zulkepely, NR, & Ahmad, H. (2014). Study of a fiber optic humidity sensor based on agarose gel. *Journal of Modern Optics, 61*(3), 244-248.

Batumalay, Malathy, Ahmad, F, Lokman, Asiah, Jasim, AA, Wadi Harun, Sulaiman, & Ahmad, H. (2014). Tapered plastic optical fiber coated with single wall carbon nanotubes polyethylene oxide composite for measurement of uric acid concentration. *Sensor Review, 34*(1), 75-79.

Batumalay, Malathy, Harun, Sulaiman Wadi, Irawati, Ninik, Ahmad, Harith, & Arof, Hamzah. (2015). A study of relative humidity fiber-optic sensors. *IEEE Sensors Journal, 15*(3), 1945-1950.

Batumalay, Malathy, Lokman, Asiah, Ahmad, Fauzan, Arof, Hamzah, Ahmad, Harith, & Harun, Sulaiman Wadi. (2013). Tapered plastic optical fiber coated with HEC/PVDF for measurement of relative humidity. *IEEE Sensors Journal, 13*(12), 4702-4705.

Beres, Carolina, de Nazaré, Fábio Vieira Batista, de Souza, Nathália Correa Chagas, Miguel, Marco Antônio Lemos, & Werneck, Marcelo Martins. (2011). Tapered plastic optical fiber-based biosensor–Tests and application. *Biosensors and Bioelectronics, 30*(1), 328-332.

Berry, Scott M, Pabba, Santosh, Crest, Jérôme, Cambron, Scott D, McKinley, Gareth H, Cohn, Robert W, & Keynton, Robert S. (2011). Characterization and modeling of direct-write fabrication of microscale polymer fibers. *Polymer, 52*(7), 1654-1661.

Bertelli, Davide, Lolli, Massimo, Papotti, Giulia, Bortolotti, Laura, Serra, Giorgia, & Plessi, Maria. (2010). Detection of honey adulteration by sugar syrups using one-dimensional and two-dimensional high-resolution nuclear magnetic resonance. *Journal of agricultural and food chemistry, 58*(15), 8495-8501.

Bhardwaj, Nandana, & Kundu, Subhas C. (2010). Electrospinning: a fascinating fiber fabrication technique. *Biotechnology advances, 28*(3), 325-347.

Bidin, Noriah, Zainuddin, Nurul Hida, Islam, Shumaila, Abdullah, Mundzir, Marsin, Faridah Mohd, & Yasin, Moh. (2016). Sugar Detection in Adulterated Honey via Fiber Optic Displacement Sensor for Food Industrial Applications. *IEEE Sensors Journal, 16*(2), 299-305.

Bilodeau, F, Hill, KO, Faucher, S, & Johnson, DC. (1988). Low-loss highly overcoupled fused couplers: Fabrication and sensitivity to external pressure. *Journal of Lightwave Technology, 6*(10), 1476-1482.

Bonaccorso, Francesco, & Sun, Zhipei. (2014). Solution processing of graphene, topological insulators and other 2d crystals for ultrafast photonics. *Optical Materials Express, 4*(1), 63-78.

Brambilla, G. (2010). Optical fibre nanowires and microwires: a review. *Journal of Optics, 12*(4), 043001.

Brambilla, Gilberto, Finazzi, Vittoria, & Richardson, David J. (2004). Ultra-low-loss optical fiber nanotapers. *Optics Express, 12*(10), 2258-2263.

Brambilla, Gilberto, Xu, Fei, & Feng, Xiang. (2006). Fabrication of optical fibre nanowires and their optical and mechanical characterisation. *Electronics Letters, 42*(9), 1.

Brambilla, Gilberto, Xu, Fei, Horak, Peter, Jung, Yongmin, Koizumi, Fumihito, Sessions, Neil P, Wilkinson, James S. (2009). Optical fiber nanowires and microwires: fabrication and applications. *Advances in Optics and Photonics, 1*(1), 107-161.

Bret, Georges, & Gires, Francois. (1964). GIANT-PULSE LASER AND LIGHT AMPLIFIER USING VARIABLE TRANSMISSION COEFFICIENT GLASSES AS LIGHT SWITCHES. *Applied Physics Letters, 4*(10), 175-176.

Bruchez, Marcel, Moronne, Mario, Gin, Peter, Weiss, Shimon, & Alivisatos, A Paul. (1998). Semiconductor nanocrystals as fluorescent biological labels. *science, 281*(5385), 2013-2016.

Bueno, Antonio, Suárez, Isaac, Abargues, Rafael, Sales, Salvador, & Pastor, Juan P Martínez. (2012). Temperature sensor based on colloidal quantum dots–PMMA nanocomposite waveguides. *IEEE Sensors Journal, 12*(10), 3069-3074.

Bures, Jacques, & Ghosh, René. (1999). Power density of the evanescent field in the vicinity of a tapered fiber. *JOSA A, 16*(8), 1992-1996.

Cafiso, Samuele Davide Di Dio, Ugolotti, Elena, Schmidt, Andreas, Petrov, Valentin, Griebner, Uwe, Agnesi, Antonio, . . . Bae, Sukang. (2013). Sub-100-fs Cr: YAG laser mode-locked by monolayer graphene saturable absorber. *Optics letters, 38*(10), 1745-1747.

Camposeo, Andrea, Di Benedetto, Francesca, Stabile, Ripalta, Neves, Antonio AR, Cingolani, Roberto, & Pisignano, Dario. (2009). Laser emission from electrospun polymer nanofibers. *Small, 5*(5), 562-566.

Camposeo, Andrea, Persano, Luana, & Pisignano, Dario. (2013). Light-Emitting Electrospun Nanofibers for Nanophotonics and Optoelectronics. *Macromolecular Materials and Engineering, 298*(5), 487-503.

Chan, Warren CW, & Nie, Shuming. (1998). Quantum dot bioconjugates for ultrasensitive nonisotopic detection. *Science, 281*(5385), 2016-2018.

Chang, Chi-Hsiu, & Lee, Yuh-Lang. (2007). Chemical bath deposition of CdS quantum dots onto mesoscopic TiO2 films for application in quantum-dot-sensitized solar cells. *Applied Physics Letters, 91*(5), 5350-5353.

Chang, Chun-Ching, Huang, Chun-Min, Chang, Yi-Hao, & Kuo, Changshu. (2010). Enhancement of light scattering and photoluminescence in electrospun polymer nanofibers. *Optics express, 18*(102), A174-A184.

Chang, Guoqing, Li, Aike, Xu, Xiaoqian, Wang, Xiaoliang, & Xue, Gi. (2016). Twisted Polymer Microfiber/Nanofiber Yarns Prepared via Direct Fabrication. *Industrial & Engineering Chemistry Research, 55*(25), 7048-7051.

Chen, George Y, Ding, Ming, Newson, Trevor, & Brambilla, Gilberto. (2013). A review of microfiber and nanofiber based optical sensors. *The Open Optics Journal, 7*(1).

Cheng, Cheng, Wang, Sunde, & Cheng, Xiaoyu. (2012). CdSe/PMMA: Plastic fiber material containing CdSe quantum dots. *Optics & Laser Technology, 44*(5), 1298-1300.

Corres, Jesús M, Arregui, Francisco J, & Matias, Ignacio R. (2006). Design of humidity sensors based on tapered optical fibers. *Journal of Lightwave Technology, 24*(11), 4329-4336.

Corres, Jesús M, Arregui, Francisco J, & Matías, Ignacio R. (2007). Sensitivity optimization of tapered optical fiber humidity sensors by means of tuning the thickness of nanostructured sensitive coatings. *Sensors and Actuators B: Chemical, 122*(2), 442-449.

Corres, Jesus M, Bravo, Javier, Matias, Ignacio R, & Arregui, Francisco J. (2006). Nonadiabatic tapered single-mode fiber coated with humidity sensitive nanofilms. *IEEE Photonics Technology Letters, 18*(8), 935-937.

Cramariuc, Bogdan, Cramariuc, Radu, Scarlet, Roxana, Manea, Liliana Rozemarie, Lupu, Iuliana G, & Cramariuc, Oana. (2013). Fiber diameter in electrospinning process. *Journal of Electrostatics, 71*(3), 189-198.

Cui, Tieyu, Cui, Fang, Zhang, Junhu, Wang, Jiayu, Huang, Jing, Lü, Changli, Yang, Bai. (2006). From monomeric nanofibers to PbS nanoparticles/polymer composite nanofibers through the combined use of γ-irradiation and gas/solid reaction. *Journal of the American Chemical Society, 128*(19), 6298-6299.

Das, Anshuman J, Lafargue, Clément, Lebental, Mélanie, Zyss, Joseph, & Narayan, KS. (2011). Three-dimensional microlasers based on polymer fibers fabricated by electrospinning. *Applied Physics Letters, 99*(26), 263303.

Dausinger, Friedrich, Lichtner, Friedemann, & Lubatschowski, Holger. (2004). *Femtosecond technology for technical and medical applications* (Vol. 96): Springer Science & Business Media.

Dawkins, ST, Mitsch, R, Reitz, D, Vetsch, E, & Rauschenbeutel, A. (2011). Dispersive optical interface based on nanofiber-trapped atoms. *Physical review letters, 107*(24), 243601.

De-Jun, Feng, Mao-Sen, Zhang, Liu, Guanxiu, Xi-Lu, Liu, & Dong-Fang, Jia. (2014). D-shaped plastic optical fiber sensor for testing refractive index. *IEEE Sensors Journal, 14*(5), 1673-1676.

Di Benedetto, Francesca, Camposeo, Andrea, Persano, Luana, Laera, Anna Maria, Piscopiello, Emanuela, Cingolani, Roberto, . . . Pisignano, Dario. (2011). Light-emitting nanocomposite CdS–polymer electrospun fibres via in situ nanoparticle generation. *Nanoscale, 3*(10), 4234-4239.

Dickerson, BD, Irving, DM, Herz, E, Claus, Richard O, Spillman Jr, WB, & Meissner, KE. (2005). Synthesis kinetics of CdSe quantum dots in trioctylphosphine oxide and in stearic acid. *Applied Physics Letters, 86*(17), 171915.

Dıez, A, Andres, MV, & Cruz, JL. (2001). In-line fiber-optic sensors based on the excitation of surface plasma modes in metal-coated tapered fibers. *Sensors and Actuators B: Chemical, 73*(2), 95-99.

Ding, Jin-Fei, Zhang, A Ping, Shao, Li-Yang, Yan, Jin-Hua, & He, Sailing. (2005). Fiber-taper seeded long-period grating pair as a highly sensitive refractive-index sensor. *IEEE Photonics Technology Letters, 17*(6), 1247-1249.

Djurišić, AB, Ng, AMC, & Chen, XY. (2010). ZnO nanostructures for optoelectronics: material properties and device applications. *Progress in Quantum Electronics, 34*(4), 191-259.

Doran, NJ, & Wood, David. (1988). Nonlinear-optical loop mirror. *Optics letters, 13*(1), 56-58.

Duong Ta, Van, Chen, Rui, Ma, Lin, Jun Ying, Yong, & Dong Sun, Han. (2013). Whispering gallery mode microlasers and refractive index sensing based on single polymer fiber. *Laser & Photonics Reviews, 7*(1), 133-139.

Empedocles, Stephen A, Norris, DJ, & Bawendi, MG. (1996). Photoluminescence spectroscopy of single CdSe nanocrystallite quantum dots. *Physical Review Letters, 77*(18), 3873.

Ertekin, Kadriye, Tepe, Mustafa, Yenigül, Berrin, Akkaya, Engin U, & Henden, Emür. (2002). Fiber optic sodium and potassium sensing by using a newly synthesized squaraine dye in PVC matrix. *Talanta, 58*(4), 719-727.

Fermann, Martin E, Haberl, F, Hofer, Martin, & Hochreiter, H. (1990). Nonlinear amplifying loop mirror. *Optics Letters, 15*(13), 752-754.

Folarin, Olujinmi M, Sadiku, Emmanuel R, & Maity, Arjun. (2011). Polymer-noble metal nanocomposites: review.

Foster, Mark A, Turner, Amy C, Lipson, Michal, & Gaeta, Alexander L. (2008). Nonlinear optics in photonic nanowires. *Optics Express, 16*(2), 1300-1320.

Fu, Li, Zheng, Yuhong, Wang, Aiwu, Cai, Wen, Deng, Bo, & Zhang, Zhi. (2016). An Electrochemical Sensor Based on Reduced Graphene Oxide and ZnO Nanorods-Modified Glassy Carbon Electrode for Uric Acid Detection. *Arabian Journal for Science & Engineering (Springer Science & Business Media BV), 41*(1).

Gambling, W Anthony. (2000). The rise and rise of optical fibers. *IEEE journal of selected topics in quantum electronics, 6*(6), 1084-1093.

Gao, Xiaohu, Cui, Yuanyuan, Levenson, Richard M, Chung, Leland WK, & Nie, Shuming. (2004). In vivo cancer targeting and imaging with semiconductor quantum dots. *Nature biotechnology, 22*(8), 969-976.

Garg, Koyal, & Bowlin, Gary L. (2011). Electrospinning jets and nanofibrous structures. *Biomicrofluidics, 5*(1), 013403.

Geim, Andre K, & Novoselov, Konstantin S. (2007). The rise of graphene. *Nature materials, 6*(3), 183-191.

Golnabi, Hossein. (2000). Simulation of interferometric sensors for pressure and temperature measurements. *Review of scientific Instruments, 71*(4), 1608-1613.

Golnabi, Hossein. (2004). Design and operation of a fiber optic sensor for liquid level detection. *Optics and Lasers in Engineering, 41*(5), 801-812.

Grattan, Kenneth TV, & Meggitt, Beverley T. (1995). *Optical fiber sensor technology* (Vol. 1): Springer.

Greenspan, Lewis. (1977). Humidity fixed points of binary saturated aqueous solutions. *Journal of research of the national bureau of standards, 81*(1), 89-96.

Grobnic, Dan, Mihailov, Stephen J, Smelser, Christopher W, & Ding, Huimin. (2004). Sapphire fiber Bragg grating sensor made using femtosecond laser radiation for ultrahigh temperature applications. *IEEE Photonics Technology Letters, 16*(11), 2505-2507.

Gu, Fuxing, Yu, Huakang, Fang, Wei, & Tong, Limin. (2013). Nanoimprinted Polymer micro/nanofiber Bragg gratings for high-sensitivity strain sensing. *IEEE Photonics Technology Letters, 25*(1), 22-24.

Gu, Fuxing, Yu, Huakang, Wang, Pan, Yang, Zongyin, & Tong, Limin. (2010). Light-emitting polymer single nanofibers via waveguiding excitation. *ACS nano, 4*(9), 5332-5338.

Gu, Fuxing, Zhang, Lei, Yin, Xuefeng, & Tong, Limin. (2008). Polymer single-nanowire optical sensors. *Nano letters, 8*(9), 2757-2761.

Guerreiro, PT, Ten, S, Borrelli, NF, Butty, J, Jabbour, GE, & Peyghambarian, N. (1997). PbS quantum-dot doped glasses as saturable absorbers for mode locking of a Cr: forsterite laser. *Applied Physics Letters, 71*(12), 1595-1597.

Guo, Menglin, Shi, Jinchun, & Li, Baojun. (2008). Polymer-based micro/nanowire structures for three-dimensional photonic integrations. *Optics letters, 33*(18), 2104-2106.

Guo, Xin, & Tong, Limin. (2008). Supported microfiber loops for optical sensing. *Optics Express, 16*(19), 14429-14434.

Guo, Xin, Ying, Yibin, & Tong, Limin. (2013). Photonic nanowires: From subwavelength waveguides to optical sensors. *Accounts of chemical research, 47*(2), 656-666.

Hamizi, Nor Aliya, & Johan, Mohd Rafie. (2010). Synthesis and size dependent optical studies in CdSe quantum dots via inverse micelle technique. *Materials Chemistry and Physics, 124*(1), 395-398.

Harfenist, Steven A, Cambron, Scott D, Nelson, Eric W, Berry, Scott M, Isham, Alex W, Crain, Mark M, . . . Cohn, Robert W. (2004). Direct drawing of suspended filamentary micro-and nanostructures from liquid polymers. *Nano Letters, 4*(10), 1931-1937.

Harith, Z, Irawati, N, Batumalay, M, Rafaie, HA, Yun II, G, Harun, SW, Ahmad, H. (2015). Relative humidity sensor employing optical fibers coated with ZnO nanostructures. *Indian Journal of Science and Technology, 8*(35), 1.

Harith, Zuraidah, Irawati, Ninik, Rafaie, Hartini Ahmad, Batumalay, Malathy, Harun, Sulaiman Wadi, Nor, Roslan Md, & Ahmad, Harith. (2015). Tapered plastic optical fiber coated with Al-doped ZnO nanostructures for detecting relative humidity. *IEEE Sensors Journal, 15*(2), 845-849.

Hayashi, Neisei, Mizuno, Yosuke, & Nakamura, Kentaro. (2012). Brillouin gain spectrum dependence on large strain in perfluorinated graded-index polymer optical fiber. *Optics express, 20*(19), 21101-21106.

He, XL, Li, DJ, Zhou, J, Wang, WB, Xuan, WP, Dong, SR, Luo, JK. (2013). High sensitivity humidity sensors using flexible surface acoustic wave devices made on nanocrystalline ZnO/polyimide substrates. *Journal of Materials Chemistry C, 1*(39), 6210-6215.

Hida, N, Bidin, N, Abdullah, M, & Yasin, M. (2013). Fiber optic displacement sensor for honey purity detection in distilled water. *Optoelectron. Adv. Mater.-Rapid Commun, 7*(7-8), 565-568.

Hjertén, Stellan, & Kunquan, Yao. (1981). High-performance liquid chromatography of macromolecules on agarose and its derivatives. *Journal of Chromatography A, 215*, 317-322.

Holzwarth, Jeremy M, & Ma, Peter X. (2011). Biomimetic nanofibrous scaffolds for bone tissue engineering. *Biomaterials, 32*(36), 9622-9629.

Huang, Chujia, Xie, Weijing, Lee, Dongwen, Qi, Chongjie, Yang, Minghong, Wang, Min, & Tang, Jianguan. (2015). Optical fiber humidity sensor with porous TiO 2/SiO 2/TiO 2 coatings on fiber tip. *IEEE Photonics Technology Letters, 27*(14), 1495-1498.

Huang, Jiaxing, & Kaner, Richard B. (2004). A general chemical route to polyaniline nanofibers. *Journal of the American Chemical Society, 126*(3), 851-855.

Huang, JY, Huang, WC, Zhuang, WZ, Su, KW, Chen, YF, & Huang, KF. (2009). High-pulse-energy, passively Q-switched Yb-doped fiber laser with AlGaInAs quantum wells as a saturable absorber. *Optics letters, 34*(15), 2360-2362.

Huang, Keji, Yang, Shuangyang, & Tong, Limin. (2007). Modeling of evanescent coupling between two parallel optical nanowires. *Applied optics, 46*(9), 1429-1434.

Island, Joshua O, Steele, Gary A, van der Zant, Herre SJ, & Castellanos-Gomez, Andres. (2015). Environmental instability of few-layer black phosphorus. *2D Materials, 2*(1), 011002.

Ivekovic, Damir, Japec, Matea, Solar, Matea, & Živkovic, N. (2012). Amperometric uric acid biosensor with improved analytical performances based on alkaline-stable H2O2 transducer. *Int. J. Electrochem. Sci, 7*, 3252-3264.

Jamieson, Timothy, Bakhshi, Raheleh, Petrova, Daniela, Pocock, Rachael, Imani, Mo, & Seifalian, Alexander M. (2007). Biological applications of quantum dots. *Biomaterials, 28*(31), 4717-4732.

Janulewicz, KA, Hapiddin, A, Joseph, D, Geckeler, KE, Sung, JH, & Nickles, PV. (2014). Nonlinear absorption and optical damage threshold of carbon-based nanostructured material embedded in a protein. *Applied Physics A, 117*(4), 1811-1819.

Jiang, Xiaoshun, Song, Qinghai, Xu, Lei, Fu, Jian, & Tong, Limin. (2007). Microfiber knot dye laser based on the evanescent-wave-coupled gain. *Applied physics letters, 90*(23), 3501.

Jin, Y, & Granville, AM. (2016a). Polymer Fiber Optic Sensors–A Mini Review of their Synthesis and Applications. *J Biosens Bioelectron, 7*(194), 2.

Jin, Y, & Granville, AM. (2016b). Polymer Fiber Optic Sensors—A Mini Review of their Synthesis and Applications. *J. Biosens. Bioelectron, 7*, 194.

John, V, Muhammad, MZ, Irawati, N, Ali, NM, & Harun, SW. (2015). Micro-ball lens based optical biosensors. *JOURNAL OF OPTOELECTRONICS AND ADVANCED MATERIALS, 17*(11-12), 1656-1660.

Jorge, Pedro, Martins, Manuel António, Trindade, Tito, Santos, José Luís, & Farahi, Faramarz. (2007). Optical fiber sensing using quantum dots. *Sensors, 7*(12), 3489-3534.

Kang, BS, Ren, F, Heo, YW, Tien, LC, Norton, DP, & Pearton, SJ. (2005). p H measurements with single ZnO nanorods integrated with a microchannel. *Applied physics letters, 86*(11), 112105.

Keller, U, Miller, DAB, Boyd, GD, Chiu, TH, Ferguson, JF, & Asom, MT. (1992). Solid-state low-loss intracavity saturable absorber for Nd: YLF lasers: an antiresonant semiconductor Fabry–Perot saturable absorber. *Optics letters, 17*(7), 505-507.

Keller, Ursula. (2003). Recent developments in compact ultrafast lasers. *Nature, 424*(6950), 831-838.

Koike, Yasuhiro, & Asai, Makoto. (2009). The future of plastic optical fiber. *NPG Asia Materials, 1*(1), 22-28.

Koike, Yasuhiro, & Koike, Kotaro. (2011). Progress in low-loss and high-bandwidth plastic optical fibers. *Journal of Polymer Science Part B: Polymer Physics, 49*(1), 2-17.

Kou, Jun-Long, Ding, Ming, Feng, Jing, Lu, Yan-Qing, Xu, Fei, & Brambilla, Gilberto. (2012). Microfiber-based Bragg gratings for sensing applications: A review. *Sensors, 12*(7), 8861-8876.

Kou, Jun-long, Feng, Jing, Ye, Liang, Xu, Fei, & Lu, Yan-qing. (2010). Miniaturized fiber taper reflective interferometer for high temperature measurement. *Optics express, 18*(13), 14245-14250.

Kovalenko, AV, Kurashov, VN, & Kisil, AV. (2008). Radiation losses in optical nanofibers with random rough surface. *Optics express, 16*(8), 5797-5806.

Kwon, Il-Bum, Choi, Man-Yong, & Moon, Hahngue. (2004). Strain measurement using fiber optic total reflected extrinsic Fabry–Perot interferometric sensor with a digital signal processing algorithm. *Sensors and Actuators A: Physical, 112*(1), 10-17.

Latiff, AA, Shamsudin, H, Ahmad, H, & Harun, SW. (2016). Q-switched thulium-doped fiber laser operating at 1940 nm region using a pencil-core as saturable absorber. *Journal of Modern Optics, 63*(8), 783-787.

Le Kien, Fam, Gupta, S Dutta, Balykin, VI, & Hakuta, K. (2005). Spontaneous emission of a cesium atom near a nanofiber: Efficient coupling of light to guided modes. *Physical Review A, 72*(3), 032509.

Lee, Jian-Hong, Leu, Chi, Chung, Yi-Wen, & Hon, Min-Hsiung. (2006). Fabrication of ordered ZnO hierarchical structures controlled via surface charge in the electrophoretic deposition process. *Nanotechnology, 17*(17), 4445.

Li, Dan, & Xia, Younan. (2004). Electrospinning of nanofibers: reinventing the wheel? *Advanced materials, 16*(14), 1151-1170.

Li, Liang-shi, Hu, Jiangtao, Yang, Weidong, & Alivisatos, A Paul. (2001). Band gap variation of size-and shape-controlled colloidal CdSe quantum rods. *Nano Letters, 1*(7), 349-351.

Li, Likai, Yu, Yijun, Ye, Guo Jun, Ge, Qingqin, Ou, Xuedong, Wu, Hua, Zhang, Yuanbo. (2014). Black phosphorus field-effect transistors. *Nature nanotechnology, 9*(5), 372-377.

Li, Sheng, Jiang, Wei-Feng, Xu, Yuan-Ping, & George, Thomas F. (2011). Invisible Cavity of a Polymeric Nanofiber Laser. *The Journal of Physical Chemistry C, 115*(35), 17582-17586.

Li, Tao, Zhao, Chun-Liu, Dong, Xinyong, Qian, Wenwen, Jin, Yongxing, & Jin, Shangzhong. (2010). *Relative humidity sensor based on photonic crystal fiber with tapered and filled in polymer*. Paper presented at the Asia Communications and Photonics Conference and Exhibition.

Li, Yuhang, Vienne, Guillaume, Jiang, Xiaoshun, Pan, Xinyun, Liu, Xu, Gu, Peifu, & Tong, Limin. (2006). Modeling rare-earth doped microfiber ring lasers. *Optics express, 14*(16), 7073-7086.

Liang, Wei, Huang, Yanyi, Xu, Yong, Lee, Reginald K, & Yariv, Amnon. (2005). Highly sensitive fiber Bragg grating refractive index sensors. *Applied physics letters, 86*(15), 151122.

Lim, Kok Sing, Jasim, Ali A, Damanhuri, Siti SA, Harun, Sulaiman W, Rahman, BM Azizur, & Ahmad, Harith. (2011). Resonance condition of a microfiber knot resonator immersed in liquids. *Applied optics, 50*(30), 5912-5916.

Lim, KS, Harun, SW, Damanhuri, SSA, Jasim, AA, Tio, CK, & Ahmad, H. (2011). Current sensor based on microfiber knot resonator. *Sensors and Actuators A: Physical, 167*(1), 60-62.

Lim, KS, Harun, SW, Jasim, AA, & Ahmad, H. (2011). Fabrication of microfiber loop resonator-based comb filter. *Microwave and Optical Technology Letters, 53*(5), 1119-1121.

Liu, Haiqing, Edel, Joshua B, Bellan, Leon M, & Craighead, HG. (2006). Electrospun polymer nanofibers as subwavelength optical waveguides incorporating quantum dots. *Small, 2*(4), 495-499.

Liu, Han, Neal, Adam T, Zhu, Zhen, Luo, Zhe, Xu, Xianfan, Tománek, David, & Ye, Peide D. (2014). Phosphorene: an unexplored 2D semiconductor with a high hole mobility. *ACS nano, 8*(4), 4033-4041.

Liu, Jiang, Wu, Sida, Yang, Quan-Hong, & Wang, Pu. (2011). Stable nanosecond pulse generation from a graphene-based passively Q-switched Yb-doped fiber laser. *Optics letters, 36*(20), 4008-4010.

Liu, Jingmin, Li, Xingliang, Zhang, Shumin, Zhang, Han, Yan, Peiguang, Han, Mengmeng, Yang, Zhenjun. (2016). Polarization domain wall pulses in a microfiber-based topological insulator fiber laser. *Scientific reports, 6*.

Liu, Xiang, Wu, Xiaohua, Cao, Hui, & Chang, RPH. (2004). Growth mechanism and properties of ZnO nanorods synthesized by plasma-enhanced chemical vapor deposition. *Journal of Applied Physics, 95*(6), 3141-3147.

Liu, Xiangming, Adachi, Yusuke, Tomita, Yasuo, Oshima, Juro, Nakashima, Takuya, & Kawai, Tsuyoshi. (2012). High-order nonlinear optical response of a polymer nanocomposite film incorporating semiconducotor CdSe quantum dots. *Optics express, 20*(12), 13457-13469.

Liu, Yanjuan, Zhang, Yao, Lei, Hongxiang, Song, Jingwei, Chen, Hui, & Li, Baojun. (2012). Growth of well-arrayed ZnO nanorods on thinned silica fiber and application for humidity sensing. *Optics express, 20*(17), 19404-19411.

Lou, Jingyi, Tong, Limin, & Ye, Zhizhen. (2006). Dispersion shifts in optical nanowires with thin dielectric coatings. *Optics express, 14*(16), 6993-6998.

Lou, Jingyi, Wang, Yipei, & Tong, Limin. (2014). Microfiber optical sensors: A review. *Sensors, 14*(4), 5823-5844.

Luo, Zhengqian, Huang, Yizhong, Zhong, Min, Li, Yingyue, Wu, Jianyu, Xu, Bin, Weng, Jian. (2014). 1-, 1.5-, and 2-μm fiber lasers Q-switched by a broadband few-layer MoS 2 saturable absorber. *Journal of Lightwave Technology, 32*(24), 4077-4084.

Luo, Zhengqian, Zhou, Min, Weng, Jian, Huang, Guoming, Xu, Huiying, Ye, Chenchun, & Cai, Zhiping. (2010). Graphene-based passively Q-switched dual-wavelength erbium-doped fiber laser. *Optics letters, 35*(21), 3709-3711.

Lye, PG, Boerkamp, M, Ernest, A, & Lamb, DW. (2005). *Investigating the sensitivity of PMMA optical fibres for use as an evanescent field absorption sensor in aqueous solutions.* Paper presented at the Journal of Physics: Conference Series.

Mägi, Eric C, Nguyen, Hong C, & Eggleton, BJ. (2005). Air-hole collapse and mode transitions in microstructured fiber photonic wires. *Optics express, 13*(2), 453-459.

Matias, Ignacio R, Arregui, Francisco J, Corres, Jesus M, & Bravo, Javier. (2007). Evanescent field fiber-optic sensors for humidity monitoring based on nanocoatings. *IEEE Sensors Journal, 7*(1), 89-95.

Matsas, VJ, Newson, TP, Richardson, DJ, & Payne, David N. (1992). Selfstarting passively mode-locked fibre ring soliton laser exploiting nonlinear polarisation rotation. *Electron. Lett, 28*(15), 1391-1393.

Mbese, Johannes Z, & Ajibade, Peter A. (2014). Preparation and characterization of ZnS, CdS and HgS/poly (methyl methacrylate) nanocomposites. *Polymers, 6*(9), 2332-2344.

Medintz, Igor L, Uyeda, H Tetsuo, Goldman, Ellen R, & Mattoussi, Hedi. (2005). Quantum dot bioconjugates for imaging, labelling and sensing. *Nature materials, 4*(6), 435-446.

Mehryar, Laleh, & Esmaiili, Mohsen. (2011). *Honey and honey adulteration detection: A Review.* Paper presented at the proceeding of 11th International congress on engineering and food-Athens, Greece.

Meinel, Anne J, Germershaus, Oliver, Luhmann, Tessa, Merkle, Hans P, & Meinel, Lorenz. (2012). Electrospun matrices for localized drug delivery: current technologies and selected biomedical applications. *European Journal of Pharmaceutics and Biopharmaceutics, 81*(1), 1-13.

Meng, Chao, Xiao, Yao, Wang, Pan, Zhang, Lei, Liu, Yanxin, & Tong, Limin. (2011). Quantum-Dot-Doped Polymer Nanofibers for Optical Sensing. *Advanced Materials, 23*(33), 3770-3774.

Mizuno, Yosuke, Hayashi, Neisei, & Nakamura, Kentaro. (2013). Brillouin scattering signal in polymer optical fiber enhanced by exploiting pulsed pump with multimode-fiber-assisted coupling technique. *Optics letters, 38*(9), 1467-1469.

Mizuno, Yosuke, & Nakamura, Kentaro. (2010). Potential of Brillouin scattering in polymer optical fiber for strain-insensitive high-accuracy temperature sensing. *Optics letters, 35*(23), 3985-3987.

Mthethwa, TP, Moloto, MJ, De Vries, A, & Matabola, KP. (2011). Properties of electrospun CdS and CdSe filled poly (methyl methacrylate)(PMMA) nanofibres. *Materials Research Bulletin, 46*(4), 569-575.

Nain, Amrinder S, Wong, Joanna C, Amon, Cristina, & Sitti, Metin. (2006). Drawing suspended polymer micro-/nanofibers using glass micropipettes. *Applied physics letters, 89*(18), 183105.

Nayak, Kali P, & Hakuta, K. (2008). Single atoms on an optical nanofibre. *New Journal of Physics, 10*(5), 053003.

Nelson, LE, Jones, DJ, Tamura, K, Haus, HA, & Ippen, EP. (1997). Ultrashort-pulse fiber ring lasers. *Applied Physics B: Lasers and Optics, 65*(2), 277-294.

Nisman, Rozalia, Dellaire, Graham, Ren, Ying, Li, Ren, & Bazett-Jones, David P. (2004). Application of quantum dots as probes for correlative fluorescence, conventional, and energy-filtered transmission electron microscopy. *Journal of Histochemistry & Cytochemistry, 52*(1), 13-18.

Noy, Aleksandr, Miller, Abigail E, Klare, Jennifer E, Weeks, Brandon L, Woods, Bruce W, & DeYoreo, James J. (2002). Fabrication of luminescent nanostructures and polymer nanowires using dip-pen nanolithography. *Nano letters, 2*(2), 109-112.

O'Brien, Garret A, Quinn, Aidan J, Tanner, David A, & Redmond, Gareth. (2006). A single polymer nanowire photodetector. *Advanced materials, 18*(18), 2379-2383.

Ong, YS, Kam, W, Harun, SW, & Zakaria, R. (2015). Fabrication of polymer microfiber through direct drawing and splicing of silica microfiber via vapor spray and flame treatment. *Applied Optics, 54*(13), 3863-3867.

Pál, Edit, Hornok, Viktória, Oszkó, Albert, & Dékány, Imre. (2009). Hydrothermal synthesis of prism-like and flower-like ZnO and indium-doped ZnO structures. *Colloids and Surfaces A: Physicochemical and Engineering Aspects, 340*(1), 1-9.

Peters, Kara. (2010). Polymer optical fiber sensors—a review. *Smart materials and structures, 20*(1), 013002.

Pilizota, V, & Tiban, NN. (2009). Advances in honey adulteration detection. *Food Saf. Mag, 15*, 62-64.

Popa, D, Sun, Z, Hasan, T, Torrisi, F, Wang, F, & Ferrari, AC. (2010). Graphene Q-switched, tunable fiber laser. *arXiv preprint arXiv:1011.0115*.

Rafailov, EU, Cataluna, MA, & Sibbett, Wilson. (2007). Mode-locked quantum-dot lasers. *Nature photonics, 1*(7), 395-401.

Rafailov, EU, Cataluna, MA, Wilcox, K, & Zolotovskaya, SA. (2009). *Compact ultrafast lasers based on quantum-dot structures.* Paper presented at the SPIE OPTO: Integrated Optoelectronic Devices.

Rahman, HA, Irawati, N, Abdullah, TNR, & Harun, SW. (2015). *PMMA microfiber coated with ZnO nanostructure for the measurement of relative humidity.* Paper presented at the IOP Conference Series: Materials Science and Engineering.

Richardson, DJ, Nilsson, J, & Clarkson, WA. (2010). High power fiber lasers: current status and future perspectives [Invited]. *JOSA B, 27*(11), B63-B92.

Rodriguez-Rodriguez, Joaquin H, Martinez-Pinon, Fernando, Alvarez-Chavez, Jose A, & Jaramillo-Vigueras, David. (2008). *Polymer optical fiber moisture sensor based on evanescent-wave scattering to measure humidity in oil-paper insulation in electrical apparatus.* Paper presented at the Sensors, 2008 IEEE.

Roskov, Kristen E, Kozek, Krystian A, Wu, Wei-Chen, Chhetri, Raghav K, Oldenburg, Amy L, Spontak, Richard J, & Tracy, Joseph B. (2011). Long-range alignment of gold nanorods in electrospun polymer nano/microfibers. *Langmuir, 27*(23), 13965-13969.

Sagué, G, Vetsch, E, Alt, W, Meschede, D, & Rauschenbeutel, A. (2007). Cold-atom physics using ultrathin optical fibers: Light-induced dipole forces and surface interactions. *Physical review letters, 99*(16), 163602.

Sato, Keiichi, Kojima, Satoshi, Hattori, Shinya, Chiba, Taeko, Ueda-Sarson, Keiko, Torimoto, Tsukasa, . . . Kuwabata, Susumu. (2007). Controlling surface reactions of CdS nanocrystals: photoluminescence activation, photoetching and photostability under light irradiation. *Nanotechnology*, *18*(46), 465702.

Schaffer, Chris B, Brodeur, Andre, & Mazur, Eric. (2001). Laser-induced breakdown and damage in bulk transparent materials induced by tightly focused femtosecond laser pulses. *Measurement Science and Technology*, *12*(11), 1784.

Schmidt-Mende, Lukas, & MacManus-Driscoll, Judith L. (2007). ZnO–nanostructures, defects, and devices. *Materials today, 10*(5), 40-48.

Schütze, K, Pösl, H, & Lahr, G. (1998). Laser micromanipulation systems as universal tools in cellular and molecular biology and in medicine. *CELLULAR AND MOLECULAR BIOLOGY-PARIS-WEGMANN-, 44*, 735-746.

Set, Sze Y, Yaguchi, Hiroshi, Tanaka, Yuichi, & Jablonski, Mark. (2004). Ultrafast fiber pulsed lasers incorporating carbon nanotubes. *Selected Topics in Quantum Electronics, IEEE Journal of, 10*(1), 137-146.

Shcherbakov, E, Fomin, V, Abramov, A, Ferin, A, Mochalov, D, & Gapontsev, Valentin P. (2013). *Industrial grade 100 kW power CW fiber laser*. Paper presented at the Advanced Solid State Lasers.

Sheehan, PE, Whitman, LJ, King, William P, & Nelson, Brent A. (2004). Nanoscale deposition of solid inks via thermal dip pen nanolithography. *Applied physics letters, 85*(9), 1589-1591.

Shi, Lei, Xu, Yonghao, Tan, Wei, & Chen, Xianfeng. (2007). Simulation of optical microfiber loop resonators for ambient refractive index sensing. *Sensors*, *7*(5), 689-696.

Sivakesava, S, & Irudayaraj, J. (2001). A rapid spectroscopic technique for determining honey adulteration with corn syrup. *Journal of Food Science, 66*(6), 787-791.

Sobon, Grzegorz, Sotor, Jaroslaw, Pasternak, Iwona, Krajewska, Aleksandra, Strupinski, Wlodek, & Abramski, Krzysztof M. (2015). Multilayer graphene-based saturable absorbers with scalable modulation depth for mode-locked Er- and Tm-doped fiber lasers. *Optical Materials Express*, *5*(12), 2884-2894.

Soffer, BH. (1964). Giant pulse laser operation by a passive, reversibly bleachable absorber. *Journal of applied physics, 35*(8), 2551-2551.

Somers, Rebecca C, Bawendi, Moungi G, & Nocera, Daniel G. (2007). CdSe nanocrystal based chem-/bio-sensors. *Chemical Society Reviews, 36*(4), 579-591.

Song, Qinghai, Liu, Liying, & Xu, Lei. (2009). Lasing action in dye doped polymer nanofiber knot resonator. *Journal of Lightwave Technology, 27*(19), 4374-4376.

Song, Yong-Won, Jang, Sung-Yeon, Han, Won-Suk, & Bae, Mi-Kyung. (2010). Graphene mode-lockers for fiber lasers functioned with evanescent field interaction. *Applied Physics Letters, 96*(5), 051122.

Stellan, H, & Yao, K. (1981). High-performance liquid chromatography of macromolecules on agarose and its derivative. *J. Chromatogr. A, 215*, 317-322.

Sulaiman, Azlan, Harun, Sulaiman Wadi, Ahmad, Fauzan, Norizan, Siti Fatimah, & Ahmad, Harith. (2012). Electrically tunable microfiber knot resonator based erbium-doped fiber laser. *IEEE Journal of Quantum Electronics, 48*(4), 443-446.

Sumetsky, M. (2008). Basic elements for microfiber photonics: Micro/nanofibers and microfiber coil resonators. *Journal of lightwave technology, 26*(1), 21-27.

Sumetsky, M, Dulashko, Y, Fini, JM, Hale, A, & DiGiovanni, DJ. (2006). The microfiber loop resonator: theory, experiment, and application. *Journal of Lightwave Technology, 24*(1), 242.

Sumetsky, Misha, Dulashko, Yury, Fini, John M, & Hale, Arturo. (2005). Optical microfiber loop resonator. *Applied Physics Letters, 86*(16), 161108.

Sun, Z, Hasan, T, & Ferrari, AC. (2012). Ultrafast lasers mode-locked by nanotubes and graphene. *Physica E: Low-dimensional Systems and Nanostructures, 44*(6), 1082-1091.

Ta, Van Duong, Chen, Rui, & Sun, Handong. (2014). Coupled polymer microfiber lasers for single mode operation and enhanced refractive index sensing. *Advanced Optical Materials, 2*(3), 220-225.

Tan, Swee Tiam, Chen, BJ, Sun, XW, Fan, WJ, Kwok, HS, Zhang, XH, & Chua, SJ. (2005). Blueshift of optical band gap in ZnO thin films grown by metal-organic chemical-vapor deposition. *Journal of applied physics, 98*(1), 013505-013505-013505.

Tang, DY, Zhao, LM, Zhao, B, & Liu, AQ. (2005). Mechanism of multisoliton formation and soliton energy quantization in passively mode-locked fiber lasers. *Physical Review A, 72*(4), 043816.

Tatavarty, Rameshwar, Hwang, Ee Taek, Park, Jee-Woong, Kwak, Jun-Hyuk, Lee, Jeong-O, & Gu, Man Bock. (2011). Conductive quantum dot-encapsulated electrospun nanofibers from polystyrene and polystyrene-co-maleic anhydride copolymer blend as gas sensors. *Reactive and Functional Polymers, 71*(2), 104-108.

Tong, Limin, Gattass, Rafael R, Ashcom, Jonathan B, He, Sailing, Lou, Jingyi, Shen, Mengyan, . . . Mazur, Eric. (2003). Subwavelength-diameter silica wires for low-loss optical wave guiding. *Nature, 426*(6968), 816-819.

Tong, Limin, Lou, Jingyi, Gattass, Rafael R, He, Sailing, Chen, Xuewen, Liu, Liu, & Mazur, Eric. (2005). Assembly of silica nanowires on silica aerogels for microphotonic devices. *Nano letters, 5*(2), 259-262.

Tong, Limin, Lou, Jingyi, & Mazur, Eric. (2004). Single-mode guiding properties of subwavelength-diameter silica and silicon wire waveguides. *Optics Express, 12*(6), 1025-1035.

Tong, Limin, & Sumetsky, Michael. (2010). Micro/nanofiber optical sensors *Subwavelength and Nanometer Diameter Optical Fibers* (pp. 187-214): Springer.

Tong, Limin, & Sumetsky, Michael. (2011). *Subwavelength and nanometer diameter optical fibers*: Springer Science & Business Media.

Tong, Limin, Zi, Fei, Guo, Xin, & Lou, Jingyi. (2012). Optical microfibers and nanofibers: A tutorial. *Optics communications, 285*(23), 4641-4647.

Tran, Vy, Soklaski, Ryan, Liang, Yufeng, & Yang, Li. (2014). Layer-controlled band gap and anisotropic excitons in few-layer black phosphorus. *Physical Review B, 89*(23), 235319.

Trivedi, Evan R, & Hatch, Shelby L. (2013). Synthesis and Size Dependent Properties of CdSe Quantum Dots. *Department of Chemistry. IL, 60208*.

Tsai, Tzong-Yow, Fang, Yen-Cheng, Huang, Huai-Min, Tsao, Hong-Xi, & Lin, Shih-Ting. (2010). Saturable absorber Q-and gain-switched all-Yb 3+ all-fiber laser at 976 and 1064 nm. *Optics express, 18*(23), 23523-23528.

Umar, Ahmad, Kim, Byoung-Kye, Kim, Ju-Jin, & Hahn, YB. (2007). Optical and electrical properties of ZnO nanowires grown on aluminium foil by non-catalytic thermal evaporation. *Nanotechnology, 18*(17), 175606.

Unnithan, Afeesh R, Barakat, Nasser AM, Pichiah, PB Tirupathi, Gnanasekaran, Gopalsamy, Nirmala, R, Cha, Youn-Soo, . . . Kim, Hak Yong. (2012). Wound-dressing materials with antibacterial activity from electrospun polyurethane–dextran nanofiber mats containing ciprofloxacin HCl. *Carbohydrate polymers, 90*(4), 1786-1793.

Vienne, Guillaume, Grelu, Philippe, Pan, Xinyun, Li, Yuhang, & Tong, Limin. (2008). Theoretical study of microfiber resonator devices exploiting a phase shift. *Journal of optics A: pure and applied optics, 10*(2), 025303.

Vienne, Guillaume, Li, Yuhang, & Tong, Limin. (2007). Effect of host polymer on microfiber resonator. *IEEE Photonics Technology Letters, 19*(17/20), 1386.

Wan, Qing, Li, QH, Chen, YJ, Wang, Ta-Hung, He, XL, Li, JP, & Lin, CL. (2004). Fabrication and ethanol sensing characteristics of ZnO nanowire gas sensors. *Applied Physics Letters, 84*(18), 3654-3656.

Wang, Debin, Kodali, Vamsi K, Curtis, Jennifer E, & Riedo, Elisa. (2011). Nanofabrication of Functional Nanostructures by Thermochemical Nanolithography *Tip-Based Nanofabrication* (pp. 265-297): Springer.

Wang, Lisheng, Zhang, Xiaozhong, Zhao, Songqing, Zhou, Guoyuan, Zhou, Yueliang, & Qi, Junjie. (2005). Synthesis of well-aligned ZnO nanowires by simple physical vapor deposition on c-oriented ZnO thin films without catalysts or additives. *Applied Physics Letters, 86*(2), 024108-024108-024103.

Wang, LY, Xu, WC, Luo, ZC, Cao, WJ, Luo, AP, Dong, JL, & Wang, HY. (2011). Passively Q-switched mode-locking erbium-doped fiber laser with net-normal dispersion using nonlinear polarization rotation technique. *Laser Physics, 21*(10), 1808.

Wang, Pan, Gu, Fuxing, Zhang, Lei, & Tong, Limin. (2011). Polymer microfiber rings for high-sensitivity optical humidity sensing. *Applied optics, 50*(31), G7-G10.

Wang, Pan, Li, Zhiyong, Zhang, Lei, & Tong, Limin. (2013). Electron-beam-activated light-emitting polymer nanofibers. *Optics letters, 38*(7), 1040-1042.

Wang, Pan, Wang, Yipei, & Tong, Limin. (2013). Functionalized polymer nanofibers: a versatile platform for manipulating light at the nanoscale. *Light: Science & Applications, 2*(10), e102.

Wang, Pan, Zhang, Lei, Xia, Younan, Tong, Limin, Xu, Xia, & Ying, Yibin. (2012). Polymer nanofibers embedded with aligned gold nanorods: a new platform for plasmonic studies and optical sensing. *Nano letters, 12*(6), 3145-3150.

Wang, Qing Hua, Kalantar-Zadeh, Kourosh, Kis, Andras, Coleman, Jonathan N, & Strano, Michael S. (2012). Electronics and optoelectronics of two-dimensional transition metal dichalcogenides. *Nature nanotechnology, 7*(11), 699-712.

Wang, XH, Li, RB, & Fan, DH. (2011). Study on synthesis and optical properties of Al-doped ZnO hierarchical nanostructures. *AIP Advances, 1*(1), 012107.

Wang, Xiaoyong, Qu, Lianhua, Zhang, Jiayu, Peng, Xiaogang, & Xiao, Min. (2003). Surface-related emission in highly luminescent CdSe quantum dots. *Nano Letters, 3*(8), 1103-1106.

Wang, Xu-dong, & Wolfbeis, Otto S. (2015). Fiber-optic chemical sensors and biosensors (2013–2015). *Analytical chemistry, 88*(1), 203-227.

Wang, Yun, Yeow, John TW, & Chen, Liang-Yih. (2008). *Synthesis of aligned zinc oxide nanorods for humidity sensing.* Paper presented at the Sensing Technology, 2008. ICST 2008. 3rd International Conference on.

Wang, Yuqing, Zhu, Heng, & Li, Baojun. (2011). Optical characterization of mechanically tunable microwire based resonators by changing ring radius and wire diameter. *Optics Communications, 284*(13), 3276-3279.

Wang, Zhong Lin. (2004). Zinc oxide nanostructures: growth, properties and applications. *Journal of Physics: Condensed Matter, 16*(25), R829.

Warken, F, Vetsch, E, Meschede, D, Sokolowski, M, & Rauschenbeutel, A. (2007). Ultra-sensitive surface absorption spectroscopy using sub-wavelength diameter optical fibers. *Optics Express, 15*(19), 11952-11958.

Wei, Ming, Zhi, Dan, & MacManus-Driscoll, Judith L. (2005). Self-catalysed growth of zinc oxide nanowires. *Nanotechnology, 16*(8), 1364.

Wo, Jianghai, Wang, Guanghui, Cui, Ying, Sun, Qizhen, Liang, Ruibing, Shum, Perry Ping, & Liu, Deming. (2012). Refractive index sensor using microfiber-based Mach–Zehnder interferometer. *Optics letters, 37*(1), 67-69.

Wood, Joshua D, Wells, Spencer A, Jariwala, Deep, Chen, Kan-Sheng, Cho, EunKyung, Sangwan, Vinod K, . . . Hersam, Mark C. (2014). Effective passivation of exfoliated black phosphorus transistors against ambient degradation. *Nano letters, 14*(12), 6964-6970.

Woodward, Robert I, Kelleher, Edmund J, Runcorn, TH, Popov, Sergei V, Torrisi, Felice, Howe, Rc T, & Hasan, Tawfique. (2014). Q-switched fiber laser with MoS2 saturable absorber. *CLEO: 2014*, SM3H-6.

Woodward, Robert I, & Kelleher, Edmund JR. (2015). 2D saturable absorbers for fibre lasers. *Applied Sciences, 5*(4), 1440-1456.

Wu, Jing, Wang, Nü, Zhao, Yong, & Jiang, Lei. (2013). Electrospinning of multilevel structured functional micro-/nanofibers and their applications. *Journal of Materials Chemistry A, 1*(25), 7290-7305.

Wu, Kan, Zhang, Xiaoyan, Wang, Jun, Li, Xing, & Chen, Jianping. (2015). WS 2 as a saturable absorber for ultrafast photonic applications of mode-locked and Q-switched lasers. *Optics express, 23*(9), 11453-11461.

Wu, Xiaoqin, & Tong, Limin. (2013). Optical microfibers and nanofibers. *Nanophotonics, 2*(5-6), 407-428.

Wu, Yu, Zhang, TianHu, Rao, YunJiang, & Gong, Yuan. (2011). Miniature interferometric humidity sensors based on silica/polymer microfiber knot resonators. *Sensors and Actuators B: Chemical, 155*(1), 258-263.

Wu, Zhichao, Fu, Songnian, Chen, Changxiu, Tang, Ming, Shum, Perry, & Liu, Deming. (2015). Dual-state dissipative solitons from an all-normal-dispersion erbium-doped fiber laser: continuous wavelength tuning and multi-wavelength emission. *Optics letters, 40*(12), 2684-2687.

Xia, Fengnian, Wang, Han, & Jia, Yichen. (2014). Rediscovering black phosphorus as an anisotropic layered material for optoelectronics and electronics. *Nature communications, 5*.

Xiao, Limin, Grogan, Michael D, Leon-Saval, Sergio G, Williams, Rhys, England, Richard, Wadsworth, Willam J, & Birks, Tim A. (2009). Tapered fibers embedded in silica aerogel. *Optics letters, 34*(18), 2724-2726.

Xing, Xiaobo, Zhu, Heng, Wang, Yuqing, & Li, Baojun. (2008). Ultracompact photonic coupling splitters twisted by PTT nanowires. *Nano letters, 8*(9), 2839-2843.

Xu, Fei, & Brambilla, Gilberto. (2007). Embedding optical microfiber coil resonators in Teflon. *Optics letters, 32*(15), 2164-2166.

Xu, Fei, Pruneri, Valerio, Finazzi, Vittoria, & Brambilla, Gilberto. (2008). An embedded optical nanowire loop resonator refractometric sensor. *Optics Express, 16*(2), 1062-1067.

Xu, Wei, Huang, Xu Guang, & Pan, Jing Shun. (2013). Simple fiber-optic refractive index sensor based on fresnel reflection and optical switch. *IEEE Sensors Journal, 13*(5), 1571-1574.

Yamashita, S, Inoue, Y, Maruyama, S, Murakami, Y, Yaguchi, H, Jablonski, M, & Set, SY. (2004). Saturable absorbers incorporating carbon nanotubes directly synthesized onto substrates and fibers and their application to mode-locked fiber lasers. *Optics letters, 29*(14), 1581-1583.

Yan, Peiguang, Lin, Rongyong, Ruan, Shuangchen, Liu, Aijiang, & Chen, Hao. (2015). A 2.95 GHz, femtosecond passive harmonic mode-locked fiber laser based on evanescent field interaction with topological insulator film. *Optics express, 23*(1), 154-164.

Yang, Qing, Jiang, Xiaoshun, Gu, Fuxing, Ma, Zhe, Zhang, Jiangyang, & Tong, Limin. (2008). Polymer micro or nanofibers for optical device applications. *Journal of applied polymer science, 110*(2), 1080-1084.

Yano, Mitsuaki, Koike, Kazuto, Ogata, Ken-ichi, Nogami, Takahiro, Tanabe, Shintaro, & Sasa, Shigehiko. (2012). Zinc oxide-based biosensors. *physica status solidi (c), 9*(7), 1570-1573.

Yao, Baicheng, Wu, Yu, Gong, Yuan, & Rao, Yunjiang. (2012). *A highly sensitive and fast response molecular sensor based on graphene coated microfiber*. Paper presented at the OFS2012 22nd International Conference on Optical Fiber Sensor.

Yeo, TL, Sun, T, & Grattan, KTV. (2008). Fibre-optic sensor technologies for humidity and moisture measurement. *Sensors and Actuators A: Physical, 144*(2), 280-295.

Yu, Dong, Wehrenberg, Brian L, Jha, Praket, Ma, Jiasen, & Guyot-Sionnest, Philippe. (2006). Electronic transport of n-type CdSe quantum dot films: Effect of film treatment. *Journal of applied physics, 99*(10), 104315.

Yu, Hao, Zheng, Xin, Yin, Ke, & Jiang, Tian. (2015). Thulium/holmium-doped fiber laser passively mode locked by black phosphorus nanoplatelets-based saturable absorber. *Applied optics, 54*(34), 10290-10294.

Yu, Huakang, Wang, Shanshan, Fu, Jian, Qiu, Min, Li, Yuhang, Gu, Fuxing, & Tong, Limin. (2009). Modeling bending losses of optical nanofibers or nanowires. *Applied optics, 48*(22), 4365-4369.

Yu, Huaqing, Xiong, Liangbin, Chen, Zhihong, Li, Qianguang, Yi, Xunong, Ding, Yu, . . . Ding, Yaoming. (2014). Solution concentration and refractive index sensing based on polymer microfiber knot resonator. *Applied Physics Express, 7*(2), 022501.

Yu, Huaqing, Zhang, Rui, & Li, Baojun. (2011). Optical properties of quantum-dot-decorated polymer nanofibers. *Nanotechnology, 22*(33), 335202.

Yuan, CT, Chou, WC, Chuu, DS, Chen, YN, Lin, CA, & Chang, WH. (2008). Photoinduced fluorescence enhancement in colloidal Cd Se Te⁄ Zn S core/shell quantum dots. *Applied Physics Letters, 92*(18), 183108.

Yuan, Shengjun, Rudenko, AN, & Katsnelson, MI. (2015). Transport and optical properties of single-and bilayer black phosphorus with defects. *Physical Review B, 91*(11), 115436.

Zan, Hsiao-Wen, Li, Chang-Hung, Yeh, Chun-Cheng, Dai, Ming-Zhi, Meng, Hsin-Fei, & Tsai, Chuang-Chuang. (2011). Room-temperature-operated sensitive hybrid gas sensor based on amorphous indium gallium zinc oxide thin-film transistors. *Applied Physics Letters, 98*(25), 253503.

Zeng, Xu, Wu, Yu, Hou, Changlun, Bai, Jian, & Yang, Guoguang. (2009). A temperature sensor based on optical microfiber knot resonator. *Optics Communications, 282*(18), 3817-3819.

Zhai, Gaoye, & Tong, Limin. (2007). Roughness-induced radiation losses in optical micro or nanofibers. *Optics express, 15*(21), 13805-13816.

Zhang, Fenfen, Wang, Xiaoli, Ai, Shiyun, Sun, Zhengdong, Wan, Qiao, Zhu, Ziqiang, . . . Yamamoto, Katsunobu. (2004). Immobilization of uricase on ZnO nanorods for a reagentless uric acid biosensor. *Analytica Chimica Acta, 519*(2), 155-160.

Zhang, Han, Tang, DY, Zhao, LM, Bao, QL, & Loh, KP. (2009). Large energy mode locking of an erbium-doped fiber laser with atomic layer graphene. *Optics Express, 17*(20), 17630-17635.

Zhang, Lei, Gu, Fuxing, Lou, Jingyi, Yin, Xuefeng, & Tong, Limin. (2008). Fast detection of humidity with a subwavelength-diameter fiber taper coated with gelatin film. *Optics express, 16*(17), 13349-13353.

Zhang, Lei, Wang, Pan, Xiao, Yao, Yu, Huakang, & Tong, Limin. (2011). Ultra-sensitive microfibre absorption detection in a microfluidic chip. *Lab on a Chip, 11*(21), 3720-3724.

Zhang, LQ, Zhuo, Z, Wang, JX, & Wang, YZ. (2012). Passively Q-switched fiber laser based on graphene saturable absorber. *Laser Physics, 22*(2), 433-436.

Zhang, Rui, Yu, Huaqing, & Li, Baojun. (2012). Active nanowaveguides in polymer doped with CdSe–ZnS core–shell quantum dots. *Nanoscale, 4*(19), 5856-5859.

Zhang, Yanfeng, Russo, Richard E, & Mao, Samuel S. (2005). Femtosecond laser assisted growth of ZnO nanowires. *Applied Physics Letters, 87*(13), 133115.

Zhao, Xiaohua, Li, Meng, & Lou, Xiangdong. (2014). Sol–gel assisted hydrothermal synthesis of ZnO microstructures: morphology control and photocatalytic activity. *Advanced Powder Technology, 25*(1), 372-378.

Zhao, Yong, Zhang, Bo, & Liao, Yanbiao. (2003). Experimental research and analysis of salinity measurement based on optical techniques. *Sensors and Actuators B: Chemical, 92*(3), 331-336.

Zheng, MJ, Zhang, LD, Li, GH, & Shen, WZ. (2002). Fabrication and optical properties of large-scale uniform zinc oxide nanowire arrays by one-step electrochemical deposition technique. *Chemical Physics Letters, 363*(1), 123-128.

Zheng, Yangzi, Dong, Xinyong, Zhao, Chunliu, Li, Yi, Shao, Liyang, & Jin, Shangzhong. (2013). Relative humidity sensor based on microfiber loop resonator. *Advances in Materials Science and Engineering, 2013*.

Zhou, Da-Peng, Wei, Li, Dong, Bo, & Liu, Wing-Ki. (2010). Tunable passively-switched erbium-doped fiber laser with carbon nanotubes as a saturable absorber. *IEEE Photonics Technology Letters, 22*(1), 9-11.

Zhu, Heng, Wang, Yuqing, & Li, Baojun. (2009). Tunable refractive index sensor with ultracompact structure twisted by poly (trimethylene terephthalate) nanowires. *ACS nano, 3*(10), 3110-3114.

Zhu, Junjie, Palchik, O, Chen, Siguang, & Gedanken, A. (2000). Microwave assisted preparation of CdSe, PbSe, and Cu2-x Se nanoparticles. *The Journal of Physical Chemistry B, 104*(31), 7344-7347.

Zibaii, Mohammad Ismail, Kazemi, Alireza, Latifi, Hamid, Azar, Mahmoud Karimi, Hosseini, Seyed Masoud, & Ghezelaiagh, Mohammad Hossein. (2010). Measuring bacterial growth by refractive index tapered fiber optic biosensor. *Journal of Photochemistry and Photobiology B: Biology, 101*(3), 313-320.

Zirngibl, M, Stulz, LW, Stone, J, Hugi, J, DiGiovanni, David, & Hansan, PB. (1991). 1.2 ps pulses from passively mode-locked laser diode pumped Er-doped fibre ring laser. *Electronics Letters, 27*(19), 1734-1735.

Zubia, Joseba, & Arrue, Jon. (2001). Plastic optical fibers: An introduction to their technological processes and applications. *Optical Fiber Technology, 7*(2), 101-140.

LIST OF PUBLICATIONS AND PAPERS PRESENTED

Journal Publications

1) Irawati, N., Suthaskumar, M., John, V., Ali, N. M., Ahmad, H., & Harun, S. W. (2015). Fabrication of polymer microfiber by direct drawing. *Microwave and Optical Technology Letters*, *57*(4), 820-823.

2) Irawati, N., Harun, S. W., Adwan, S., Alnowami, M., & Ahmad, H. (2015). PMMA microfiber coated with al-doped ZnO nanostructures for detecting uric acid. *Microwave and Optical Technology Letters*, *57*(10), 2455-2457.

3) Rahman, H. A., Irawati, N., Abdullah, T. N. R., & Harun, S. W. (2015). PMMA microfiber coated with ZnO nanostructure for the measurement of relative humidity. In *IOP Conference Series: Materials Science and Engineering* (Vol. 99, No. 1, p. 012025). IOP Publishing.

4) Lokman, A., Irawati, N., Arof, H., Harun, S. W., & Ali, N. M. (2015). Dumbbell shaped inline MachZehnder interferometer for sensor applications.

5) Rafis, H., Irawati, N., Rafaie, H. A., Ahmad, H., Harun, S. W., & Nor, R. M. (2015). Detection of Different Concentrations of Uric Acid Using Tapered Silica Optical Sensor Coated with Zinc Oxide (ZnO). *Jurnal Teknologi*, *74*(8).

6) Yasin, M., Soelistiono, S., Yhun Yhuwana, Y. G., Khasanah, M., Arof, H., N, Irawati., Harun, S. W. (2015). Intensity based optical fiber sensors for calcium detection. *Optoelectronics and Advanced Materials – Rapid Communications*, Vol. 9, 1185 – 1189.

7) John, V., Muhammad, M. Z., Irawati, N., Ali, N. M., & Harun, S. W. (2015). Micro-ball lens based optical biosensors. *JOURNAL OF OPTOELECTRONICS AND ADVANCED MATERIALS*, *17*(11-12), 1656-1660.

8) Aris, A. M., Irawati, N., Rahman, H. A., Harun, S. W., & Ahad, I. Z. M. (2015, August). Fiber Bragg grating sensor for humidity measurement. In *2015 5th IEEE International Conference on System Engineering and Technology (ICSET)* (pp. 55-59). IEEE.

9) Harith, Z., Irawati, N., Batumalay, M., Rafaie, H. A., Yun II, G., Harun, S. W., ... & Ahmad, H. (2015). Relative humidity sensor employing optical fibers coated with ZnO nanostructures. *Indian Journal of Science and Technology*, *8*(35), 1.

10) Irawati, N., Rahman, H. A., Ahmad, H., & Harun, S. W. (2017). A PMMA microfiber loop resonator based humidity sensor with ZnO nanorods coating. *Measurement*, *99*, 128-133.

11) Irawati, N., Yusuf, N. A. M., Rahman, H. A., Yasin, M., Ahmad, H., & Harun,

S. W. (2017). Potassium permanganate (KMnO 4) sensing based on microfiber sensors. *Applied Optics*, *56*(2), 224-228.

12) Latiff, A. A., Shamsudin, H., Aziz, N. S. A., Hashim, A. M., Irawati, N., Ahmad, H., & Harun, S. W. (2016). Mode-locked generation in thulium-doped fiber linear cavity laser. *Optik-International Journal for Light and Electron Optics*, *127*(23), 11119-11123.

13) Ahmed, M. H. M., Banabila, A. M., Latiff, A. A., Irawati, N., Ali, N. M., Harun, S. W., & Arof, H. (2016). Tunable Q-switched erbium doped fiber laser with graphene oxide paper based saturable absorber. *OPTOELECTRONICS AND ADVANCED MATERIALS-RAPID COMMUNICATIONS*, *10*(11-12), 791-796.

14) Aris, A. M., Rahman, H. A., Irawati, N., Harun, S. W., & Sarnin, S. S. (2017). Tapered Fiber Bragg Grating Sensor Coated with Zinc Oxide Nanostructures for Humidity Measurement. *Journal of Telecommunication, Electronic and Computer Engineering (JTEC)*, *9*(1-5), 1-5.

15) Mohamed, H., Irawati, N., Ahmad, F., Ibrahim, M. H., Ambran, S., Rahman, M. A. A., & Harun, S. W. (2017). Optical Humidity Sensor Based on Tapered Fiber with Multi-walled Carbon Nanotubes Slurry. *Indonesian Journal of Electrical Engineering and Computer Science*, *6*(1).

16) Irawati, N., Abdullah, T. N. R., Rahman, H. A., Ahmad, H., & Harun, S. W. (2017). PMMA Microfiber Loop Resonator For Humidity Sensor. *Sensors and Actuators A: Physical*.

17) Irawati, N., Rahman, H. A., Yasin, M., Al-Askari, S., Hamida, B. A., Ahmad, H., & Harun, S. W. (2017). Relative Humidity Sensing Using A PMMA Doped Agarose Gel Microfiber. *Journal of Lightwave Technology*.

18) Mahyuddin, M. B. H., Latiff, A. A., Rusdi, M. F. M., Irawati, N., & Harun, S. W. (2017). Quantum dot cadmium selenide as a saturable absorber for Q-switched and mode-locked double-clad ytterbium-doped fiber lasers. *Optics Communications*, *397*, 147-152.

19) Irawati, N., Harun, S. W., Rahman, H. A., Chong, S. S., Hamizi, N. A., & Ahmad, H. (2017). Temperature sensing using CdSe quantum dot doped poly (methyl methacrylate) microfiber. *Applied Optics*, *56*(16), 4675-4679.

Papers Presented at Conferences

1) John, V., Irawati, N., Ali, N. M and Harun, S. W. (2015). Measuring Various Biomedical Concentration Using Micro-ball Lens Probe. paper presented at **2015 5th International Conference on Biomedical Engineering and Technology (ICBET 2015), Hanyang University,** Seoul, South Korea

2) Irawati, N., Harun S.W and Ahmad, H. (2015). Optical Trapping and Transport of Polystyrene Microssphere's Evanescent Wave on Microfibers. Paper presented at **ONNA 2015: Optical Nanofiber Applications : From Quantum to Bio Technologies, Okinawa Institute of Science and Technology,** Okinawa, Japan.

3) Aris. A. M., Irawati, N., Rahman, H. A., Harun, S.W., Ahad, I. Z. M. (2015). Fiber Bragg Grating Sensor For Humidity Measurement. Paper presented at **2015 International Conference on System Engineering and Technology (ICSET 2015), UniversitiTeknologi Mara,** Shah Alam, Malaysia

4) Yasin, M., Irawati, N., Abdullah, T. N. R., Rahman, H. A., Ahmad, H. Harun, S. W. (2015). Relative Humidity Sensor Using A PMMA Microfiber Coated WithZnO Nanostructure. Paper presented at **10th International Symposium on Modern Optics and Its Applications (ISMOA 2015), InstitutTeknologi Bandung**, Bandung, Indonesia

5) Rahman, H. A., Irawati, N., Harun, S. W. (2015). PMMA Microfiber Coated with ZnO Nanostructure for The Measurement ofRelative Humidity. Paper presented at **4th International Conference on Electronic Devices, Systems and Applications (ICEDSA), Hotel Istana,**Kuala Lumpur, Malaysia

6) Rosol, A.H.A, Irawati, N., Rahman, H. A, Harun, S. W. (2015). Microfiber Knot Resonator Based Humidity Sensor. Paper presented at **International Conference on Research in Science and Technology, Intercontinental Hotel,** Kuala Lumpur, Malaysia.

7) Aris. A. M., Irawati, N., Rahman, H. A., Harun, S.W., Lim, K. S., Ahad, I. Z. M. (2016). Enhanced Relative Humidity Sensing Based on A Tapered Fiber Bragg Grating with Zinc Oxide Nanostructure-Embedded Coatings. Paper presented at **2016 3rd International Conference on Computer, Communication and Control Technology, Promenade Hotel, Kota Kinabalu, Malaysia.**

8) Rosol, A.H.A., Irawati, N., Rahman., N. M. Isa., H. A, Harun, S. W. (2016). *Detection of Honey Adulteration by Addition of Glucose Via a Microfiber Coupler.*Paper presented at **2016 3rd International Conference on Computer, Communication and Control Technology, Promenade Hotel, Kota Kinabalu, Malaysia.**

9) N. M. Isa., Irawati, N.,Rosol, A.H.A., Rahman., M. H. M. Yusoff., N. N. fadzlina., Harun, S. W. (2016). Silica Microfiber Sensor for the Detection of Honey Adulteration. Paper presented at **2016 3rd International Conference on Computer, Communication and Control Technology, Promenade Hotel, Kota Kinabalu, Malaysia.**